# Laser-assisted epicutaneous vaccination of mice with ovalbumin-dextran nanoparticles

## Master thesis

**To obtain the title "Master of Science"**
**University of Salzburg**

Stephan Drothler
1420875

Submission: 2021, March
Version update: 2021, June

Supervisors: Prof. Dr. Richard Weiss
Dr. Sandra Scheiblhofer

Department of Biosciences

’A poet once said, " The whole universe is in a glass of wine." We will probably never know in what sense he meant that, for poets do not write to be understood. But it is true that if we look at a glass of wine closely enough we see the entire universe. There are the things of physics: the twisting liquid which evaporates depending on the wind and weather, the reflections in the glass, and our imagination adds the atoms. The glass is a distillation of the Earth’s rocks, and in its composition we see the secrets of the universe’s age, and the evolution of stars. What strange arrays of chemicals are in the wine? How did they come to be? There are the ferments, the enzymes, the substrates, and the products. There in wine is found the great generalization: all life is fermentation. Nobody can discover the chemistry of wine without discovering, as did Louis Pasteur, the cause of much disease. How vivid is the claret, pressing its existence into the consciousness that watches it!’

– Richard P. Feynman
*The Feynman Lectures on Physics (1964)*
*Volume I, 3-10*

# Statutory declaration

I, Stephan Drothler, hereby declare that the thesis submitted is my own unaided work, that I have not used other than the sources indicated, and that all direct and indirect sources are acknowledged as references.

This printed thesis is identical with the electronic version submitted.

Date, Signature

(Original Version was signed on 03.03.21 and is available on the Paris Lodron University (Salzburg) publication server)

# Version Update

The following corrections were made without distorting the content of the work:

## Update June 2021

Page 11: α-Glucan instead *α-Glucans*

immunologists instead of *immunologist*

Page 15: Hollow needles ~~are~~ [...]

Page 42: Closed second bracket in: [...] *(NetSurfP1.1/NetSurfP2) [1, 2] (Fig. 3.4(**B**)*).

Page 44: Removed wrong Figure caption: ~~(**B**) Summary of exposed~~ [...]

Page 57: Changed Fig. to Tab. in: *Spleenocytes were largely unaffected by OVA* [...]

Page 68: Closed second bracket in: *In contrast, only OVADex 15F1 was able to stimulate CD86 upregulation of GM-CSF DCs (see. Fig. 2.2.4(**A,B**)*)

If you find additional mistakes, please send me an email to: stephan.drothler@gmail.com

# Contents

# Preface

Vaccination is generally considered to be an unparalleled triumph for global human health, backed up by a large scientific body [3–7]. The groundwork of vaccination is rooted in the principle of equipping the body with immunological weapons by transferring a safe dose of pathogen. Induced by this challenge, the organism upholds a long-term protection against the administered infectant.

With the up-rise of molecular biology in the last decades, novel vaccination approaches enriched the traditional range. Traditionally, vaccines consisted of pathogen-subunits, attenuated- or inactivated- whole-pathogen agents.

Whole agents excel at mimicry of the pathogen, resulting in a broad range of different antibodies. While inactivated microbes fail to induce cellular immunity, attenuated pathogens can elicit potent immune stimulation, hence evoking rich humoral and cellular responses. Sub-unit vaccination exploits single components of pathogens, like surface molecules. This technique usually produces an antibody-dominant response and requires several booster injections.

More recent approaches aim at lower costs of production while increasing safety and immunogenicity [3]. Peptide and protein based vaccines reduce pathogen-related antigens down to the immunogenic epitopes, to drive down costs, reduce allergenic potential and increase overall safety. To compensate for the low immunogenicity of the stand-alone antigens, formulations are often spiked with adjuvants or incorporated into bio-polymer constructs [7, 8]. In this regard, polysaccharide functionalization has gained thrust over the last decades. Since carbohydrates are often naturally occurring on the surface of pathogens, they are recognized by the immune system via specialized pattern recognition receptors of the C-type lectin family. These receptors are broadly present on the surface of dendritic cells, the major orchestrators of powerful adaptive immune responses [9]. Consequently, spiking immune therapeutics with various polysaccharides in order to target dendritic cells and elicit potent immune responses has been highly researched. Moreover, these carbohydrates are bio-compatible and associated with high safety profiles, which has been demonstrated in several clinical trials [10]. Dextran is a glucan widely used in food and medicine and was generally regarded as a biologically inert molecule. In the last years, research has shown that dextran also binds multiple C-type lectin receptors, some with size-dependent efficiency [11, 12].
In addition to biochemical upgrades of novel immuo-therapeutics, routes and methods of administration are also under active investigation. Currently, the dominant methods for drug delivery are intramuscular or subcutaneous injection, targeting anatomical sites low in naturally occurring, professional immunocytes. Alternatively, intradermal injection is also

performed since 1908 and studied exhaustively since the skin is a tissue highly infiltrated with immunocytes. Strong immunogenicity and safety have even been shown in clinical trials before [13–15], yet intradermal injection is only broadly used for tuberculosis and rabies vaccines in developing countries [16]. Successful intradermal injection is hard to perform and requires trained personnel [17], and is often accompanied by harmless but undesirable local adverse events [18]. Hung et al. reviewed data from multiple studies and meta-analyses of intradermal influenza vaccination. They also concluded that intradermal immunization had greater or similar immunogenicity but stressed the high technical demand of correct injection [19]. Therefore it is reasonable to assume that the technical hurdle and factors contributed to slowing down the mainstream spread of intradermal injections.
Excitingly, novel epicutaneous, laser-facilitated approaches, promise direct targeting of immuno-competent cells, without the need for trained personnel. Furthermore, the technique comprises a natural adjuvant effect and is associated with a low occurrence of local side effects [16]. Korotchenko et al. have recently demonstrated the feasibility of epicutaneous immunization using β-glucan-ovalbumin glycoconjugates upon ablative laser-facilitated microporation. The Authors used a mouse model for allergenic asthma to compare immunogenicity and safety of neoglycoconjugates to the uncoupled allergen. Both treatments were delivered through micropores created by thermal laser ablation. Additionally, one treatment with uncoupled ovalbumin was delivered by sub cutaneous injection adjuvanted with alum. In the study they observed lower levels of lung inflammation and IgE titers, but higher IgG1 levels in the laser group with glycoconjugated allergen. The inflammatory reduction was also seen in the laser-treated mice immunized with uncoupled ovalbumin, but IgG1 levels were lower while the IgE concentration was increased [20]. Furthermore, targeting of dendritic cells via C-type lectin receptors has also been researched for inducing anti-cancer therapy. Especially Dectin-1 and DC-SIGN receptor mediated immunity has been studied and shown to induce $CD8^+$ T cell responses through cross-presentation [21]. Successful induction of cytotoxic T lymphocytes is critical for developing a promising cancer therapy, since these $CD^+$ cells are dominantly responsible for tumor eradication [22]

This work was focused on the interplay of innate and adaptive immunity based on *in vitro* cultured dendritic cells and T-cells from mice expressing an ovalbumin (OVA)-specific T-cell receptor, as well as an *in vivo* vaccination model with C57BL/6 mice. The treatments consisted of in-house produced OVA-dextran conjugates, purified by size exclusion chromatography. For the glycoconjugate production, polyaldehyde dextran was coupled to surface accessible Lysines on ovalbumin by reductive amination. To test the immunogenic and allergenic potential of the particles, two differently stimulated dendritic cell cultures were set up *ex vivo*. Subsequently, the degree of activation and the induction of T cell proliferation and maturation by these dendritic cells was measured. Furthermore, we studied the extent of degranulation from anti-OVA-IgE loaded rat basophilic leukemia cells upon treatment with our neoglycoconjugates. This is important for allergen-specific immunotherapy because

cross-linking of pre-existing IgE in allergic patients can induce serious side effects. Lastly, we immunized C57Bl/6 mice epicoutaneously through laser generated micropores. In this study we used an 2940 nm diode-pumped, erbium:yttrium-aluminum-garnet (ER:YAG) ablative laser P.L.E.A.S.E. ® device (Pantec Biosolutions, Lichtenstein).
After the low initial immunogenicity readouts from the first *in vivo* immunization protocol, we decided to co-administer CpG-ODN in the second immunization experiment. This adjuvant is known to boost $T_H1$ immunity, which enabled us to discriminate the induction of a cytotoxic $CD8^+$ response. All treatments were compared to uncoupled ovalbumin and adjusted to equal treatment doses by weight.

The production of glycoconjugates with three different dextrans (15 kDa, 100 kDa and 450 kDa) yielded two distinct size peaks upon chromatographic separation. Those distinct fractions were subsequently pooled, which left us with two, differently sized particle suspensions for each ovalbumin-dextran (OVADex) neoglycoconjugate. In summary, we generated a total of six treatments, one large particle fraction pool, which we termed "F1" and one small particle fraction pool termed "F2". In this work, treatments are therefore referred to as 15F1, 15F2, 100F1, 100F2, 450F1 and 450F2 - with the numeric prefix identifying the molecular weight of the coupled dextran. The co-culture of naive $CD4^+$ T-cells with GM-CSF generated bone marrow derived dendritic cells yielded a 48% - 150% increase in absolute $CD4^+$ T cell numbers in the highest dose groups (20 μg), where the biggest conjugates induced higher proliferation than the smaller conjugates. The minimum effective dose was shown to be lower for dextran constructs, where induction of proliferation was observable in the 4 μg groups, but not in the 4 μg OVA group. The same experiment with FLT3L generated bone marrow derived dendritic cells with a lower maximum dose of 10 μg showed similar trends, with a 123% - 290 % increase in CD4 proliferation. The lower treatment dose (2 μg) generated a similar response as 10 μg in the OVA group, while the dextrans constructs still showed a dose-dependent effect. Activation of the respective dendritic cells was also monitored, where strong CD86 and CD40 upregulation was observed for 15F1 treated groups in both DC cultures. In addition, FLT3L DCs showed a higher response to 100F2 and 450F2 OVADex treatment than GM-CSF derived DCs. IgE-loaded rat basophilic leukemia cells treated with conjugates showed less degranulation up to the maximum tested dose of 10 $\frac{\mu g}{mL}$ compared to uncoupled OVA. Therefore, all conjugates were hypoallergenic, whereby the small particle fraction of the dextran with the lowest molecular weight (15 kDa) showed the least effective allergenic epitope shielding. Readouts from the *in vivo* immunizations showed elevated $T_H1$ associated antibody titers (IgG2c) in OVADex groups. Anti-OVA ELISA resulted in tenfold higher titers compared to the OVA immunized group. Moreover increased OVA specific T-lymphocyte proliferation and activation was observed in the spleens of animals treated with 100 kDa and 450 kDa F2 OVADex conjugates. Conversely, we observed a decrease of cytotoxic activity in OVADex treated mice compared to plain OVA with increased dextran chain length, against SIINFEKL-pulsed target cells from naive syngeneic donor mice. Interestingly, at the cellular level, 15F2 OVADex produced

comparable results to uncoupled OVA but showed stronger induction of antibodies.

Taken together, these results illustrate the potential of dextran conjugated antigens to induce and activate immunocytes *in vivo* and *in vitro* while being hypoallergenic. Unfortunately, the production process had a low turnout efficiency for large conjugates (F1), thus the promising candidates from the cell culture studies could not be tested in the living organism. Interestingly, even though antibody stimulation and induction of T cell proliferation were high for the 100F2 and 450 F2 conjugates, induction of target-specific cell lysis was poor in these groups.

The following manuscript outlines the path for reaching those conclusions and aims to provide an understanding of the considerations and decisions gauged in this thesis. Finally, the results will be discussed in more detail.

# Goals and Hypotheses

In this work, we investigated immune stimulation of dextran functionalized ovalbumin neoglycoconjugates. We aimed to target C-type lectin receptors (CLR) present on the surface of dendritic cells (DC) to study the subsequent immune reactions. Dendritic cells are well known as the most competent inducers of adaptive immunity, thus DC targeting approaches have been researched in various immunological disciplines. Among these, allergology and oncology have both been investigating the immune-modulatory capabilities of various polysaccharides before. Both fields aim to potentiate the immunogenicity of their formulations, while allergen-specific therapies aim to create hypoallergenic therapeutics which also generate blocking IgGs. In contrast, cancer treatments mostly seek to induce cytotoxic T lymphocytes and aim to circumvent tumor mediated immune evasion. DC targeting has already shown encouraging pre-clinical results for allergen-specific immunotherapy and cancer treatment. Moreover, carbohydrate-based adjuvants appear as ideal candidates with regard to their high safety profile. Additionally, bio-technical advances have offered new means of effective and safe drug delivery. In this study, we administered our glycoconjugates epicutaneously on laser generated micropores. To test for size-dependent differences, we coupled dextran with different molecular weights to ovalbumin and tested their effects on several immune-related parameters. To determine immunogenicity and allergenicity we measured the activation of dendritic cells, T cell proliferation and basophil degranulation *in vitro*. Furthermore, we analyzed antibody levels, antigen specific cell polarization, lymphocyte mediated cellular toxicity and cytokine production in immunized C57BL/6 mice. After our first immunization protocol, we decided to include CpG-ODN as an adjuvant, so we were able to distinguish target specific lysis between treatment groups. Takahara et al. have demonstrated that some CLRs preferentially take up dextrans with higher molecular weight [11]. Korotchenko, Weinberger and Machando et al. also tested neoglycoconjugates and observed high immunogenicity and low allergenicity of their novel particles[20, 23, 24] Thus our research goals in this thesis can subsequently be formulated into the following scientific hypothesis.

**Hypothesis$_1$**: Conjugated ovalbumin-dextran particles have a higher immunogenic potential than ovalbumin alone.

**Hypothesis$_2$**: Ovalbumin-dextran glycoconjugates potentiate immune response with an increase in size

**Hypothesis$_3$**: Antigen-specific type I hypersensitivity is reduced upon conjugation

**Hypothesis$_4$**: Allergenicity of OVADex particles decrease with size

# Abstract

Safe and effective immunization strategies are of very high interest for global human health. A high safety profile can be achieved by reducing vaccine formulations down to single pathogen associated antigens. Yet, these subunit vaccines are poorly immunogenic and require adjuvants to potentiate the immune response. Carbohydrates are naturally occurring on pathogens and are increasingly popular as immune stimulants due to their high bio-compatibility. It is known, that professional immunocytes are resident in upper dermal layers, which are able to induce powerful adaptive immune responses in the draining lymph nodes. In this work, we studied the immunogenic effect of dextran as an adjuvant, by conjugation to a model antigen (ovalbumin). For efficient targeting of c-type lectin receptors on dendritic cells in the skin, we delivered the neoglycoconjugates through micropores using an ablative P.L.E.A.S.E. ® laser.

To study size dependent uptake and subsequent immune reactions, we generated neoglycoconjugates from three differently sized dextrans (15kDa, 100kDa and 450kDa). We purified the OVADex conjugates via size exclusion chromatography and pooled two distinctly sized fractions per dextran for a total of six glycoconjugates. After testing the particles *in vitro*, we found evidence for size-dependent activation of dendritic cells. In our setup, the largest fractions showed significantly higher activation. Consequently, these particles induced higher T cell proliferation and maturation rates than uncoupled ovalbumin and the smaller conjugates. Using an *in vitro* degranulation assay, we found a reduction of the allergenic potential of all conjugates compared to uncoupled ovalbumin. Due to a low coupling rate of the largest fraction pools, we were unable to test their immunogenicity in the final *in vivo* experiment. Nevertheless, immunization of C57BL/6 mice with the smaller fraction pools of 100kDa and 450 kDa OVADex showed an increase in $T_H1$ associated antibodies, as well as expanded immunocyte proliferation compared to ovalbumin. Conversely, we observed almost no target specific lysis in those groups, which might be attributable to coupling related damage of the dominant cytotoxic epitope.

In summary, we collected evidence *in vitro* and *in vivo* that indicates a higher degree of humoral and cellular immune activation, as well as a reduction of allergenicity by conjugating ovalbumin to dextran.

# Abbreviations

**AAA** amino acid analysis

**APC** antigen presenting cell

**BCR** B cell receptor

**CD** cluster of differentiation

**CTL** cytotoxic T lymphocytes

**DAMP** danger associated molecular pattern

**DC** dendritic cell

**Dex/DEX** dextran

**DLS** dynamic light scattering

**ELISA** enzyme linked immunosorbent assay

**F1/F2** fraction 1/fraction 2

**FLT3-L/FLT3L** fms like tyrosine kinase 3 ligand

**FPLC** fast protein liquid chromatography

**GM-CSF** granulocyte macrophage colony-stimulating factor

**HPLC** high performance liquid chromatography

**Ig** immunoglobulin

**kDa** kilo dalton

**LC** langerhans cell

**LN** lymph node

**LPS** lipopolysaccharide

**MHC** major histocompatibility complex

**MST** microscale thermophoresis

**OD** optical density

**OVADex** ovalbumin-dextran conjugates

**OVA** ovalbumin

**PAMP** pathogen associated molecular pattern

**PRR** pattern recognition receptor

**SDS-PAGE** sodium dodecyl sulfate - polyacrylamide gel electrophoresis

**SEC** size exclusion chromatography

**SFU** spot forming units

**$T_H$** T helper

**TCR** T cell receptor

**TLR** toll like receptor

# Introduction 1

## 1.1 Vaccinology - a short history

> *"It is said that only those who have seen the beginning of things can understand the present."*
>
> – Stanley Plotkin, *2011*

Documentation of humans, battling infectious diseases via immunization, dates back to ancient China between 1000 - 1500 A.D. It is helpful to know that traditional Chinese medicine relied heavily on the *vis medicatrix naturae*, the body's inherited healing process. Based on two essential principles - *kung* ( "attack")[1] and *pu* ("revitalization")[2] a core guideline was *i tu kung tu* - "using poison to combat poison". This phrase is linked to the original attempts of early medicos to protect patients against smallpox by controlled inoculation with the pathogen itself. The remains describe different immunization practices, either by transferring grinded smallpox scarbs from infected people into the patient´s nostrils, or by transmission of infected lymph fluid into the epidermis of the patient. While the former was the dominant procedure in China, the latter technique spread over to Turkey and further then to Europe in the 17th century [25]. The method was known under the name of variolation, derived from latin *varus*,[3] "mark of the skin". It got introduced to England in 1715, triggered by the hunt for a treatment of the English aristocrat Lady Mary Wortley Montague. She commissioned Charles Maitland to variolate her five year old son, at that time in Turkey, in 1718. Three years later, back in England, Charles Maitland performed the smallpox inoculation also on Lady Montague´s four year old daughter successfully - sparking her to advocate and popularize variolation. The death rate of the variolation procedures itself, is not precisely historically confirmed, but was probably around 1-3% - approximately ten times lower than the disease itself. The first documented statistical approach was conducted by Mather and Boylston in Boston, 1721 - covering 12000 individuals, amongst whom the case fatality rate of non-immunized persons was 14% contrary to 2% in variolated beings. The death toll was indeed dramatically lower, but safer procedures were desired - a procedure later known as vaccination [18, 26, 27].

In the late 18th century, Edward Jenner and Benjamin Jesty pioneered in the development of the first smallpox vaccine - through



1: meaning the active combat of pathogens

2: meaning the strengthening of internal defense mechanisms

3: inoculation was often used interchangeably, derived from the latin word *inoculare*, "to graft", which explains another popular term for the procedure in europe "engrafting"

protection offered by cowpox viruses. At that time there was a known connection between cowpox exposed milkmaids and a resistance against smallpox. Jetsy successfully vaccinated his family, while Jenner pursued further testing and delivered scientific confirmation,[4] leading to a rapid spread of the vaccine.[5] The exact contents of Jenner´s *vaccinia* remain unknown, speculations circle an extinct strain of horsepox or a genetic hybrid between smallpox and cowpox, namely *variola*, a virus with no natural host. The publication eventually gave rise to the global eradication of smallpox [25, 29] - as confirmed by the WHO in 1980 [18].

4: Variolae Vaccinae in 1798 [28]

5: Jesty was honored in 1805 by the Original Vaccine Pock Institute in an open statement, recognizing Jesty's cowpox vaccination. Furthermore his portrait arranged in the institute. Nevertheless Jenners paper is accepted as the first scientific shot to regulate a extensively present disease, without transmitting the disease itself [6].

Louis Pasteur characterized 80 years later the monumental process of attenuation. Whether on purpose, or by accident, Pasteur documented the mitigation of *Pasteurella multocida* by exposure to adverse conditions. Subsequently, he continued to work on Anthrax and rabies, shedding more and more light into the mysteries of vaccination. Decisive discoveries of bacterial toxins, antitoxins, viruses, inactivation of whole bacteria or toxin- and replication-neutralizing agents in serum - now known as antibodies - followed between 1890 and 1900. Shortly after, inactivated whole-cell vaccines against typhoid, cholera and plague were created. Antibodies, were described in animals surviving exotoxin-secreting *diphtheria bacilli* infections. Further investigation of the toxin led to the formulation of a stable non-toxic formalin-inactivated diphtheria antigen toxoid. Further insight arose in the selection of avirulent strains by passage through unnatural hosts. Strikingly, the development of a *Mycobacterium bovis* vaccine through 230 serial passages took 14 years, offering protection against tuberculosis [29]. Jules Bordet demonstrated in the late 19th century, that target lysis was based on heat-labile agents (complement) and a heat-stable factors (antiodies) - while the exact terminology and functionality was developed steadily over time [18]. Being smaller than bacteria and parasites, filterable agents,[6] were described and the yellow fever strain 17D was attenuated through serial passage. Simultaneously, whole-cell *Bordetella pertussis* vaccine and *influenza virus* vaccines were employed, whereby the original pertussis formulation became refined to only the antibody-inducing bacterial proteins. Influenza - although successfully immunizable initially - emerged as greatly variable in antigens, swinging the original vaccine impotent. Countering this variability, still remains subject to research, in a quest to identify conserved, antigenic domains.

6: virus; The first reported specimen, *Tobacco mosaic virus* was described by Ivanoski in 1892, showing that extracts from infected leaves remained infectious upon filtration. (typically removing bacteria and parasites). Seven years later, Beijerinck coined the term *"virus"*, describing the tobacco mosaic virus as a soluble, infectious agent [30].

Viral cell culture,[7] was certainly a milestone in vaccine development, taken advantage of by Jonas Salk and Albert Sabin, in developing a *poliovirus* vaccine. Awareness, that neutralizing antibodies correlated positively with immunity, built the credo to reduce reactivity of viruses, while maintaining immunogenicity. These findings also paved the road for measles, mumps, and rubella

7: Pioneered by John F. Enders, Thomas H. Weller and Frederick C. Robbins, who tested conditions for extraneural replication of a *poliomyelitis virus* strain. The culture media consisted of a salt solution, and ox serum ultra-filtrate supplemented with various human embryo tissue [31].

vaccines (MMR).[8] Protein - polysaccharide conjugation was already discovered but failed to deliver potent results, until Robbins and Rachel Schneerson successfully coupled diphtheria with the type b capsule protein of *H. influenza*. Successive experiments, also with tetanus toxoid, spawned conjugate vaccines for *meningococci* and *pneumococci*.

Stanley Cohen and Herbert Boyer have launched the protein production in various cell types via the means of genetic engineering, at that time with using baculovirus vectors. This enabled the development of the first engineered vaccine - a hepatitis B surface antigen. Subsequently, protective antigens were expressed for *human papillomavirus*, *Borrelia burgdorferi* and *rotaviruses*. Other than the humoral component of immunity, T cell activation also plays a crucial role in various infections and ensures a long-time protection into the future. The classification of cellular and molecular orchestration is currently object of scientific research and advances the creation of high precision formulations [29].

In the following sections, a coherent outline of the relevant immune machinery is given, leading to the techniques and scientific foundation for the latter experiments.

8: MMR controversy (Box):

**Vaccine safety**

Myths, that MMR vaccination leads to autism has been among the most harmful controversies in vaccine safety. Reported in 1998 - "Ileal-lymphoid-nodular hyperplasia, non-specific colitis, and pervasive developmental disorder in children" - the article was retracted by the publisher (The Lancet), because of suspicious subject recruitment and financing. The authors observed twelve children with pervasive developmental disorder (9 with autism) and intestinal problems. Additionally, the central message of the study was based on the note of the parents or doctors, observing a worsening of pervasive developmental disorder in eight children. Even though a great number of studies demonstrated no correlation between autism and MMR vaccination, the large initial panic still lingers in the heads of many parents and resulted in a re-occurrence of the diseases in some places [32].

## 1.2 Molecular mechanism of immunization

### 1.2.1 Basic concept of immunization

The immunological cascade obviously depends on the type of vaccine, route of administration and nevertheless a condensed summary of events can be quite useful. Briefly summarized - upon administration of the compound, active and/or passive transport to the draining lymph node(s) occurs (1/3). Presented and recognizable antigenic domains lead to B and T - cell expansion (2/3). After the effector phase, memory cells serve for follow-up protection (3/3).

| **Polarization:** | | |
|---|---|---|
| **$T_H1$** | **$T_H2$** | **$T_H17$** |
| **Cytokines**: | | |
| IFN-γ | IL-4 | IL-17A |
| | IL-5 | IL-17F |
| | IL-13 | IL-22 |
| **Transcription factors**: | | |
| T-bet | GATA3 | RORγ t |

**Table 1.1:** Rough classification of T helper subsets. Cytokine expression and transcription factors can have large overlaps with other immunocytes, such as innate lymphoid cells and their expression levels can vary depending cell stage [33]. Additional helper subsets exist, and their classification is likely expanding in the future.

### 1.2.2 Initial response to antigens

More delicately speaking, inflammation and subsequent immunocyte recruitment, alongside increased vascular permeability enables the passive transport of antigen to the draining lymph node via the lymph fluid itself, as well as the active transport via the recruited cells. Upon passive arrival in the marginal sinus, the antigenic domains of the proteins are broken up into MHC[9] compatible peptides, predominantly by subcapsular macrophages.[10] Subsequently these epitopes are displayed to naive lymphocytes in

their respective departments by the incoming antigen loaded cells (from the active transport) or freshly loaded lymph node resident macrophages [35].

### 1.2.3 Lymphocyte mediated defense

B lymphocyte[11] activation usually occurs in the intranodal follicles through BCR[12] signaling and initiates an orchestrated response starting with the quick extrafollicular production of low affinity - short lived antibodies with a IgM/IgG ratio >1 due to presence of IgM on naive B cells. The affinity of initial IgM roughly approximates the binding strength - of the antigen to the IgM-BCR - whereby upon T-cell help, subsequent isotype switching and affinity maturation ensure a refined supply of high-precision antibodies of the IgG/IgA/IgE class directly or sequentially [37, 38]. This striking process is enabled by costimulation of activated B cells via $T_H$ cells at the T/B zone border. These B cells then wander towards the follicle hub and undergo hypermutation in the "dark zone" before selection in the "light zone" occurs through fDCs.[13] Finally selected "higher" affinity clones can leave the germinal center via support by follicular $T_H$ cells, pursuing either a long lived plasma cell - or memory B cell fate or re-enter the "dark zone" for enhanced maturation [39]. In addition to the MHC restricted affinity maturation, B cells are also able to respond to non-protein antigens in a T - cell independent manner. These antibodies are consequently less specific and typically IgM isotypes. Currently, therapeutic vaccines against several maladies like tumors, allergy, addiction and atherosclerosis are under active investigation. Yet for most preventative vaccines, creation of high affinity $IgG^{+14}$ memory B cells is of critical interest for a long term protective, humoral immunity.

Evoking cellular immunity, manifested as a T lymphocyte response, also depends on an antigen dependent activation reaction. Naive T cells circulate through the system until they get confronted with their specific antigen by loaded, activated APCs in a MHC dependent manner. Helper type responses root in the signal transduction via MHC-II and the respective TCR and the CD4 co-receptor, whereas cytotoxic strikes rely on MHC-I interaction with the TCR and the CD8 co-receptor. Activation of these respective T lymphocytes is also dependent on the co-stimulation, as the lack of it, pushes the T cell into an anergic state. The most eminent co-stimulating agent, known to date is the CD28 receptor, triggering an intracellular cascade upon binding to its ligands C80 / CD86 provided by APCs. Additional adhesion molecules enable the formation of a secure transmission cluster, often called the *immunological synapse*. Successful interaction of MHC-TCR complex

9: Major histocompatibility complex - These are central immunological receptors classified into two types (I / II). All nucleated cells mount peptides onto their MHC-I receptors (consisting of 2x α- chains with a pocket size of 8–10 amino acids), while professional APCs can load peptides onto their MHC-II receptors (consisting of one α& one β-chain with a groove of 13-25 amino acids) [34]

10: For some antigens, a distinct type of medullary DC might be more important. This topic is currently under investigation

11: Representative for the humoral defense cascade mediated by γ-immunoglobulins (antibodies).

12: B-cell receptor, which is decisively important for antigen recognition. Similar to the T-cell receptor variety, clonal diversity is achieved by RAG-mediated genetic recombination of the coding V-D-J segments [36].

13: Follicular dendritic cells, which are able to store antigens over long periods of time in non-decomposing endosomal compartments and can therefore present antigens repeatedly in various time intervals. fDCs also release B and T cell targeted chemoattractants (eg.CXCL13) and B cell survival signals (eg. IL-6 / BAFF). The germinal centers are technically predefined micro-compartments with respective CXCL12 / CXCL13 gradients that enable dynamic sampling of novel, draining antigens by B cells and control their subsequent affinity maturation [39, 40].

14: IgG is the most abundant circulating immunoglobulin and is able to initiate antibody dependent cellular toxicity and complement activation. Depending on the scientific issue, other isotypes eg. IgA which is critical in mucosal immunity might be of interest.

then kicks off manifold intracellular activation processes leading to rapid expansion and differentiation. Among the different mechanisms, phosphorylation via tyrosine kinases is a hallmark of lymphocyte activation. Upon activation of the TCR complex, the tyrosine kinase Lck[15] is moved mechanically into proximity of the immunoreceptor tyrosine-based activation motifs. The phosphorylated patterns provide a docking platform for a ZAP-70 kinase, which subsequently becomes a mobile tyrosine kinase itself - involved in the activation of downstream signaling molecules. Ultimately, the fine-tuned signaling leads to the activation of distinct transcription factors and shapes the individual phenotype. Furthermore, positive feedback is provided by activated T lymphocytes themselves, via secretion of pro-inflammatory cytokines like IFN-γ or IL-2 and upregulation of CD154 (CD40L) - which are able to bolster APC activation, a process known as "licensing" [41, 42].

15: Intracellularly associated with the CD4 / CD8 co-receptors.

The presentation of peptides via MHC-I and MHC-II differ in their respective loading processes. Intracellular proteins are degraded in the proteasome and shuttled into the endoplasmatic reticulum via *transporter associated with antigen processing*(TAP) and loaded onto MHC-I via tapasin. In contrast MHC-II compatible peptides are prepared by cathepsins and mounted to MHCs in late endosomes or lysosomes. A key exception is the mechanism of cross-presentation, where exogenous immunogens are also mounted onto MHC-I complexes mainly in specialized dendritic cells. Classical DCs type 1 (cDC1)[16] are one of two subgroups from the cDC pool, present in humans and mice. cDC1 cells are known as strong cross-presenters, with $103^{+}$ roaming the skin, intestine and lung in mice. Murine lymphoid antigens are cross-presented by $CD8^{+}$ resident cDC1s.[17] While cDC2 and even pDCs are theoretically able to cross-present, the current literature suggests that they are largely dispensable in MHC-I dependent immune reactions [43, 44]. $CD8^{+}$ T cells are also termed cytotoxic T lymphocytes (CTL) for their prominent role in the clearance of infected and neoplastic host cells. Effector CTLs upregulate the expression of perforin and granzymes for their cytotoxic activity, driven by the signature transcription factors T-bet. Stimulation of CTLs through activated APCs, leads to a metabolic switch to aerobic glycolysis and a dramatic expansion of antigen specific clones that migrate to the target site [42, 45]. Essential for the induction of this process it the presence of helper T cells, characterized by their expression of the CD4 co-receptor. Constant efforts have been directed to classify subsets of these helper cells, with three major categories often found in the literature. These subsets are termed $T_H1$, $T_H2$ and $T_H17$ - distinguished by the release of signature cytokines and the presence of transcription factors (Tab. 1.1). This classification is not exhaustive as additional cell types and corresponding cytokines play important roles in

16: Characteristic transcription factors are IRF8 and Batf3. Typically classified by expression of the XCR1 receptor. cDC1 cells express high levels of MHC-I components and low endosomal acidification.

17: Conversely human cDC1s are characterizable by CD141, instead of CD8 and CD103 [43].

immune responses. The affinity maturation described above, or the dampening of immune responses and maintaining peripheral tolerance is mediated by follicular $T_H$ cells and regulatory T cells respectively [33].

## 1.3 Novel vaccine designs

The triumph of vaccines against infectious diseases and the inherent increase in life expectancy has led to a shift in disease burden - an uprise in non-communicable related deaths. Among cancer, cardiovascular disease, nicotine addition and alzheimer's, also type-I allergy vaccines are under investigation [46, 47]. With ever-growing insight into molecular immunology, it is clear that a protective immune response is in many instances only dependent on a few immunogenic proteins. These vaccine formulations are also developed against non-communicable diseases. Whole-pathogen vaccines or their subunits, may not only contain unnecessary components but also allergenic ones. The sources might be intrinsic and dependent on the type of vaccine or are caused by unwanted trace elements. These might be generated during the production process or found in packaging/syringes (eg. OVA, latex, gelatin) [7, 48]. [18] Attractive techniques have revolved around protein and peptide based vaccines, coupled to polysaccharides, spiked with soluble immune-stimulants or water-oil emulsions. Not only drug design, but also the method of delivery is under investigation, ensuring high safety profiles with optimal efficiency[3, 4, 16, 23].

18: In this case, the immunologically mediated hypersensitivity requires a pre-exposure of the patient to the antigen with produces IgE-mounted granulocytes (Type I - Hypersensitivity). These cells granulate upon re-exposure to the allergen, which lead to the release of inflammatory mediators and can result, at worst, in anaphylaxis. Most hypersensitivity reactions are mild and not reproducible, therefore thought not to be immune mediated [48]

### 1.3.1 Sub-unit vaccines

The mild immunogenicity associated with protein and peptide based vaccines, called for the development of boosters - enhancing the magnitude and duration of these vaccines. So called adjuvants are often ligands to pattern recognition receptors of the innate immune system. Thereby, the adjuvant mimics conserved domains of natural pathogens, to trigger the distinctly evolved immune cascades [49].

Aluminum salts were the first adjuvants used and licensed by the FDA in 1926, followed by water in oil emulsions. A lot of time passed before novel formulations came to market, due to high safety regulations and a lack of knowledge about the underlying mechanisms [50]. In 2009 the FDA approved a cervix vaccine for human papilloma virus (HPV) containing a new mixed-adjuvant formulation of monophosphoryl lipid and aluminum salt. This collection of adjuvants acts through release of damage associated patterns (DAMPs), thereby largely reinforcing the humoral immune

response via IL-1β production [4]. The major effect of alum is reported to be based on the stimulation of the inflammasome and secretion of the $T_H2$ inducing cytokines IL-4, IL-6 and IL-25. Additionally, some cells become necrotic, secrete DAMPS[19] and the complement system might be activated [50, 51] As previously mentioned, cellular immunity is the key to tackle diseases like tuberculosis, HIV and malaria, and is therefore an interesting target for adjuvant design.

19: Damage associated molecular patterns - eg .DNA, uric acid, ATP and HSP-70

Popular PAMPs[20] for mobilizing a boosted immune response are targeting TLRs[21] which are expressed on a broad range of immune cells. They are extensively studied and downstream signaling is typically well described [52]. Monophosphoryl- and glucopyranosyl[22] - lipid A are widley used for TLR4 targeting, polyI:C for TLR3, remiquimod and imiquiumod for TLR7/8 targeting [53]. CpG-ODN is used as a TLR9 agonist, bacterial flagellin for TLR5. Roughly, TLR3, TLR4, TLR7, TLR8 and TLR9 bolster $T_H1$ - while TLR2 and TLR5 don't skew polarization. Important adaptor in the downstream signaling triggered by PRR activation are MyD88, TRIF, RIP2, CARD9, and IPS1, activating key transcription factors NF-κB, IRF3, and IRF7 [54]. Multi-PRR targeting has also been shown to potentiate adjuvant effects. Creation of covalently bound multimers or nano-encapsulation of single-molecule adjuvants, have shown to be more effective than the untouched, mixed analogs[23] [55]. Taken together, sub-unit vaccines appear as promising and safe candidates for future vaccines, but effective and tolerable adjuvants are necessary to provide sufficient immunity. Many carbohydrate comprise a natural adjuvant effect because they are naturally occurring on pathogens and trigger specific immune responses by binding to pattern recognition receptors on antigen presenting cells. In the subsequent section, this interaction will be explained in more detail.

20: Pathogen associated molecular patterns

21: Toll like receptors

22: Used in a emulsion based formulation

23: Data from cell culture and mouse studies.

### 1.3.2 Ovalbumin as a model antigen

For the creation of novel immunizing therapeutics or comparing means of administration - model antigens and organisms are crucial. In immunologic research - mechanistic insight and potential therapeutic value are often assessed in mice. One of the major pillars of immunological research was thereby the generation of "knockouts" - genetically modified mice, with targeted, specific gene disruption in germline cells. Since the first report in the 1980s - the disruption of the β2-microglobulin gene - research with knockouts has shed light on many important biological questions [56]. Even though components of the immune system differ between organisms, the translational value was derived from mouse models,[24] while "humanizing" murine immune responses

24: Mouse models are certainly not the only model organism in immunology, but have several characteristics eg. low cost, size or traceability. A problem is the low predictive value for immune responses against certain diseases [57].

is under active investigation [58, 59]. Cell culture studies are also important immunological tools, especially for mechanistic insights. As published by several research groups before [60–62], DC phenotypes diverge based on the stimulant used and generally comprise heterogeneous cell suspensions. FLT-3-L[25] and GM-CSF[26] derived DCs before and found higher pre-activation in GM-CSF DCs compared to FLT-3s. Both were suitable for studying naive T cell activation, yet FLT-3 DCs might be better suited to detect treatment specific activation due to their steady-state phenotype

25: fms-like tyrosine kinase 3 ligand

26: granulocyte-macrophage colony-stimulating factor

Ovalbumin (OVA) is a very popular antigen used to model immune responses in biomedical research. A big part of OVA's dominant role can be contributed to Hogquist et al. and Barnden et al. - who generated $CD8^+$ OVA-specific (OT-I) and $CD4^+$ OVA-specific (OT-II) T cell clones, respectively [63, 64]. The use of a single transgene induced the expression of Vβ2 and Vβ5 regions of the TCR, recognizing $OVA_{257\text{-}264}$ (Seq: SIINFKEL) for OT-I and $OVA_{323\text{-}339}$ (Seq: ISQAVHAAHAEINEAGR) for OT-II. The transgenic mice have a narrow repertoire of T cells with a high frequency of the described clones and thereby enable uncluttered tracing of immune responses. OVA makes up for the largest protein fraction (60-65%) in egg whites and is home to the serpin family - although lacking the characteristic protease inhibitory activity. It has a molecular weight of $\approx$ 45 kDa and is typically mannosylated at Asn293. A more stable form called "S-ovalbumin" exists and is based on conformational change with differences in stability, 3D shape and hydrophobicity [65].

## 1.4 Immunocyte targeted therapies

It is well established, that innate immunity contains specialized cells, capable of recognizing foreign substances via pattern recognition receptors (PRR). Subsequently, those cells internalize, process and present antigens, and provide co-stimulatory signals for adaptive immune responses. Professional antigen presenting cells are capable of processing invasive substances - conserved domains in countless pathogens called PAMPs[27] - via DC-SIGN family receptors,[28] mannose, scavenger and toll-like receptors [12]. The initial focus of dendritic cell targeting approaches was mainly set on *ex vivo* stimulation. This procedure was especially prominent in the cancer therapy research, but failed to produce significant success. Even though clinical trials have demonstrated good safety and induction of immune responses, tumor regression was often not achieved. Nowadays, treatments are increasingly *in vivo* targeted, whereby monoclonal antibodies or ligands are used as antigen carriers to dendritic cell receptors [66]. The broad range

27: Pathogen associated molecular pattern

28: Dendritic cell - specific intracellular adhesion molecule 3-grabbing nonintegrin - a family of C-type lectin receptors

of receptors and the expression of cross presenting machinery makes dendritic cells the most prominent target for cell specific immunizations. Interestingly, dendritic cells counteract the rapid degradation of immunogenic epitopes in lysosomes by active alkalization and reduced expression of lysosomal proteases. Furthermore, receptor dependent internalization also has an impact on subsequent antigen processing. Studies with MR (CD206) and scavanger receptors have shown that MR-internalized antigens are transported to distinct endosomes, which did not undergo lysosomal fusion. The MR targeted antigens where therefore efficiently cross-presented whereas scavenger receptor-mediated endocytosis led to antigen degradation. Strikingly, antigen interaction with different regions of the DEC-205 receptor leads to differences in cross-presentation efficiency. Targeting of the carbohydrate recognition domain is associated with poor antigen presentation on MHC-I, while antigens targeted to the neck domain of DEC-205 are efficiently cross-presented [43].

### 1.4.1 C-type lectin receptors

C-type lectin receptors (CLRs) are critical for the orchestration of downstream signaling molecules bridging the innate side of dendritic cells with the appropriate polarization of adaptive immunity (Tab. 1.1). CLRs are $Ca^{2+}$ dependent, soluble or transmembrane proteins with at least one carbohydrate binding domain. Two major groups of CLRs are distinguished - mannose and asialoglycoprotein - which both contain immunoreceptor tyrosine-based inhibitory motif (ITIM) and immunoreceptor tyrosine-based activation motif (ITAM) representatives. Typically ligand binding triggers NF-κ B driven gene expression and often works hand in hand with TLRs or other PRRs [9]. Since CLRs have evolved to combat different pathogenic immune subversion techniques, they play a role in shaping immune polarization.

Dectin-1 initiates $T_H1$ or $T_H17$ biased immune responses but is mainly expressed on cDC2s in mice, which are weak at cross-presenting antigens [16, 66]. Langerin targeting has been attributed to tolerogenic and immune-stimulating responses. This is due to the expression of Langerin (CD207) on Langerhans cells and cDC1s, which are responsible for determining the subsequent immune response. Langerhans cells mediate the induction of tolerance, while cDC1s are able to cross-present antigens and stimulate potent T cell responses in mice. Interestingly, human Langerhans cells closely resemble the cDC1 phenotype of mice rather the murine Langerhans cells. Targeting of Mannan receptor (CD206) has been shown to elicit antigen specific CD8 and CD4 responses in murine tumor models. The induction of CD8 mediated immunity

is thereby of high interest for human cancer therapies and already studied in clinical trials [66]. In order to evoke the desired T cell polarization upon binding to CD206, the chemical composition of the ligands is critical. It has been shown that reduced and oxidized Mannan can determine the polarization into $T_H1$ or $T_H2$ direction. In that, antigen conjugates with oxidized mannan showed early endosomal escape and $T_H1$ biased responses, whereas reduced mannan elicited mainly CD4 driven $T_H2$ immunity [67]. cDNA screening revealed SIGN-R1 -R2, -R3, -R5, -R7 and R8[29] as murine analogs to the human DC-SIGN, which have distinct carbohydrate binding motifs and vary in their function. SIGNR1 and SIGNR3 are the only ones known mediate endocytosis [68]. SIGNR3 has the closest ligand binding specificity to DC-SIGN and is known to participate in anti-fungal responses in the gut where it recognizes terminal fucose or high mannose residues [69]. SIGNR1 has generally lower binding affinities compared to SIGNR3 and is expressed on marginal zone macrophages [70]. Because of their endocytic function and endosomal release, SIGNR1 and R3 are attractive targets for novel therapeutics.

29: SIGNR6 is encoded by a pseudogene and thus hypothetically possible but not yet observed.

In the mouse, two distinct macrophage galactose-type lectins variants, MGL1 and MGL2 are present, whereas only one (CD310) is found in humans. They are expressed on macrophages, $CD1a^+$ dDCs and immature moDCs, and mediate endocytosis with subsequent CD4 / CD8 Tcell induction [66].

The innate recognition system acts as a sensor for the distinct carbohydrate signatures of pathogens. Mannose is associated with viruses, fungi and mycobacteria, fucose is often found on bacteria and helminths, while glucan residues are occurring on bacteria and fungi. Thus, downstream signalling pathways of CLRs vary between the different receptor types depending on the respective threat, but are also influenced by signaling cascades from TLRs. It has been shown that binding of highly mannosylated structures to DC-SIGN potentiates already present TLR3/4/5 dependent NF-κB activation. After co of DC-SIGN, RAF1 is activated and phosphorylates NF-κB at Ser276, which leads to prolonged transcription at the Il8 and Il10 promotor [9].

Additionally, CLRs are able to bind and take up non-carbohydrate bio-molecules. DEC205 is known to take up CpG-ODN and shuttle it to the endosomal TLR9 receptors [71], while soluble collectins are able to bind lipids [72].

### 1.4.2 Dendritic cell targeting with dextran

The ability of dendritic cells to function as a sentinel as well as an activator, shapes immune responses in their intensity and

manner. Therefore, extensive research has been directed towards efficient DC targeting in the last decade. While valuable mechanistic insights and potent DC inducers have been discovered, there is still a lot to be learned in this field - especially considering the sparse outcome in clinical trials[30] so far [73]. Carbohydrates have been regarded as attractive stimulative substances, because of their safety and bio-compatibility profile. Currently[31] 12 clinical trials involving carbohydrate adjuvants, as reported by Garcia-Vello et al, are enrolled [10]. Among these carbohydrates, dextran is reported to enter cells via the mannose receptor (CD206), DC-SIGN, L-SIGN, SIGN-R1, and SIGN-R3 and Langerin (CD207) through clathrin-mediated endocytosis. Receptor independent entry is also possible through nonspecific fluid-phase endocytosis but less common [12]. Takahara et al. tested dextran compatibility of murine C-type lectin receptors expressed in transfected non-macrophage cells [32] . Langerin and SIGN-R1 were able to take up dextrans ≥ 40 kDa (tested up to 2000 kDa) - (only expressed in mice (Human analogue: DC-SIGN)). SIGN-R3 seems to accept only larger dextran starting at 250 kDa, while DC-SIGN was not able to take up dextran. Inhibition of dextran binding was also tested by the group. Mannan reliably blocked dextran uptake in all receptors with higher efficiency at Langerin, followed by SIGNR1 and SIGNR3 [11]. Finally, dextran uptake via MGL[33] is reported in the literature, yet no size dependent efficiency data was determined [74]. There is a strong incentive to maximize active transport to the draining lymph nodes because passive transport is not targeted and the intranodal filamentous collagen bundles only allow for the passage of particles < 70 kDa with a hydrodynamic radius up to 5.5 nm [39]. Moreover, tolerability and safety of dextran is classified as "type 2"[34] by SCOGS[35] standards [75].[36]

Targeting dendritic cells with carbohydrates has been demonstrated by our group and others before [20, 23, 24, 76]. The glycoconjugates produced in our institute consistently demonstrated good safety profiles, reduced allergenicity and potent immunogenicity. Among the most popular carbohydrate-adjuvants are β-Glucans - eg. mannan, laminarin and zymosan - which are prominently found on the surface of pathogens, especially fungi [77, 78]. In contrast, dextran as an αGlucan[37] is mostly considered pharmacologically inert and is broadly used - from clinical produce to food. As discussed above, immunologists have studied the targeting potential of dextran and it has already been used as a platform for drug delivery, ranging from cancer, liver to colon targeting [81]. The literature describes dextran as a wildly used adjuvant - yet it is usually a chemically different version (eg. polycationic - diethylaminoethyl dextran [82]) or coupled to an adjuvant (eg. 3'3'-cGAMP [10]). Another dextran related vaccine approach is the design of an anti-dextran vaccine - explored for possible H.pylori immunizations[83] or by blocking

30: Mainly focused on *ex vivo* loaded dendritic cells

31: Status: October 2020

32: To exclude

33: Macrophage galactose-type lectin

34: "There is no evidence in the available information on [substance] that demonstrates a hazard to the public when it is used at levels that are now current and in the manner now practiced. However, it is not possible to determine, without additional data, whether a significant increase in consumption would constitute a dietary hazard."

35: Select Committee on GRAS Substances

36: Database was searched for "dextran". Currency was confirmed in Nov. 2020. Latest update date declared on the site was July. 2020.

37: ≈ 95 % α1↦6 linked, 5 % α1↦3 linked - might also have some 1↦2 / 1↦4 [79]. Since this branching can vary, the chemical composition was verified at the website of the Manufacturer (Sigma Aldrich) [80].

C-type lectin receptor entry of pathogens [12]. Taken together the literature shows great safety and flexibility of dextran and highlights uptake mechanisms, still no strong picture for $\alpha\,1\mapsto6^{high}$,$\alpha\,1\mapsto3^{low}$ dextran mediated immunity emerges.[38] In the current thesis, we aim to shed more light on this issue.

38: Our group coupled dextran to papain before - yet immunological assays were carried out with mannan [23].

### 1.4.3 Cutaneous drug delivery

Intramuscular (i.m) injection is the main strategies for vaccine administration. In contrast to the popularity of the method, relatively little was known about the exact immunological mechanisms. Nowadays, is is recognized that the intramuscular routes of immunization benefit from the slow clearance of antigen and the of non-professional antigen presentation by muscle cells. Expression of TLR2, TLR3, TLR4, TLR5, and TLR9 is found in most muscle cells - with myoblasts lacking TLR2 and TLR9 [14, 84]. Even though i.m injections work, the high popularity might be more attributed to convenience than high effectiveness. Thereby the sparse occurrence of professional immunocytes in muscle tissue is often criticized today [14]. A growing body of research explores the advantages of cutaneous antigen delivery. By now, several comparative studies have demonstrated a dose sparing effect by delivering Rabies, Influenza or Hepatitis B vaccines intradermally [15]. In a randomized trial with 100 healthy persons between age 18 and 40, intramuscular versus intradermal injection efficiency were compared. Thereby, the intradermal delivery yielded similar or better antibody levels (geometric mean fold increase), seroconversion, and seroprotection rates at an 80% lower treatment dose [13]. As stated above, alternative administration strategies to classical injection are also continuously explored. Taddio et al. even showed in a survey, that nearly a quarter of parents and approximately two thirds of the questioned children had fear of needles. As stated, this fear even prompted 7 % of parents and 8 % of children to refuse vaccination [85]. Alternative vaccination routes are nothing new - oral polio vaccine were delivered to millions of people in the 60s [86], the live attenuated nasal influenza vaccine FluMist® was approved by the FDA in 2003 [87] - certainly not sufficiently popular. In the following subsections an abstract of the current literature - concerning strategies for skin immunization - is presented.

#### 1.4.3.1 Dermal immunology

Dermal directed immunization can capitalize on an broad cellular landscape, comprising a diverse immunocyte depot.[39] . Several cell types in the viable epidermis are described in the literature. Langerhans cells, keratinocytes and melanocytes -are usually found in the

39: The distinct immunobiology of the skin was already recognized in 1983 by Streilein, who coined the term "*skin-associated lymphoid tissues'* (SALT) [88]. In 1986 Bos and Kapsenberg expanded the term with the inclusion of further immuno related cells (e.g. mast cells, tissue macrophages and granulocytes). They proposed the label *"skin immune system"* (SIS), which outlines a neat pool of immune reactive biomass in the dermal compartment [89]

upper skin layers, while in the deeper laying dermis, macrophages, dendritic - , natural killer -, innate lymphoid - and T - cells can be found.

The first steps of cutaneous immune response are generally mediated through keratinocytes, the most abundant cell type in the viable epidermis. They act as first line sensors and are capable of secreting a broad array of cytokines and chemokines [40] and also act as non-professional APCs [90]. Other epidermal key players are Langerhans cells[41] . They are hard to characterize and act as a hybrid between dendritic cell and macrophage. Their roles are diverse and range from the induction of tolerance to the mediation of preemptive and acute immune responses. They are skillful probers, constantly monitoring this delicate environment and migrate to the draining lymph node (DC-like behavior). On the other hand, they share a common lineage and express self-renewal genes under a macrophage specific transcription factor (Macrophage-like behavior). Their immune-stimulatory ability might be dependent on the way they acquire antigen - uptake through intact junctions enhances their initiation of humoral immunity, while tissue damage prompts them to stimulate cell-mediated immunity [91]. Generally, two subsets of dermal conventional DCs are found in human and mouse skin. They are categorized as cDC1 or cDC2 and distinguishable by XCR1 or SIRPα expression in mice and CD141 and CD1c/SIRPα in humans. This specialization is already determined in the bone marrow and is driven by the transcription factors IRF8 and IRF4 respectively. This early lineage determination of cDCs is probably expended by tissue specific transcription programs which allow for highly flexible occupation of anatomical niches. Lastly, skin resident moDCs are also important in dermal immunizations. They were also primarily used for *ex vivo* cancer therapies and are hard to distinguish from macrophages. Currently, PD-L2 and CD209a upregulation are used to differentiate moDCs from iNOS producing macrophages [66, 92].

Phagocytosis, complement activation and inflammation through TNF-α, IL-6, and IL-1β are fast acting, innate immune reactions, whereas antigen processing by professional APCs evoke powerful but slow adaptive immune responses[90]. The innate immune reactions are rather unspecific compared to the adaptive immune responses, but are immediately present, while building effective long lasting adaptive immune responses can take multiple weeks [93, 94]. For designing an effective immunization program, penetration depth, degree of tissue damage and physio-chemical properties of the therapeutic are major factors which shape the corresponding immune response. But for determining a viable, clinically applicable delivery system, economics, safety and ease-of-use have to be considered as equally important factors. Dendritic

40: L-1, TNF-α, IL-6, G/M-CSF, TGF-β , IL-1, CXCL-8 and IP-10

41: The hallmark characteristic was thought to be langerin (CD207). By now several other $CD207^+$ cell have been described in mice, but not in humans. Birbeck granules however are exclusively found in Langerhans cells and serve as distinct marker for identification.

cells are critical for determining the intensity and polarization of a T cell response. Whereby specific subsets of dendritic cells can decide the immunogenicity of administered antigens.

#### 1.4.3.2 Methods for epicutaneous and transdermal drug delivery

For proper stimulation, all skin directed immunization approaches need to bypass the stratum corneum in order to capitalize on the immunocompetence of the subjacent layers - stratum granulosum, stratum spinosum, stratum basale and the dermis [90]. It has been shown that skin vaccination is able to trigger cellular and humoral immunity and looks to be more efficient than intramuscular injections. Several techniques have been employed for targeting the SIS, which fundamentally differ by the means of barrier circumvention.

Non invasive, passive transport methods simply rely on diffusion of the active compound though the stratum corneum. This method is cheap and doesn't require skilled workers, but does suffer from diffusion related limitations like molecular weight or polarity. Mondoulet et al. reported an interesting approach to combat food related allergies by epicutaneous immunotherapy. In that, they applied allergenic proteins via a Viaskin® (DBV Technologies, Paris) patches on the intact skin of patients. In a pilot study skimmed milk power was well tolerated but failed to induce significant improvements in cumulative tolerated doses, due to high standard deviations. Subsequent phase I and II/b trials with peanut protein showed good tolerability and immunogenicity. Local adverse events were observed frequently in all trials, but most were mild and patient adherence was very high (> 95 %). Allergen specific IgG4 was increased in treatment groups while a reduction in IgE was observed in parallel. Preclinical animal studies with Viaskin patches, provided mechanistic insight, of the underlying mechanisms. Interestingly, epicutaneous immunization on intact skin induced a shift in T helper polarization from $T_H2$ towards $T_H1$. In contrast, immunizations on tape stripped skin were increasing type 2 T-Helper responses. This observation is consistent with findings in humans, where skin inflammation is recognized as an important risk factor for sensitization [95, 96].

Active immunization techniques comprise a large potpourri based on injections, micro-porations and creation of local transport regions [97]. A non-exhaustive selection of relevant methods is introduced in the following paragraph.

Intra-dermal injection with a syringe and a fine-gauge needle is usually performed with the mantoux method, developed in the

early 20th century. The needle is inserted roughly 3 mm in a flat angle (5 - 15 degrees). Proper execution results in a visible, temporary bleb. Comparisons to i.m. injections have demonstrated a dose sparing effect and good tolerability, but the technique is demanding to perform and requires trained personnel [13, 17].

Needle-free injection approaches like jet injection and powder injection have also been established. Jet injection has a relatively long history with reports dating back to the 1800s. It has already been employed in large scale vaccination programs conducted against measles, polio and smallpox. It uses a focused beam of fluid to penetrate the skin and create a liquid reservoir with active compound intradermally or intramuscularly. It can be adopted for high throughput immunizations ( $\leq 1000$ /hour), but contamination risks and high local side reactions limit the usage [98]. In contrast, ballistic injection launches solid particles into the dermis and epidermis, using a helium pulse. It was originally developed in 1987 for DNA based therapeutics and is therefore often called "gene gun". Until now, It has mainly been used to deliver gold particles and sugar particles. Gold particles generally have a high transfection efficiency, but coating is limited to the surface capacity of the particles, additionally particle cost is relatively high. Sugar particles are cheaper and easier to manufacture but suffer from lower density which handicaps efficient delivery [99].

Microneedle mediated delivery is a low-cost and effective way to circumvent the stratum corneum in a nearly painless manner. Five different types of needles have been utilized to transport active compound to the stratum granulosum, stratum spinosum and stratum basale. Solid needles are used to create micro-pores in the skin before the therapeutic formulation is applied, enables transport of molecules via diffusion. Coated needles deliver compounds which are layered onto the spikes before application. After insertion and subsequent retraction of the needles, the compound is deposited and dispersed relatively quickly. In contrast, dissolving micro needles have incorporated active ingredients in their matrix, which are released over time. The breakdown rate is determined by the material, therefore the antigen release can be adjusted to the respective application. Hollow needles are act as a tunnel, which allow for administration of liquid therapeutics comparable to classical injection or a slower release over time. Finally, hydrogel-forming polymeric micro needles are the latest developments among the five described techniques. Here, the inserted needles quickly absorb body fluids and enable rapid diffusion of drug formulations stored in a patch on top of the needle array [100].

Other interesting permeabilization approach is electroporation, which uses shortly pulsed high-voltage electric currents, for non-invasive transdermal drug delivery. Iontophoresis uses a similar,

electric based procedure, but with a constant flow of current at low-voltage. Both techniques are quite easy to perform but electroporation acts stronger on the barrier than the drug, and reaches higher transmission efficiency at the macro-molecular level [101]. Sonoporation is a related method which uses ultrasonic waves to enhance the degree of transport in a non-invasive manner. The treatment induces the spontaneous formation of micro-bubbles, resulting local cavities which enhance drug delivery transiently [102].

Ablation methods aim to disrupt the stratum corneum by creating micro-pores to allow for transport of bio-active material. Pore formation can be achieved with radio-, thermal- or laser - operated devices, while the drugs are generally delivered with patches. The radio-frequency waves stimulate vibrations and thus heat production, which causes water evaporation and thereby creates micropores. Closely related, the thermal based method ablates corneocytes by releasing a single thermal energy pulse for channel creation [103].

Combined immunization procedures - like pre-treatment with micro-needles before electroporation - are also of great interest and might create novel synergistic delivery procedures [104].

#### 1.4.3.3 Laser assisted microporation

Laser facilitated dermal drug delivery has gained traction over the past decades, offering several practical advantages to conventional therapy[42] while comprising an immune-stimulatory adjuvant effect. To this date, four types of medical lasers are put to work, ultra-short pulsed, non-pulsed ablative fractional and non-ablative fractional. Apart from the enhanced drug transport, laser light triggered adjuvant effects differ in their effect between the laser classes [106]. Non tissue-damaging lasers like ultra-short pulsed and non-pulsed lasers (Conterminal Lasers) date back to 1967 in Hungary (Non-pulse, helium-neon) and 1978 in Russia (Pulsed, copper laser). At that time tested for wound healing, conterminal lasers are now investigated for immunocyte stimulation. The wavelengths typically range between 510 - 1064 nm, with newer systems preferably using ≈ 1000 nm. This is due to the absorption characteristics of water, hemoglobin and melanin, which have high transmission around this wavelength [107]. A study from Morse et al. in 2017 showed better mobilization of migratory DC subsets by using Nd:$YVO_4$ Laser ($\lambda$= 1064 nm) in continuous rather than a pulsed setting[43] [108].

Fractional lasers can be differentiated in non-ablative and ablative systems. A non-ablative device (1410 nm) has been shown to in-

42: E.g. omission of bio-hazardous, sharp waste, painless application and long-term economics [105]

43: Intradermal injection of influenza vaccine in C57BL/6 mice - followed by laser illumination. No skin damage was observed, AG-loaded migratory DCs could be observed in the draining lymph nodes.

duce transient, local micro-inflammation through the creation of thermally, coagulated columns - by Wang et al. in 2015 [109]. The stimulatory effect was mediated by pDCs and TNF-α- tolerability and efficiency was tested in mice and swine. Ablative lasers generally fire at a wavelength with high water absorption - 2790, 2940 or 10600 nm. The rapid excitation of water then leads to local super-heating and consequent pore formation [110]. Efficient uptake of protein antigens by Langerhans cells was demonstrated with a $CO_2$ Laser by Chen et al. in 2012 [111]. The laser used in this work, is based on a 2940 nm diode-pumped, erbium:yttrium-aluminum-garnet (ER:YAG) emitter. It is fitted into a P.L.E.A.S.E.® (Precise Laser Epidermal System) machine developed by Pantec Biosolutions AG (Ruggell, Liechtenstein). Device settings allow for variation in pore depth and diameter ($\leq$ 300 μm) - largely depended on pulse energy[44] - with a re-epithelialization duration of ≈ 24 hours. The extent of thermal related damage was positively correlated with the duration of the pules [112]. The device has been shown to generate a pro-inflammatory environment, which can be driven in $T_H1$, $T_H2$ or $T_H17$ directions, depending on the physio-chemical properties of the therapeutic, laser parameters or upon co-administration of fitting biochemical adjuvants [110, 113]. Weiss et al., demonstrated the uptake of FITC-dextran (MW: 2000 kDa) by langerin negative $CD11b^+$ and $CD11b^-$ DCs in mice. They showed a $T_H2$ biased response[45] , which was re-programmable to $T_H1$ upon co-administration of CpG-ODN. Generally, deeper penetration into the dermis yielded a stronger $T_H1/T_H17$ response than epidermal targeting. Interestingly, pore healing took up to 2 days in this study - more in line with reports from Kali et al. in human subjects [113]. Interestingly, Machando et al. observed a strong local pro-inflammatory milieu with high levels of TNF-α IL-6, CCL2, CCL3, CCL7, CXCL-10, and TSLP. The authors concluded, that combination of laser facilitated delivery and allergen coupling to mannan resulted in attraction and subsequent activation of DCs. After antigen uptake and maturation, active transport to the draining lymph nodes was observed. In contrast intradermal injection was associated with passive transport to the skin draining lymph nodes [24]. Moreover, Scheiblhofer et al. determined the magnitude and polarization of immune responses upon varying parameters of fractional laser ablation and co-administration of different adjuvants. They tested CpG ODN1826, $CRM_{197}$, heat labile enterotoxin subunit B (LT-B), monophosphoryl lipid A and Alum adjuvants, co-administered with Hepatitis B surface antigen. After a dose testing experiment, the authors immunized BALB/c mice three times in 14 day intervals. Interestingly, they saw diminished antibody responses in the Alum group compared to non adjuvanted antigen. Among the other treatment groups, LT-B and monophosphoryl lipid A group showed the highest antibody

44: Energy is usually expressed as fluence, which is related to the illuminated area ($\frac{J}{cm^2}$)

45: 6 pulses delivered at 1.9 ($\frac{J}{cm^2}$) - 3 model antigens (OVA, bGal, Phl p 5)

titers, but not significantly different than in the non-adjuvanted Hepatitis B surface antigen group. They proceeded to compare immune responses of LT-B[46] after transcutaneous immunization to the current gold standard, the intramuscular injection with Alum. Both treatment methods generated similar antibody responses, while only transcutaneous immunization showed a dose response effect. Moreover, the authors found a difference in the humoral IgG response upon varying laser fluence[47] , corresponding to different pore depths. 34 days after the second immunization, the 6 pulse treatment group demonstrated the highest titer and lowest standard deviation. The IgG levels were significantly higher than in the 1 pulse group, but not higher than in the 2,4 and 8 pulse groups. Finally, the authors found no significant IgE or IgA responses at any of the tested laser parameter [105]. Recently, the P.L.E.A.S.E.® laser has also been successfully deployed in a phase I clinical trial with 102 volunteers - testing the potential for reviving anti pertussis-toxin memory. The treatment was well tolerated - binding IgG and neutralizing antibodies were not increased with the licensed therapeutic Boostrix® [114].

46: The strongest adjuvant after epicutaneous application in their study

47: 1, 2, 4, 6, or 8 pulses corresponding to a fluence of 2.1, 4.2, 8.4, 12.6, and 16.8 $\frac{J}{cm^2}$ at 500 Hz, 50 µs pulse length, 0.5 W with 5% pore density. Mice were treated with non-adjuvanted HBsAg

# Materials and Methods 2

In this chapter, chemicals used and experimental procedures conducted during the thesis are described. The Bulk of the work was performed at the University of Salzburg, Hellbrunnerstr. 34, Division of Allergy & Immunology, AG Weiss. Dynamic light scattering (DLS) analysis was performed by Mark Geppert in the Laboratory for Chemistry and Physics of Materials, Jakob-Haringer-Straße 2, Salzburg. Microscale thermophoresis (MST) was performed by Elfriede Dall in the Research Centre of Biosciences and Health, Billrothstraße 11, Salzburg. Amino acid analysis (AAA) was performed by Sabrina Wildner at the University of Salzburg, Hellbrunnerstr. 34, Division of Allergy & Immunology.

Statistical analysis was performed with mainly GraphPad Prism (v 7/ 8.2.1) or Rstudio (V 1.3.1) with `Tidyverse()` as the main workhorse [115, 116]. Multiple comparisons in GraphPad were carried out with Dunnett's and Tukey's multiple comparisons tests, depending on the multiple testing against a control. When used with matched pairs, both tests were always corrected with the Geisser-Greenhouse method. Preferably Dunnett's test was performed for multiple comparisons against the OVA group, so less irrelevant comparisons were computed and test power was increased. Multiple testing against all groups was generally not performed, unless stated otherwise. Significance levels were labeled with * when adj. p <0.05, ** when adj. p <0.01, adj. p <0.001 and **** when adj. p <0.0001. Photos were annotated with Inkscape (V 0.92). Figures 2.5 on page 32, 2.2 on page 25 and 2.1 on the following page were created using BioRender. Estimates and confidence intervals mentioned in the text were usually transformed according to $x = (-1) \cdot x$, so mean increase and decrease are easily recognized (Tables contain the untransformed values).



## 2.1 Glycoconjugate production

### 2.1.1 Triton method

For removal of protein associated endotoxin, 400 mg commercially available Ovalbumin (Sigma-Aldrich, Lot# 038K7012) was weighed in and diluted in 20 ml $dH_2O$ (2 stocks). 200 µL Triton-X114 (5%, Sigma-Aldrich, 8x washed) were added drop-wise to the solutions while vortexing. Next, the samples were incubated at 4 °C for 60


**Figure 2.1:** Workflow for the generation of nanoparticles. Firstly OVA and Dextran were chemically treated before conjugation. Size exclusion chromatography was used to extract coupled particles. Subsequent fractions were tested for binding strength via micro-scale thermophoresis, while size was measured by dynamic light scattering.

minutes while shaking, then centrifuged at $10^4$ rpm for 30 minutes at 37 °C. Supernatants were carefully collected and processed as described above for three additional times. For purification, the samples were treated as above for another two times, but without further addition of Triton-X114. Finally, the samples were passed through a 0.22 µm pre-warmed (37 °C ) syringe filter (Starlab). The concentration of the solutions was assessed via Bicinchoninic acid assay while the residual LPS[1] was quantified via Limulus amebocyte lysate assay. The samples were stored at +4 °C in the dark.

1: Lipopolysaccharide

### 2.1.2 Bicinchoninic acid assay

Protein quantification was performed via Pierce™ BCA Protein Assay Kit (Thermo Fischer). For this purpose, samples and standards were diluted in ef-$H_2O$ and 25 µL pipetted into a 96-well flat-bottom plate (Greiner). 50 parts of Reagent A were mixed with 5 parts of Reagent B, then 200 µL of this working reagent were added to each well. The plates were incubated for 30 minutes at 37 °C before measuring the absorbance at 562 nm (Tecan infinite M200PRO). Poly-aldehyde dextran was also measured with the BCA assay [117], due to the lack of a verified standard the data is

not presented here - only the observations are briefly described: Relative oxidation levels and storage lengths were compared. Readouts seems to correlate well with theoretical relative oxidation. Storage (up to 6 months) time didn't seem to alter the presence of aldehyde groups in a strong manner.

### 2.1.3 Limulus amebocyte lysate assay

50 µL of samples and LPS standards (Pyroquant, Cat No. 32500A) were diluted in endotoxin-free Water (Sigma-Aldrich) and loaded onto a clear 96-well V-bottom plate (Greiner). Then, 50 µL of LAL reagent (lysate 2018) were carefully added to each well and stirred 20x with pipette tips before performing a time kinetic measurement of the absorption at 405 nm at 37 °C for 30 minutes (9 time points, Tecan infinite M200PRO).

### 2.1.4 Oxidation of Dextrans

15-25 kDa, 100 kDa and 450-650 kDa Dextrans (from *Leuconostoc spp.*, Sigma-Aldrich) were oxidized to a degree of 40%, 20% and 20%[2] respectively, using sodium periodate ($NaIO_4$) (99%, Fisher Scientific U.K.). Briefly, 800 mg of Dextrans were dissolved in 20 mL endotoxin-free Water (Sigma-Aldrich) by vortexing and mild heating (< 75 °C). The Dextrans were oxidized by addition of 2350 µL (100 kDa, 450 kDa) and 4700 µL (15 kDa) of 90 $\frac{mg}{ml}$ $NaIO_4$ (in ef-$H_2O$). After incubating the samples for 75 minutes while shaking at 450rpm (dark, RT), they were dialysed (Cut-Off$_{MW}$: 3500 Da, Roth) against 2 L PBS overnight (stirring, 3x PBS change, final dilution 1:5x10$^5$). The generated solutions were measured via Anthrone assay and stored at 4 °C in the dark. Oxidation status was

2: Percentage of possible functional aldehyde groups, as modeled by a 1:1 ($\frac{mol}{mol}$) reaction stoichiometry.

### 2.1.5 Anthrone assay

50 µL of samples and standards were added to a 96-well flat-bottom plate (Greiner) and incubated at 4 °C for 15 minutes. Next, 200 µL of anthrone reagent (2 $\frac{mg}{ml}$ anthrone in ice cold $H_2SO_4$ (95%, Merck)) were added to the wells, while keeping the plate on ice. The plate was briefly shaken, then transferred to a boiling water bath (microwave, 5 minutes 600 W) for three minutes, for hydrolysation of carbohydrates to hydroxymethyl furfural. Afterwards, the plate was cooled to room temperature in a water bath for 5 min, before measuring the absorption of the samples and standards at 620 nm (Tecan infinite M200PRO)

### 2.1.6 One-pot conjugation

For conjugation, 1.5 mL of 2-picoline-borane [0.25M, solved in MetOH] (pic-$BH_3$, Merck) was added to 200 mg of oxidized Dextrans (27, 30, 32 $\frac{mg}{ml}$) while vortexing. Next, 1 mL of acetate buffer [pH 5.8] was added, before 588 µL of efOVA (17 $\frac{mg}{ml}$) was added and mixed. The final solution with a ratio of 20:1 (DEX:OVA $\frac{w}{w}$ ) was rotated for 72h in the dark at 23 °C. The solutions were then stored at 4 °C in the dark.

### 2.1.7 Size exclusion chromatography

Size exclusion chromatography (SEC) was performed on a Agilent (1050 Series) HPLC in order to identify optimal coupling conditions for the respective Dextrans efficiently. Purification of the desired conjugates was executed with a BioCAD 700E FPLC on a sephacryl S-400 HR column equipped with SF-2120 (Advantec) fraction collector.

#### 2.1.7.1 Coupling control via SE-HPLC

Coupling efficacy was assessed via HPLC[3] (Agilent) with a TSKgel G4000SWXL size exclusion column (Tosoh BiosCIENCE). The mobile phase $KH_2PO_4$ (filtered through 0.2 µm (Starlab) and degasssed) flow was set to 1 $\frac{ml}{min}$, with a runtime of 30 min, a injection volume of 70 µL and detection set to 280 nm. Differently oxidized Dextrans (0-40%) were coupled to OVA at a 20:1 and 10:1 ratio ($\frac{w}{w}$) under various buffer conditions. Highest coupling efficiency was determined by largest shifted peak area.[4] Accordingly, the following conditions were chosen for production of glycoconjugates: Buffer - Acetate pH 5.8, Ratio (Dex:OVA) - 20:2, Oxidation - 15 kDa Dex = 40%, 100 kDa & 450 kDa = 20%, Oxidizing agent: 15% ($\frac{v}{v}$) pic-$BH_3$ [0.25M] .

3: high performance liquid chromatography

4: Exemplary chromatograms included in the Appendix Fig. A.3 on page 81

#### 2.1.7.2 Purification via SE-FPLC

To purify the glycoconjugates, FPLC[5] was performed on a BioCAD 700E (Perspective Biosystems), equipped with a sephacryl 200 SE[6] column. 5 mL of the conjugates in DPBS were loaded into the loop and eluted with degassed and sterile filtered (Starlab, 0.2 µm) PBS at a flow rate of 1 $\frac{mL}{min}$. 2 mL fractions were collected and analyzed with Anthrone assay and BCA assay. Two fractions of each conjugate were pooled (Tab. 2.1). The fraction pools were then centrifuged in a Vivacon® spin column (50 kDa MWCO) (Satorius) until the respective volumes were reduced to ≈ 1 mL.

| Conjugate | Fractions |
|---|---|
| 15F1 | F38-F46 |
| 15F2 | F66-F74 |
| 100F1 | F37-F46 |
| 100F2 | F60-F72 |
| 450F1 | F38-F46 |
| 450F2 | F55-F72 |

**Table 2.1:** Summary of the pooled fractions generated by SE-FPLC

5: fast protein chromatography

6: size exclusion

### 2.1.8 SDS-PAGE

10% acrylamide based gels were used to confirm coupling of pooled OVADex Fractions. Therefore, separating gels and stacking gels were prepared according to Tab. 2.2. Samples were diluted in PBS and 4x Loading Dye (Tab. 2.3) and denatured at 95 °C for 5 minutes. The solutions were centrifuged at 14000 rpm for 5 minutes at room temperature, then 4.25 µg of each sample (17 µl) was loaded onto the gels, as well as 5 µL of prestained protein ladder (Thermo Scientific). Gels were run at 75 V (BioRad), then at 150 V for up to an hour. Staining was performed as described in 2.1.8.1 and 2.1.8.2.

**Separation**:

| **Reagent** | **Proportion** | **Manufacturer** |
|---|---|---|
| Acrylamide | 31.6 [%] | |
| Run Buffer | 28.4 [%] | |
| $dH_2O$ | 39.3 [%] | |
| APS | 0.6 [%] | |
| TEMED | 0.2 [%] | Sigma-Aldrich |

**Stacking**:

| **Reagent** | **Proportion** | **Manufacturer** |
|---|---|---|
| Acrylamide | 12.9 [%] | |
| Stack Buffer | 49.6[%] | |
| $dH_2O$ | 36.7 [%] | |
| APS | 0.6 [%] | |
| TEMED | 0.2 [%] | Sigma-Aldrich |

**Table 2.2:** Recipe for polyacrylamide stacking (bottom) and separation (top) gels. Run and Stack Buffer were prepared in the Lab and are Tris-based with pH 8.8 and 6.8 respectively. TEMED was always added last. *Abb:* APS: Ammonium persulfate, TEMED: Tetramethylethylenediamine

#### 2.1.8.1 Coomassie stain

After separation, gels were transferred to plastic boxes, washed three times with $dH_2O$ and incubated in colloidal coomassie blue staining solution (Tab.2.3). Gels were incubated at least 12, but up to 48 hours while shaking. Gels were washed three times with $dH_2O$, trans-illuminated and photographed (12MP (1/2.55") sensor, aperture f/1.5-2.4, automatic mode, SM-G970)

| Ingredient | Content |
|---|---|
| **Coomassie** | |
| CBB G-250 | 0.02% |
| $Al_2(SO_4)_3$ | 5% |
| $H_3PO_4$ | 2% |
| EtOH (96%) | 10% |
| **Loading dye:** | |
| DTT | 0.2M |
| SDS | 20% |
| Glycerol | 20 % |
| TRIS | 0.12 M |
| Bromphenol blue | "spatula-tip" |

**Table 2.3:** Recepie for coomaasie staining solution on top - loading dye on the bottom. *Abb:* CBB G-250: cooassie brilliant blue G250, TRIS: tris(hydroxymethyl)aminomethan, SDS: sodium dodecyl sulfate, DTT: Dithiothreitol

#### 2.1.8.2 Periodic acid-Schiff´s stain

Glycostaining was performed, using a microwave assisted protocol by Moravec and Mares [118]. Gels were transferred to plastic boxes, then the samples were fixed in 50 ml of 50% $CH_3OH$, by microwaving for one minute then for 45 seconds (600 W)[7] . Oxidation was performed in 25 ml of 1% $HIO_4$ while microwaving for 45 seconds. Gels were washed three times with 50 mL $dH_2O$ while heating for one minute. Staining was performed with 25 ml of Fuchsin Stain (Sigma) while heating for 30 seconds. Washing was performed first in 0.1 % $Na_2S_2O_5$ (50 mL, microwave 1 minute), then in 50 mL of 0.5 % $Na_2S_2O_5$ at room temperature. Gels were then transilluminated and photographed (12MP (1/2.55") sensor, aperture f/1.5-2.4, automatic mode, SM-G970)

7: All residual microwaving steps were performed at 600 W

### 2.1.9 Dynamic light scattering

Dynamic light scattering (DLS) analysis was performed by Mark Geppert in the Laboratory for Chemistry and Physics of Materials using a Zetasizer Nano ZS with a DTS1070 capillary cell (Malvern Instruments). Samples were diluted in PBS and all measured three times.

### 2.1.10 Microscale thermophoresis

To test the interaction of soluble ConA with DexOVA conjugates microscale thermophoresis (MST) experiments were performed. CF488A-labeled ConA (Thermo Fischer). To determine the binding affinity of different DexOVA conjugates, 1:2 dilution series were prepared. The highest concentrations used in the assay were 75 µM (DexOVA-15), 18.1 µM (DexOVA-100), and 3.5 µM (DexOVA-450). The 1:2 dilutions series were prepared in MST buffer (20 mM Hepes pH 7.5, 150 mM NaCl, 5 mM CaCl2, 5 mM MgCl2, 0.005% Tween-20). Labeled ConA was diluted to a final concentration of 400 nM in MST-buffer. 10 µl of the respective ligand solution were mixed with 10 µl labeled ConA and incubated for 15 min at 20 °C in the dark. To remove possible aggregates, the complexes were centrifuged at 13.000 g and 4 °C for 15 min. Immediately after centrifugation, the reactions were transferred into standard coated capillaries and MST traces were measured at 25 °C, 30% LED and medium MST power in an NT.115 Blue instrument. Control reactions using Dex15 (756 µM), Dex100 (125 µM), Dex450 (25.5 µM) and OVA (11.5 µM) as a ligand were similarly set up. Ligand binding was investigated by analyzing changes in MST traces. Data were recorded with the MO.Control 1.5.1 (NanoTemper) software and further analyzed using MO-Affinity Analysis 2.2.6 (NanoTemper). MST traces were processed using an MST on-time of 15 sec (DexOVA-450 and Dex450 treated samples) or 10 sec (all other samples) and fitted using $K_D$ (assuming 1:1 binding) fit models. Apparent $K_D$ values were determined from at least three independent binding experiments. To confirm that the shift in MST signal was due to complex formation rather than unspecific aggregation, samples were incubated with 10% SDS and 10 mM DTT and heated to 95 °C for 5min before measuring MST traces.

### 2.1.11 Amino acid analysis

Amino acid analysis (AAA) was performed by Sabrina Wildner as described before [119].

## 2.2 Cell culture

*In vitro* testing was focused on the dendritic cell based activation of naive T cells, as shown in Figure 2.2. Activation of dendritic cells alone was performed in parallel, but with an incubation time of 16 hours. The whole procedure is described in 2.2.1 to 2.2.7. The conjugates were additionally tested for allergenicity using a basophil cell line, as described in 2.2.8 on page 31.


.

**Figure 2.2:** Schematic representation of dendritic cell and naive T cell co-culture, as described in 2.2.5 on page 27. Created with BioRender

### 2.2.1 Murine bone marrow isolation

C57BL/6 mice were sacrificed via cervical dislocation. Under sterile conditions, femur and tibia bones were isolated, extricated from residual flesh and placed in a 10 cm sterile dish (Greiner) with DPBS (Sigma-Aldrich). Next, the bones were sterilized in 70% EtOH, washed with DPBS and placed in fresh DPBS. Finally, the ends of the bones were cut open and the bone marrow was washed out with cold DPBS, using a 27G needle. The solution was passed multiple times through a 22G needle before being filtered through a 70 µm cell strainer (Starlab). The cell mix was centrifuged for 5 minutes at 1200 rpm, 20 °C. Supernatants were discarded by suctioning, then the pellet was resuspended in 5 ml BMDC Medium (Tab. 2.4) and counted manually in a Neubauer chamber or by electronic current exclusion (CASY - OMNI Life Science).

| Reagent | Content | Manufacturer |
|---|---|---|
| RPMI-1640 | | Sigma-Aldrich |
| $\beta$-MeOH | 50 µM | Sigma-Aldrich |
| Pen-Strep | 1x | Sigma-Aldrich |
| L-Glutamine | 0.3 $\frac{mg}{ml}$ | Sigma-Aldrich |
| FBS | 10% | |
| Optional: | | |
| GM-CSF | 200 $\frac{ng}{ml}$ | ImmunoTools |

**Table 2.4:** Recipe for bone marrow derived dendritic cells medium. For the maturation of GM-CSF stimulated dendritic cells, the stated reagent, listed under 'optional' is supplemented. FBS was heat inactivated at 56 °C for 30 minutes prior to use. *Abb:* Pen-Strep: Penicillin-Streptomycin, FBS: Fetal bovine serum, $\beta$-MeOH: $\beta$-Mercaptoethanol, RPMI: Roswell Park Memorial Institute

### 2.2.2 FLT3-Ligand stimulated DCs

Cell suspensions were prepared as described in 2.2.1. The solutions were diluted to 2.5x$10^6$ $\frac{cells}{ml}$ and 3 mL dispensed into non-tissue-treated 6-well plates (Greiner). The wells were spiked with FLT3-

L[8] (AcroBiosystems) to a final concentration of 200 $\frac{ng}{ml}$, gently resuspended and incubated at 37 °C 5% $CO_2$ and 95 % $\phi$. After five days, BMDC Medium (Tab. 2.4) equal to 50 % of starting volume was added. After nine days of maturation, cells were pooled and centrifuged at 1200 rpm for 7 minutes at room temperature. Supernatants were removed via a vacuum pump and pellets resuspended in 1 mL BMDC or T cell medium (Tab. 2.4/2.7). Afterwards, cells were counted manually in a Neubauer chamber or via electronic current exclusion (CASY - OMNI Life Science), appropriately diluted and seeded (2.2.4, 2.2.5 on the following page).

8: human fms-like tyrosine kinase 3 - Ligand

### 2.2.3 GM-CSF stimulated DCs

Cell suspensions were prepared as described in 2.2.1 on the previous page. The solutions were diluted to 2x$10^5$ $\frac{cells}{ml}$ in GM-CSF spiked BMDC medium (Tab. 2.4/optional), 10 mL dispensed into 10 cm, non-tissue treated plates (Greiner) and incubated at 37 °C 5% $CO_2$ and 95 % $\phi$. After three days GM-CSF spiked BMDC medium equal to 100 % of the starting volume was added. After four or five days 50 % of total volume was carefully removed, centrifuged at 1200 rpm for 5 minutes at 4 °C resuspended in fresh GM-CSF medium and evenly distributed among the dishes. After seven days of maturation, cells were pooled, centrifuged at 1200 rpm for 7 minutes at room temperature and resuspended in 5 ml BMDC or T cell medium (Tab. 2.4/ 2.7). Afterwards, cells were counted manually in a Neubauer chamber or via electronic current exclusion (CASY - OMNI Life Science), appropriately diluted and seeded (2.2.4, 2.2.5 on the next page).

### 2.2.4 Dendritic cell activation

Harvested GM-CSF/FLT-3 BMDCs, as previously described in 2.2.2 and 2.2.3, were diluted to 8x$10^5$ $\frac{cells}{ml}$ or 16x$10^5$ $\frac{cells}{ml}$, so 1x$10^5$ $\frac{cells}{well}$ or 2x$10^5$ $\frac{cells}{well}$ could be seeded out in 125 µL, respectively. Treatments were diluted in T cell medium (Tab. 2.7) based on OVA equivalent concentrations and ranged typically from 20 - 0.08 $\frac{\mu g}{mL}$ (specified in Chapter 3). 25 µL of treatments were added to the DCs before incubating at 37 °C 5% $CO_2$ and 95 % $\phi$ for 16 hours. For analysis, cells were centrifuged at 1500 rpm for 5 minutes at 4 °C. 50 µL of supernatants were carefully collected and residual medium was discarded by pipetting. The pellets were resuspended in 20 µL anti-CD16/CD32 supernatants and incubated for 5 minutes at 4 °C. Next, 20 µL of staining mix (Tab. 2.5) was added to the wells and incubated 30 minutes at 4 °C in the dark. 95 µL cold PBS (4 °C) was added to the wells before centrifuging at 1400 rpm

| Marker | Fluorophore | Manufacturer |
|---|---|---|
| CD11c | eFluor450 | eBioscience |
| L/D | eFluor506 | eBioscience |
| CD11b | perCP-Cy5.5 | eBioscience |
| CD40 | APC | Biolegend |
| CD80 | FITC | Immunotools |
| CD86 | PE | Biolegend |
| MHC-II | APC-eFluor780 | eBioscience |

**Table 2.5:** Staining mix, used to asses FLT-3 stimulated dendritic cell activation. ef450 was used at a 1:100, ef506 at 1:800, perCP-Cy5.5 at 1:200, APC at 1:100, FITC at 1:100, PE at 1:200 and MCH-II at 1:200 dilution respectively. *Abb:* APC: allophycocyanin, BV: brilliant violet, PE: phycoerythrin, FITC: Fluorescein isothiocyanate

| Reagent | Content | Manufacturer |
|---|---|---|
| PBS | | |
| BSA | 1% | Serva |
| EDTA | 2 mM | Sigma-Aldrich |

**Table 2.6**

for 5 minutes at 4 °C. Wells were washed two times with 150 µL cold FACS Buffer (Tab. 2.6) under the same centrifugation settings. Finally the cells were resuspended in 100 µL cold FACS Buffer and analyzed as described in 2.2.7 on the next page.

### 2.2.5 Naive CD4$^+$ T cell activation

C57BL/6 mice were sacrificed via cervical dislocation. Under sterile conditions, brachial, inguinal, mesenteric and axillary lymph nodes, as well as spleens were removed. The tissues were placed into 70 µm cell strainer within a 35 mm petridish containing 1 ml DPBS. The organs were mashed with the back of a syringe plunger, transferred to a 15 mL tube (Greiner) and briefly centrifuged with the strainer. The suspension was resuspended in 7 mL ACK buffer and incubated for 5 minutes at room temperature. The tubes were filled up with DPBS and centrifuge at 1200rpm for 5 minutes at 24 °C. Supernatants were discarded by suction and pellets were solved in 1 mL DPBS. The solutions were resuspended with 9 mL pre-warmed DPBS (37 °C) containing 1 µM CFSE.[9] Cell solutions were incubated at 37 °C for 10 minutes, while swirling regularly. Upon addition of 1 mL FBS, the solution was centrifuged at 1500 rpm for 4 minutes at 4 °C. The pellet was washed once with 500 µL T cell medium (Tab. 2.7) at the same centrifugation settings, then solved in 500 µL T cell medium. Naive CD4$^+$ T cells (CD62L$^+$) were either purified via a cell sorter (BD FACS Aria™ III) or by magnetic bead separation (MojoSort™)[10] (see. 2.2.6). In the meantime, Harvested GM-CSF/FLT-3 BMDCs (see. 2.2.2/2.2.3), were diluted to 2x10$^5$ $\frac{\text{cells}}{mL}$ with T cell medium or BMDC medium (Tab. 2.7,2.4), so 5x10$^3$ $\frac{cells}{well}$ could be seeded out in 25 µL. Treatments were diluted in T cell medium (Tab. 2.7) based on OVA equivalent concentrations, which typically ranged from 20 - 0.08 $\frac{\mu g}{mL}$ (specified in Chapter 3) and added to the settled DCs. Finally, purified naive T cells were diluted to 3x10$^5$ $\frac{\text{cells}}{mL}$ in T cell medium (Tab. 2.7), so 1.5x10$^3$ $\frac{\text{cells}}{\text{well}}$ could be added, in 50 µL portions (Final mixture: 25 µL DCs, 25 µL treatments, 50 µL naive T cells). The cultures were incubated at 37 °C 5% $CO_2$ and 95 % $\phi$ for 3-5 days, while bulk proliferation was monitored by light microscopy every day. For analysis, cells were centrifuged at 1500 rpm for 5 minutes at 25 °C. 50 µL of supernatants were carefully collected and residual medium was discarded by pipetting. The pellets were resuspended in 100 µL DPBS and centrifuged at 1500 rpm for 5 minutes at 25 °C. Supernatants were discarded by pipetting and the pellets were resuspended in 30 µL of staining mix (Tab. 2.9) then the plates were incubated for 30 minutes at 4 °C in the dark. 100 µL cold FACS Buffer (4 °C, Tab. 2.6) was added to the wells before centrifuging at 1500 rpm for 4 minutes at 4 °C. Cells were washed two times with 150 µL cold FACS Buffer under the same centrifugation settings.

| Reagent | Content | Manufacturer |
|---|---|---|
| RPMI-1640 | | Sigma-Aldrich |
| HEPES | 25 mM | Sigma-Aldrich |
| Pen-Strep | 1x | Sigma-Aldrich |
| L-Glutamine | 0.3 $\frac{mg}{ml}$ | Sigma-Aldrich |
| FBS | 10% | |

**Table 2.7:** Recipe for T cell medium. FBS was heat inactivated at 56 °C for 30 minutes prior to use. *Abb:* Pen-Strep: Penicillin-Streptomycin, FBS: Fetal bovine serum, HEPES : hydroxyethyl piperazineethanesulfonic acid, RPMI: Roswell Park Memorial Institute

| Reagent | Content | Manufacturer |
|---|---|---|
| $dH_2O$ | | |
| $NH_4Cl$ | 0.15 M | |
| $KHCO_3$ | 10 mM | Fluka AG |
| EDTA | 0.1 mM | Sigma-Aldrich |

**Table 2.8:** Recipe for ACK based lysis Buffer. $NH_4Cl$ and $KHCO_3$ were filled up to 1 L with $dH_2O$ (pH adjusted to 7.2). Next, EDTA was added, the final solution was autoclaved and sterile filtered (Starlab, 0.2 µm). *Abb:* ACK: Ammonium-Chloride-Potassium, $NH_4Cl$: ammonium chloride, $KHCO_3$: potassium bicarbonate, EDTA: ethylendiaminetetraacetic acid

| Marker | Fluorophore | Manufacturer |
|---|---|---|
| CD4 | APC | BioLegend |
| L/D | eFluor780 | Invitrogen |
| CD44 | BV650 | BioLegend |
| CD62L | eFluor450 | eBioscience |
| V$\beta$5.1/5.2 | PE | BioLegend |

**Table 2.9:** Staining mix, used to asses naive T cell activation.´APC was used at 1:400, ef780 at 1:3000, BV650 at 1:100, ef450 at 1:100, PE at 1:200 dilution respectivley. *Abb:* APC: allophycocyanin, BV: brilliant violet, PE: phycoerythrin

9: carboxyfluorescein diacetate succinimidyl ester

10: CFSE staining was alternatively performed after sorting with the MojoSort Kit.

Finally the cells were resuspended in 80 µL cold FACS Buffer and analyzed as described in 2.2.7.

### 2.2.6 Cell sorting

Cell sorting was either performed by positive selection using a FACS Aria™ III (BD BioSciences) or by negative selection with the MojoSort™ naive $CD4^+$ Kit (Biolegend)

#### 2.2.6.1 Positive selection

For positive selection, the cell suspensions were stained (Tab. 2.10 and the solutions were incubated 30 minutes at 4 °C in the dark. 10 mL DPBS was added, tubes centrifuged at 1200rpm for 5 minutes at 24 °C and the pellets were solved in 300 µL T cell medium. Naive T cells were sorted into tubes containing either T cell medium or FBS. Cells were counted manually in a Neubauer chamber or via electronic current exclusion (CASY - OMNI Life Science), their concentration calculated taking the purity factor into account, appropriately diluted and seeded as described in 2.2.5 on the previous page.

| Marker | Fluorophore | Manufacturer |
|---|---|---|
| CD4 | ef450 | eBioscience |
| CD62L | APC-eF780 | eBioscience |

**Table 2.10:** Staining mix for naive cell sorting. ef450 was used at a 1:250 dilution, APC-ef780 at a 1:166 dilution. *Abb:* APC: allophycocyanin

#### 2.2.6.2 Negative selection

Cell suspensions were prepared (see. 2.2.5) and purified according to the manufacturers protocol with slight modifications. Briefly, 600 µL of cell suspensions ($6x10^7$ cells) were used, FACS buffer (Tab. 2.6) was used instead of MojoSort™ Buffer, unlabeled cells were magnetized two times instead of the labeled fraction. Purity was monitored on a Cytoflex S flow cytometer (Beckman-Coulter) with antibodies shown in Table 2.11. Cells were counted manually in a Neubauer chamber or via electronic current exclusion (CASY - OMNI Life Science), their concentration calculated taking the purity factor into account, appropriately diluted and seeded as described in 2.2.5 on the preceding page.

| Marker | Fluorophore | Manufacturer |
|---|---|---|
| CD4 | APC | BioLegend |
| CD62L | eFluor450 | eBioscience |

**Table 2.11:** Staining mix, used to for quality control of negative selection. APC was used at a 1:400 dilution, ef450 at a 1:100 dilution. *Abb:* APC: allophycocyanin

### 2.2.7 Flow cytometry

Prepared samples as described in 2.2.4 on page 26 and 2.2.5 on the preceding page were analyzed on a Cytoflex S flow cytometer (Beckman-Coulter) in plate mode. Volume to record was set 10 µL lower than the dispensed amount. Figures 2.3 and 2.4 show the exemplary gating strategies for the activation and co-culture experiments respectively. For co-culture analysis, populations were gated as shown, subsequent cell counts were used for analysis. For

dendritic cell activation, the final gate (singlets) was exported and the MFI[11] for the markers of interest as well as cell counts were analyzed.

11: median fluorescence intensity

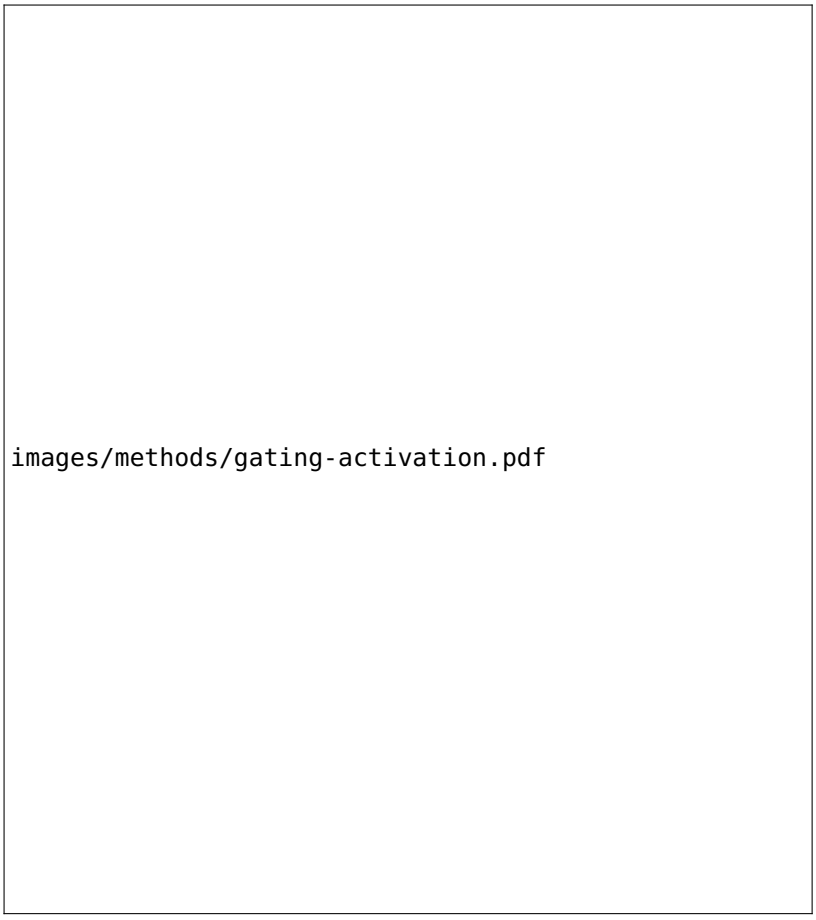


**Figure 2.3:** Exemplary gating strategy for dendritic cell activation (2.2.4) as gated on CytExpert 2.0.4.28. The presented sample is the positive control (LPS) of the experiment using FLT3L BMDCs. Starting from top left, live MHC-II$^+$ cells were gated, then artifacts were excluded based on FSC and SSC (top-right). CD11b$^+$ and CD11c$^+$ cells were selected (bottom-right), before doublet exclusion on the bottom-left. MFI values from those populations were exported for analysis. *Abb:* FSC: forward scatter, SSC: side scatter, MFI: median fluorescence intensity, MHC: major histocompatibility complex


**Figure 2.4:** Exemplary gating strategy for OT-II co-cultures (2.2.5) as gated on CytExpert 2.0.4.28. The presented sample is the positive control ($OVA_{323-339}$) of the experiment using GM-CSF BMDCs. Starting from top left, live $CD4^+$ cells were gated, then artifacts were excluded based on FSC and SSC (top-middle) Singlets were selected in the bottom-middle plot, then proliferation (bottom-left) and activation (bottom-right) was gated. The activation plots was split into four quartiles were the top-left represents the naive T cells, top-right central memory T cells and the bottom-right the effector cells. *Abb:* FSC: forward scatter, SSC: side scatter, MFI: median fluorescence intensity

### 2.2.8 RBL assay

Frozen RBL[12] (p18, 2018) were thawed, washed two times with 10 mL DPBS (1200 rpm, 5 minutes, 22 °C ), finally solved in 5mL RBL medium (37 °C Tab. 2.12 and incubated in a cell culture flask (Greiner) at 37 °C 5 % $CO_2$, 95 % $\phi$. RBL cells were passaged every 2-3 days based on visual inspection. Thereby old medium was decanted, cells were washed three times with DPBS and detached with Trypsin-EDTA (Sigma-Aldrich) at 37 °C for 5 minutes. The suspension was washed with RBL medium, transferred to a tube with RBL medium and centrifuged at 1200 rpm for 5 minutes at 25 °C. The pellet was solved in 5 mL RBL medium and transferred to a 200 mL cell culture flask (Greiner) containing 15 mL RBL medium. Depending on confluence, cells were split additionally 1:10. One day before measurement, cells were washed as described above and counted using electronic current exclusion (CASY - OMNI Life Science). Cells were diluted to 7x$10^5$ $\frac{\text{cells}}{mL}$, seeded out in 100 µL for 7x$10^4$ $\frac{\text{cells}}{well}$ in a cell-culture plastic F-bottom plate (Greiner) and incubated at 37 °C 5 % $CO_2$, 95 % $\phi$ overnight. OVA specific antiserum was diluted 1:10 or 1:50 in RBL medium, then 50 µl of cell media was replaced by 50 µl of the diluted antisera and plates were incubated at 37 °C 5 % $CO_2$, 95 % $\phi$ for two hours. Cells were washed three times with Tyrode´s Buffer (Tyrode´s salts + $NaHCO_3$ pH 7.2), then treatments were added (pre-diluted in Tyrodes Buffer) and incubated at 37 °C 5 % $CO_2$, 95 % $\phi$ for one hour.[13] Plates were centrifuged at 1200 rpm for 5 minutes at 25 °C then 50 or 75 µL of supernatant was carefully transferred to a fresh plate, diluted 1:2 with assay solution (4-MUG[14] (Merck) in citrate buffer pH 4.5) and incubated at 37 °C 5 % $CO_2$, 95 % $\phi$ for one hour. Reaction was stopped by adding equal volume of glycine buffer. Fluorescence ($A_{Ex}$: 360 nm, $A_{Em}$: 465 nm) was measured using a plate reader (Tecan M200PRO, optimal gain for each plate).

| Reagent | Content | Manufacturer |
|---|---|---|
| MEM | 66.7% ($\frac{v}{v}$) | Sigma-Aldrich |
| RPMI-1640 | 19% ($\frac{v}{v}$) | Sigma-Aldrich |
| Na-Pyr | 2 mM | Sigma-Aldrich |
| Pen-Strep | 1x | Sigma-Aldrich |
| L-Glutamine | 4 mM | Sigma-Aldrich |
| FBS | 9.5% | Sigma-Aldrich |

**Table 2.12:** Recipe for RBL medium FBS was heat inactivated at 56 °C for 30 minutes prior to use. *Abb:* MEM: Minimal essential media, Pen-Strep: Penicilin-Streptomycin, FBS: Fetal bovine serum, $\beta$-MeOH: $\beta$-Mercaptoethanol, RPMI: Roswell Park Memorial Institute

12: Rat basophilic leukemia cells

13: Triton-X100 served as a positive control and was added to the wells after 45 minutes of incubation. Cells were checked under the microscope for lysis.

14: 4-Methylumbelliferyl-β-D-glucosaminide

## 2.3 In vivo immunization

C57BL/6 mice were housed in the animal facility of the University of Salzburg according to the local animal care guidelines. All animal experiments were approved by the austrian federal ministry for eduucation, science and research, permit No. BMBWF-66.012/0014-V/3B/2019.

### 2.3.1 Immunization procedure


**Figure 2.5:** Graphical representation of the immunization procedure as described in 2.3.1. The timeline summarizes the whole method and marks days of interest. Laser head graphic was kindly provided by Evgeniia Korotchenko.

Five groups of five C57BL/6 (female, 7-8 weeks old) mice each, [15] were immunized for a total of three times at 14 day intervals (Tab. 2.13). Prior to each immunization, the mice were shaved[16] under anesthesia with isoflurane (2.5% $\frac{v}{v}$), then a depilatory cream (Veet) was applied for 30 seconds. Next, the cream was washed off thoroughly with a wet sponge and the mice were dried with paper towels. Upon laserporation, the mice were anesthetized via an injection of 90 µL of a Ketamine/Xylazine mix (1.2 $\frac{\text{mg}}{\text{mouse}}$/ 0.12$\frac{\text{mg}}{\text{mouse}}$), then an eye cream (Oleovit) was applied. The mice were lasered using a P.L.E.A.S.E device (Pantec Biosolutions, Tab. 2.14), next 25 µl of treatments were spread evenly on the microporated areas and rubbed in with the pipette tips.[17] The therapeutics were allowed to soak in, while the mice were placed on a heating mat (37 °C). After the spots were completely dry, pre-cut patches (OpSite Flexifix) were fixed over the area. One day after the immunization, patches were removed with tweezers. After three immunizations, the mice were narcotized by intraperitoneal terminal anesthesia via injection of 150 µl Ketamine/Xylazine/Acepromazine (30 $\frac{\text{mg}}{\text{mouse}}$/ 1$\frac{\text{mg}}{\text{mouse}}$/ 1 $\frac{\text{mg}}{\text{mouse}}$) formulation. After absence of reflexes, up to 1 ml of blood was collected from the retrobulbar sinus. Afterwards the mice were euthanized by cervial dislocation, to ensure an unequivocal exitus. Spleens and lymph nodes were harvested as described in 2.2.5 on page 27. Cell counts were assessed via CEDEX XS Cell Analyzer and cells were appropriately diluted for the respective down-stream analysis (2.3.3 on the following page, 2.3.4 on page 34, 2.3.5 on page 35). During organ preparation, blood samples were allowed to coagulate at room temperature for at least one hour. Samples were centrifuged for 30 minutes at $10^4$ rpm, then the sera were collected in PCR tubes, sealed and stored in a humidified box at 4 °C in the dark until analysis with IgG ELISA.

| Group | Treatment | Adjuvant |
|---|---|---|
| 1 | OVA | CpG |
| 2 | 15F2 | CpG |
| 3 | 100F2 | CpG |
| 4 | 450F2 | CpG |
| 5 | PBS | CpG |
| Doses: | 40 µg | 10µg |

**Table 2.13:** All treatments contained 40 µg of OVA equivalent (except for the control group with PBS), adjuvanted with 10 µg of CpG (ODN 1826, Invivogen). The treatments were brought to equal volumes with DPBS and delivered as 25 µl doses. Groups consisted of 5 mice, except for group 1 (OVA) where 1 mouse died (n = 4).

| Parameter | Setting |
|---|---|
| Fluence | 8.3 $\frac{J}{cm^2}$ |
| Pulse duration | 50 µs |
| Pore density | 9% |
| Frequency | 500 Hz |
| Number of pulses | 3 /per pore |
| Array size | 12 mm |

**Table 2.14:** Parameters of setting: "medium" from the P.L.E.A.S.E Device.

15: One mouse from the OVA group died during the immunization procedure. The mouse died after waking up from anesthesia, the suspected cause of death is shock.

16: Electric shaver (Oster) with a 1/20 mm, size 50 shaving head (Oster)

17: Sites of laserporation were alternated between immunizations: First immunization was performed dorsal, the second one ventral and the third one dorsal again.

### 2.3.2 IgG ELISA

White 96-Well F-bottom plates (Greiner) were filled with 50 $\frac{\mu l}{well}$ of EndoFit™ OVA (InvivoGen) in DPBS (10 $\frac{\mu g}{ml}$). The plates were shaken briefly and stored at 4 °C in dark, overnight. On the next day, the plates were washed with program 6 (PBS + Tween 0.05%, Tecan platewasher), beaten out, filled with 200 µl blocking buffer (2.15) per well and incubated for one hour at room temperature. In the meantime, sera were diluted 1:100, 1:1000 and 1:10000 in blocking buffer. After incubation, the plates were washed with program 6 again, then 50 µl of the diluted sera were transferred to the wells and the plates were incubated for one hour at room temperature. Meanwhile, HRP[18] labeled antibodies (Tab 2.16) were diluted in blocking buffer. The plates were washed with program 5, the secondary antibodies added to the wells and then the plates incubated for one hour at room temperature.[19] Luminescence substrate was prepared according to the manufacturers protocol (Roche, BM (POD)) and added to one plate at a time. After washing the plate with program 5, the substrate was incubated for 3 minutes at room temperature before the luminescence was measured (Tecan infinite M200PRO).

| Reagent | Content | Manufacturer |
|---|---|---|
| PBS | | |
| Tween 20 | 0,1% | |
| Milk powder | 2% | Roth |

**Table 2.15:** Skim milk was weighed in and dissolved in PBS. Tween 20 was added to the stirring solution and the final volume was adjusted with PBS. *Abb:* PBS: Phosphate Buffered Saline

| Reagent | Dilution | Manufacturer |
|---|---|---|
| $IgG_{total}$ | 1:2000 | Biolegend |
| IgG2c | 1:2000 | BioRad |
| IgG1 | 1:1000 | BioRad |

**Table 2.16:** The Antibodies were diluted individually in blocking buffer *Abb:* Ig: Immunoglobulin

18: Horse radish peroxidase

19: Blank values were derived from wells receiving the respective secondary antibodies only.

### 2.3.3 IFN-γ / IL-4 ELISpot

PVDF filter bottom plates (Millipore, Merck) were wetted with 100µl of 70% EtOH and incubated for 10 minutes at room temperature. Then, the plates were washed three times with 200 µl DPBS and incubated with 50 $\frac{\mu l}{well}$ of IFN-γ (BioLegend) or IL-4 Antibodies (BioLegend) in DPBS (4 $\frac{\mu g}{ml}$). The plates were stored in a humidified box at 4°C overnight. On the next day the plates were beaten out and washed with 200 µl PBS per well. The surface was blocked with 100 µl T cell medium (Tab. 2.7) for at least one hour at room temperature. Stimulation media were prepared at a concentration of 20 $\frac{\mu g}{ml}$ of EndoFit™ OVA and 10 $\frac{\mu g}{ml}$ SIINFEKL (Promega), and 50 $\frac{\mu l}{well}$ were dispensed. As negative control, regular T cell medium (Tab. 2.7) was deployed. Cells suspensions as generated in , were diluted to 2x$10^5$ and carefully pipetted to the center of the wells in a drop-wise fashion. After incubation for 24 hours in an incubator at 37 °C 5% $CO_2$ and 95 % $\phi$, the plates were washed three times with 200 µl PBS and three times with PBS + Tween 0.1 %. Next, 50 µl of detection antibodies (IL-4 and IFN-γ 2 $\frac{\mu g}{ml}$ in DPBS + 1% BSA) were added and plates were incubated in a humidified box at room temperature for two and a half hours. Plates were washed four times with PBS + Tween 0.1 %, then 50 $\frac{\mu l}{well}$ of HRP-conjugated strepavidin (BioLegend) were added at a 1:1000 dilution (in PBS + 1% BSA). After incubation for two hours

in a humidified box, plates were washed three times with PBS + Tween 0.1 %. Next, the protective rubber bottom was removed and washed with permeate. The backside of the wells was washed with 200 µl of PBS, then the bottom was re-installed and plates were washed four times with PBS. AEC stock solution is diluted in substrate buffer 1:15 and filtered (0.45 µm, Starlab). 30% $H_2O_2$ is added to the solution (1:1500), before dispensing 50 $\frac{\mu l}{well}$. The plates were incubated at room temperature until spot formation was visible, and subsequently washed thoroughly with permeate. The rubber bottoms were discarded and plates were allowed to dry at 4 °C in the dark for 72 hours. The membranes within the wells of the dried plates were stamped onto adhesive foil using a single-well puncher. The foils were then scanned at 2000 dpi resolution, transformed with a photocopy filter (Adobe Photoshop V. 9.0x211) and single-well selections (ellipse tool) analyzed on ImageJ[20] (V. 1.53 C).

20: Counting was performed automatically with a macro written by Richard Weiss (Appendix A.0.1.1, Code A.1). IL-4 coated plates were counted manually, due to low number of spots.

### 2.3.4 Immunocyte restimulation

After incubation for four days, the restimulated cells were centrifuged for 5 mins at 1200 rpm, then 50 µL of supernatants were carfully transferred to a 96-well plate and stored at -20 °C for LEGENDPlex® assay (2.3.4.2 on the next page). Cells were washed with 100 µL dPBS at 1500 rpm for 3 minutes before the pellets were dissolved in 20 µL anti-CD16/32 hybridoma supernatant. After incubation at 4 °C in the dark for 5 minutes, 20 µL of extracellular staining mix (see. 2.17) was added to the wells and the plates were subsequently incubated at 4 °C in the dark for 30 minutes. Next, cells were washed with additional 100 µL of FACS buffer (see. 2.6, pre-cooled) at 1200 rpm, 4 °C for 5 minutes. The pellets were resuspended in 150 µL Fix/Perm buffer (eBioscience, FoxP3-fix/perm concentrate, 1:3, pre-cooled) and incubated 4 °C in the dark for 60 minutes. Then, the plates were centifuged at 1500 rpm, 4 °C for 3 minutes and washed two times with 100 µL Perm buffer (eBioscience, Perm buffer, 1:10, pre-cooled). The pellets were blocked in 20 µL of 10 % mouse serum ($\frac{v}{v}$ in Perm buffer) 4 °C in the dark for 5 minutes. The intracellular staining mix (see. 2.17) was added to the cells, before incubation at room temperature in the dark for 30 minutes. Finally, the cells were washed with 100 µL Perm buffer (1500 rpm, 4°C 3 minutes), 100 µL DPBS (1500 rpm, 4°C, 3 minutes) and resuspended in 80 µL DPBS for analysis (3.3.3 on page 59).

| Marker | Fluorophore | Manufacturer |
|---|---|---|
| CD4 | FITC | ImmunoTools |
| L/D | eFluor506 | eBioscience |
| CD44 | BV650 | BioLegend |
| CD62L | APC-eFluor780 | eBioscience |
| CD25 | APC | ImmunoTools |
| CD8 | PerCP-Cy5.5 | eBioscience |
| Ki67 | ef450 | eBioscience |
| FoxP3 | PE | eBioscience |

**Table 2.17:** Fluorophores used for intra and extracellular staining of re-stimulated immunocytes. The extracellular mix consisted of CD4, CD8, CD25, CD44, CD62L and L/D. Intracellular markers were FoxP3 and Ki67. Final dilutions were: APC at 1:200 (Antibody didn't stain well), APC-ef780 at 1:200, BV650 at 1:150, ef450 at 1:200, PE at 1:150, FITC at 1:400, eF506 at 1:1000 and PerCP-Cy5.5 at 1:200 - in DPBS.

#### 2.3.4.1 Flow cytometry

Prepared samples as described in 2.3.4 on the previous page were analyzed on a Cytoflex S flow cytometer (Beckman-Coulter) in plate mode. Volume to record was set 10 µL lower than the dispensed amount. Figure 2.6 show the gating strategies used for analysis.

#### 2.3.4.2 Cytokine analysis

Cytokines from the frozen supernatants of restimulated lymphocytes (see. 2.3.4) were analyzed using a LEGENDplex® 13-plex $T_H$ panel. The supernatants were centrifuged at 1000g for 10 minutes and 5 µL were carefully removed and mixed with 5 µL assay buffer. One master mix was prepared for samples and one for the standards to control for matrix effects (Assay buffer, beads, detection antibodies /+ Tcell medium (matrix)). 5 µL of standards and samples were dispensed in a 96-well V-bottom plate, then the respective master mixes were pipetted to the wells. The plates were briefly centrifuged, wrapped in aluminum foil and placed on a shaker for two hours at room temperature. The wells were washed two times with wash buffer (125 µL and 150 µL respectively) at 1000g for 3 minutes.[21] Next, 25 µL of strepavidin-PE (Diluted 1:5 in assay buffer) was added to the wells, the plates were centrifuged briefly, wrapped in aluminum foil and placed on a shaker for 30 minutes. The wells were washed two times as described above, then the pellets were solved in 80 µL wash buffer, briefly shaken and analyzed on a Cytoflex S flow cytometer (Beckman-Coulter) in plate mode. Generated data was subsequently processed with the provided LEGENDPlex® software (V 8.0). PE signal was used for analysis, as the standard was mixed up one time and no quantitative statement is desired.

21: In the second washing step, the plates were additionally incubated for one minute on the shaker before centrifugation. Plates were beaten out on a paper towel after centrifugation.

### 2.3.5 Cytotoxicity assay

Three donor mice (C57BL/6, female, 7-8 weeks old) were sacrificed for cell transfer one day before harvest. Lymph nodes (brachial, mesenteric, axillary) and spleens were isolated. Lymph nodes were mashed in a 1.5 mL micro-centrifuge tubes (Eppendorf). Spleen were mashed with the back of a syringe in a 35 mm petridish containing 1 ml DPBS. Those solutions were transferred to 1.5 mL micro-centrifuge tubes (Eppendorf), cell solutions were withdrawn as soon as larger tissue shreds had settled. Erythrocytes from spleens were lysed in 7 mL ACK Buffer (Tab. 2.8 on page 27) for 5 minutes. The cells were washed with 8 mL DPBS at 1200 rpm for 5 minutes at 24 °C and supernatants were discarded, using a vacuum pump. The cells were solved in 1.8 mL DPBS, split in two parts of

equal volume and stain with 4 µL ef450 and ef670 proliferation dye respectively. Stained cells were washed with T cell medium (5 mL + 1 mL FBS) and solved in 5 mL T cell medium. 5 µL of SIINFEKL (Promega) (final concentration: 10 $\frac{\mu g}{mL}$) was added to the eF450 stained cells before incubation at 37 °C for 65 minutes. The pulsed and control cells were washed three times with 10 and 2 x 15 mL PBS (same procedure as above) and finally resuspended in 1 mL PBS. 500 µL from each of the two populations were mixed and analyzed on a Cytoflex S flow cytometer (Beckman-Coulter). After observing the desired 50:50 cell ratio, the residual volumes were also pooled, filtered through a 70 µm cell strainer and analyzed again via flow cytometry. The 50:50 mixture was then counted by electronic current exclusion (CASY - OMNI Life Science) and diluted to 30 x $10^6$ $\frac{cells}{mL}$. The tails from the immunized recipient mice (see. 2.3.1) were heated with pre-warmed water (≈ 43 °C) and 100 µL of the stained cell mixture was injected to the tail vein. After 16 hours, spleenic and lymphoid cell suspensions were prepared as described in 2.3.1 on page 31 and the injected cell populations analyzed on a Cytoflex S flow cytometer (Beckman-Coulter) in plate mode.


**Figure 2.6:** Gating strategy for OT-II co-cultures (2.3.4) as gated on CytExpert 2.0.4.28. Starting from top left, live cells were gated based on size. Next, in the plot in the top middle additional dead cells were excluded based on a dead cell stain. On the top righ panel, doublets were excluded based on FSC-W and FSC-A. Populations were split up into $CD4^+$ and $CD8^+$ cells and further analyzed. CD4 cells are displayed on the left-hand side (3 Plots), with proliferation on the top, activation in the middle and FoxP3 $T_{regs}$ and the bottom. CD8 cells are shown on the right, with proliferation on the bottom and activation on the top. The activation plots for CD4 and CD8 cells were split into four quartiles were the top-left represents the naive T cells, top-right central memory T cells and the bottom-right the effector cells. Proliferation was analyzed with a Ki67 maker. *Abb:* FSC: forward scatter, SSC: side scatter

# Results 3

*"Most people use statistics like a drunk man uses a lamppost; more for support than illumination".*

– Andrew Lang, *1937*



## 3.1 Generation of ovalbumin - dextran glycoconjugates

The generation of ovalbumin - dextran (OVADex) glycoconjugates was performed by creating covalent bonds via reductive amination. Before coupling, ovalbumin was purified to remove endotoxin contaminations. For the reaction we need $NH_2$ groups on the protein (primary amines) and aldehyde groups on dextran. The polyaldehyde dextrans were generated by mild oxidation with sodium periodate ($NaIO_4$). Then, the covalent links between dextran and ovalbumin were formed by reductive amination. The fractions of interest were purified by size exclusion chromatography and analyzed. Glyco- and protein- stains were performed on the samples - separated by polyacrylamide gel electrophoresis. Additionally, binding against the lectin concanavalinA was assessed by micro-scale thermophoresis. Furthermore protein concentration was assessed amino acid analysis, while dextran content was measured by anthrone assay.

### 3.1.1 Reduction of ovalbumin endotoxin contamination

LPS[1] , also known as endotoxin, has been shown to trigger DC maturation, by activating TLR4 [120, 121]. To analyze the stimulatory properties of new formulations, low endotoxin content is therefore critically important for immune studies *in vitro* and *in vivo*. Since the manufacturer (Sigma-Aldrich) states on their product website that this product is not tested for endotoxin [122], we chose to purify the product to ensure cell culture and vaccination grade quality.

Treatment of commercial OVA with Triton-X114, as described in 2.1.1 on page 19 resulted in endotoxin levels lower than 0.39 $\frac{ng}{\mu g}$. The measurement was performed according to 2.1.3 on page 21, commercial OVA from the same Lot was used as a reference (OVA sigma) (Fig. 3.1). After the purification we tested for residual

1: Lipopolysaccharide

Triton contamination by UV-absorption at 280nm as Triton strongly absorbs at this wavelength. We measured the protein concentration of cleaned and commercial OVA via Bicinchoninic acid assay and UV spectroscopy at 280nm (Eppendorf BioSpectrometer® / Tecan M200PRo). Protein concentrations determined by BCA served as reference and were compared to protein concentrations measured by UV absorption. Any increase in the ratio of OD280 to the protein concentration determined by the BCA assay were assumed to be caused by residual triton. After the cleanup, OVA had a slightly lower ratio compared to the untreated OVA and thus contained no detectable Triton contamination (see. A.1 on page 80).

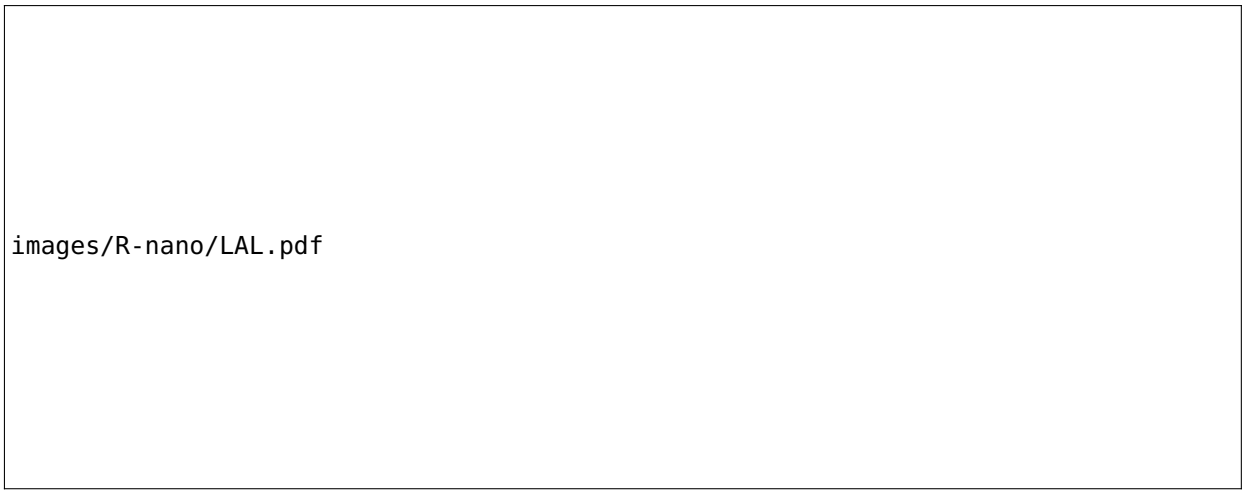


**Figure 3.1:** Endotoxin levels of commercial and cleaned ovalbumin, measured with limulus amebocyte assay. **(A)** Time series of LAL assay of OVA before and after Triton-X114 treatment (OVA sigma = before, OVA clean = after). **(B)** First order derivative of the time series, in order to illustrate the inflection points.

### 3.1.2 Conjugation of OVA to dextran results in the formation of two different size pools

Concentrations of protein and carbohydrate were assessed for controlled coupling reactions. Protein concentration was assayed by Bicinchoninic acid assay and OD280 measurement and was estimated to 17 $\frac{mg}{mL}$ (5 dilutions measured (3x BCA, 2x OD), 3 technical replicates) (Fig. A.1). Carbohydrate concentration was determined by Anthrone assay and estimated to 27, 30 and 32 $\frac{mg}{mL}$ respectively (2 dilutions measured, 4 technical replicates) (Fig. A.2 on page 80).

Upon coupling, aliquots were drawn from the samples and loaded on the SEC-HPLC for quality control, before separating 2 mL fractions on the BIO-CAD (SEC-FPLC). Each specimen produced two distinct, size-shifted peaks compared to pure OVA (OD280), reflecting complexed DEX-OVA (Fig. 3.2). To exclude signal bleeding from the Dextrans into the 280 channel, a control run with uncoupled Dextrans was performed respectively (Fig.A.4(**A**)). The collected

| Conjugate | Fractions | OVA $\frac{mg}{mL}$ |
|---|---|---|
| 15F1 | F38-F46 | 0.3 |
| 15F2 | F66-F74 | 2.45 |
| 100F1 | F37-F46 | 0.45 |
| 100F2 | F60-F72 | 2.5 |
| 450F1 | F38-F46 | 0.45 |
| 450F2 | F55-F72 | 1.85 |

**Table 3.1:** The table summarizes the generated conjugate fraction pools with the concentration of OVADex conjugates measured by amino acid analysis (third column). The first column shows the name of the respective neoglycoconjugate (The prefix identifies the dextran chain length (15 kDa - 450 kDa). F1 stands for the large fraction pool, F2 for the small one). The second column shows the fraction number used for pooling.

fractions were initially analyzed via UV absorption and Anthrone assay in order to asses the protein and dextran content, respectively (Dextran controls: Fig.A.4(**B**)). As UV absorption turned out to be not reliable to determine the protein concentration in the conjugates amino acid analysis was performed (Tab. 3.1). Results for OVA:DEX ratio based on AAA and anthrone method are described in Section 3.1.4. Interestingly, F1 and F2 fractions turned out to have very different protein:carbohydrate ratios. While in the F1 fraction, a high protein:carbohydrate ration was measured, the opposite was true for the F2 fractions. The volumes of the respective fraction pools are summarized in Table 3.2.


**Figure 3.2:** Size exclusion chromatogram of 15 kDa, 100 kDa and 450 kDa dextrans coupled to ovalbumin. Purification of neoglycoconjugates was performed on a BioCAD 700E equipped with a sephacryl 200 $SE^2$ column. 2 x 5 mL of the respective conjugates were loaded into the loop and separated with PBS at a flow rate of 1 $\frac{ml}{min}$. The SEC-chromatogram shows OD280 means (center of lines) + standard deviation (thickness if lines) of two runs from the individual OVADex conjugates (One run for OVA). The peaks for the first and second collected fraction pools were labeled "F1" and "F2" respectively. 2 mL fractions were collected, the exact collected fractions can be extracted from Table 3.2 on the following page, the corresponding volume is shown in the third column "Vol. (mL)"

### 3.1.3 F1 particles more than tenfold larger than F2 particles

After separating the glycoconjugates via size exclusion, the hydrodynamic radii of the OVADex conjugates were assessed by dynamic light scattering. Korotchenko et al. coupled 4.5 kDa laminarin to ovalbumin and measured a mean hydrodynamic radius of 8.27 nm. The neoglycoconjugate pool had a 6:1 molar ratio of carbohydrate to protein, corresponding to a 0.6 mass ratio [20].

As expected from the size exclusion chromatogram (Fig. 3.2),

pooled F1 fractions from the different conjugates had larger hydrodynamic radii, ranging from 58.8 to 80 nm, while F2 fractions ranged from 4.1 to 5.8 nm.

Typically, the z-average diameter $Z_D$ values of particles with a polydispersity index lower than 1 are calculated via the intensity-weighted mean formula, which gives a reliable representation of the true particle size [123]. In our case, aggregation can be observed for all particles, with extreme clusters of up to 40+$\mu$m. The high light scattering intensity of these aggregates skews the $Z_D$ value and increase the inaccuracy. Even though all samples have a polydispersity index (Pdl) < 1, it is more suitable to characterize our particles based on the dominant appearance. To avoid biased results, we therefore analyzed the particle size distributions based on number of particles (Fig. 3.3). Among the F2 fractions, higher molecular weight dextrans were more heterogeneous. 450F2 had two distinct size peaks at 4.8 nm and 11.7 nm. Although most 100F2 particles were 4.1 nm in size, the distribution of particles were slightly skewed to the right. 15F2 was closest to a normal distribution among the F2 fractions, with a mean size of 5.8 nm. F1 fractions appear more homogeneous and normally distributed than F2 fractions, thus arithmetic mean values adequately describe the central tendency of the F1 size distributions. Thereby, 15F2 had an average size of 80 nm, while 100F2 and 450F2 particles had and average size of 58.8 nm (see. Tab. 3.2)

Depending on steric configuration and distribution of aldehyde groups during the reductive amination reaction, functionalized dextran chains might lead to cross-linking of OVA, resulting in multimeric OVA complexes. Based on work from Armstrong et al. and Erickson et al. the hydrodynamic radii of the Dextrans can be estimated to ≈ 3 nm (15 kDa), ≈ 8 nm (100 kDa) and ≈ 16 nm (450 kDa), whereas OVA has been shown to have a hydrodynamic radius of ≈ 3 nm [124, 125]. A simple 1:1 binding model can not be assumed because oxidation and amination happened at multiple accessible sites at random. However, considering the average size (4.1 - 5.6 nm) of the pooled F2 fractions, complexes containing only a single OVA complexes are the only possible model. Interestingly, the high dextran content measured in 100F2 and 450F2 is not directly expressed in an increased hydrodynamic radius. Probably, single dextran chains were wrapped around the globular ovalbumin protein, which would only result in a small radial increase. This would explain the lower radii of 100 and 450F2 compared to 15F2, where the dextran might not be able to wrap around the protein effectively - thus resulting in a larger radius. A clear second peak is visible for 450F2 (≈ 15 nm), these particles might either be the only OVA dimers or protruding 450 kDa dextran chains. This simple model can not

| Conjugate | $\text{Radius}_\text{H}$ | Vol. (mL) |
|---|---|---|
| 15F1 | 80 | 76-92 |
| 15F2 | 5.8 | 132-148 |
| 100F1 | 58.8 | 74-92 |
| 100F2 | 4.1 | 120-144 |
| 450F1 | 58.8 | 76-92 |
| 450F2 | 4.8 | 110-144 |

**Table 3.2:** The table shows a summary of the generated conjugate fractions with their respective hydrodynamic radii and the volumes used for pooling. The first column shows the name of the respective neoglycoconjugate (The prefix identifies the molecular weight of the dextran (15 kDa - 450 kDa). F1 stands for the large fraction pool,F2 for the small one). The second column displays the size of the OVADex fraction pools, as determined by DLS. The third columns shows the elution volume of the SEC-FPLC run, used for pooling the respective OVADex fractions. *Abb:* $\text{Radius}_\text{H}$ = hydrodynamic radius

make valuable predictions for the larger, more complex F1 particles. Based on their size, multimeric cross-linked OVA complexes can be assumed, however no precise number of OVA molecules can be calculated. Korochenko et al. generated monomeric ovalbumin particles comparable to our 15F2 fractions. Interestingly, coupling of 4.5 kDa laminarin [3] resulted in a higher peak hydrodynamic radius (8.3 vs. 4.1 - 5.8 nm) than the larger dextrans (15 kDa - 450 kDa). According to the assumptions above, shorter carbohydrate chains might protrude more from the center, thus creating a bigger three dimensional conformation. Furthermore, 1↦6-linkage has a higher calculated degree of flexibility than 1↦3-linkages [127], which may rationalize the unexpected larger hydrodynamic radius of laminarin-ovalbumin conjugates.

3: A (1 ↦3)-β-d-Glucan with a low degree of β-(1↦6) branching [126]

### 3.1.4 F1 and F2 fractions have divergent protein:carbohydrate ratios

In order to characterize the biochemical composition, amino acid composition and carbohydrate content were measured (Amino acid analysis, Anthrone assay). Both values are critical for subsequent experiments, so antigen can be dosed equally in all treatment groups *in vivo* and *in vitro*. Carbohydrate content is important to model the appearance of our nanoparticles and for comparability of the dextran - concanavalinA interaction during the microscale thermophoresis experiment.

Interestingly, the bigger "F1" fractions have a higher OVA content with a ratio ≥ 1 (OVA:DEX). In contrast, the F2 fractions have higher DEX content. Generally, the higher the molecular weight of the dextran, the higher the Dextran content - as determined by the $\frac{w}{w}$ ratio (Tab. 3.3). Absolute protein concentrations from the AAA enabled bona-fide protein concentration estimates and investigation of individual amino acid content. Production efficiency in terms of total protein content is ≥ 4 times higher for F2 fractions than F1 (Tab. 3.3). For the reductive amination reaction (see. 2.1.6 on page 22), lysin content is essential due to the terminal primary amine groups. Analysis of uncoupled OVA showed 22 Lys instead of the 20 expected [128], which is attributed to imperfect measurement accuracy. The Lys content of the conjugates varied between 10-14, thus indicating 6-10 bound carbohydrate residues. Using two surface accessibility predicting algorithms, 17/20 Lys residues were found to be surface exposed (threshold 25 %) - with one difference in surface prediction at K229/207 (NetSurfP1.1/NetSurfP2) [1, 2] (Fig. 3.4(**B**)). Korotchenko et al. reported 6 surface accessible lysines, based on predictions from the VADAR server with surface access threshold ≥ 0.5. Variations between these in silico predictions, can be attributed to different thresholds and

calculation algorithms [20]. Predictions from both methods were in line with the respective experiments and might be explained in steric differences between the proteins or carbohydrates used.


**Figure 3.3:** Size distribution of OVADex conjugates as determined by dynamic light scattering. Hydrodynamic radii ($Log_{10}$) are shown against the fraction of total particles (%) for 15 kDa OVADex (**A**), 100 kDa OVADex (**B**) and 450 kDa OVADex. Peak sizes were added to the legends of the respective conjugates. Data is shown as the mean of three technical replicates. The experiment was performed one time. *Abb.* Pdl = polydispersity index, F1 stands for the large fraction pool, F2 for the smaller ones. The prefix (15, 100, 450) identifies the respective coupled dextrans in kDa.

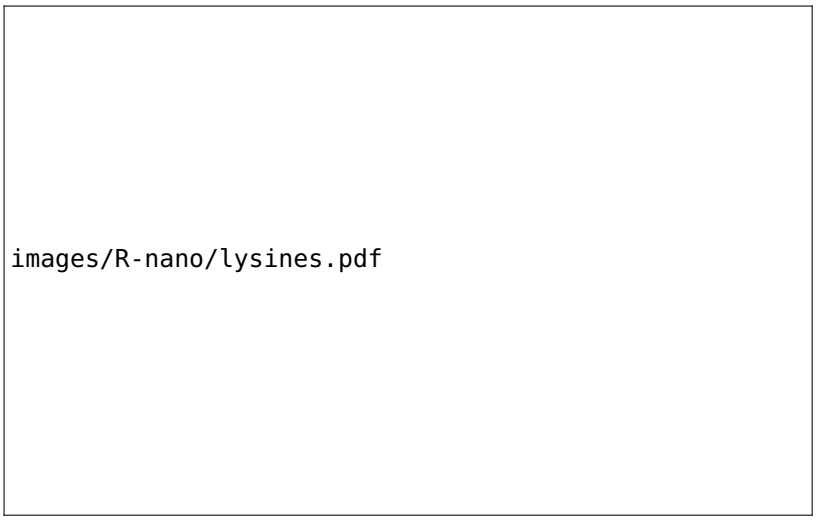


**Figure 3.4:** Lysine content and surface accessibility prediction of OVA. The amino acid composition of OVADex glycoconjugates and OVA were analyzed in order to estimate total protein concentration and number of coupled Lysine residues (**A**). Lysine residues were covalently linked to aldehyde groups of oxidized dextrans during the reductive amination reaction - and therefore not recovered during AAA (One experiment, two technical replicates). (**B**) shows the surface accessibility of Lysine residues, which could sterically participate in the reaction. The predictions were performed with (NetSurfP1.1/NetSurfP2) on P01012-1 (Uniprot).

| | 15F1 | 15F2 | 100F1 | 100F2 | 450F1 | 450F2 |
|---|---|---|---|---|---|---|
| OVA:Dex $\frac{(w)}{(w)}$ | $\frac{9.5}{1}$ | $\frac{1}{1}$ | $\frac{5.4}{1}$ | $\frac{1}{11.8}$ | $\frac{2.7}{1}$ | $\frac{1}{14}$ |
| OVA ($\frac{mg}{mL}$) | 0.3 | 2.45 | 0.45 | 2.5 | 0.45 | 1.85 |
| OVA (µg \| mg) | ≈ 420 µg | ≈ 2.5 mg | ≈ 585 µg | ≈ 2.3 mg | ≈ 630 µg | ≈ 2 mg |

**Table 3.3:** Summary table of protein and carbohydrate composition of the neoglycoconjugates. The first row shows the ratios of protein to carbohydrate in the OVADex constructs. Second row shows the absolute concentration of OVA in $\frac{mg}{mL}$ and the third row shows the total collected protein in µg or mg. 10 mg of OVA were used for glycoconjugation.

Coupling was also monitored via polyacrylamide gel electrophoresis. As expected, uncoupled OVA had a molecular weight of ≈ 45 kDa. We also monitored the impact of lyophilization and endotoxin removal and found no migratory difference between the protein bands (A.0.2.5 on page 82, Fig. A.5). The large F1 fractions with


**Figure 3.5:** Protein and carbohydrate mass ratios, determined by amino acid analysis and anthrone assay. Mass ratio of OVA and Dextran content of the individual nanoparticles. Columns to the left indicate a excess of OVA, the centerline marks an equal 1:1 ratio and columns to the right imply a higher Dextran content.

over 50 nm in hydrodynamic radius, did not enter the stacking gel and persisted as faint bands on top of the sample pockets. The F2 fractions (4.1 - 5.8 nm) were all bigger than the highest standard (180 kDa). 100F2 and 450F2 did appear more homogeneous than 15F2 on the coomassie gel (Fig. 3.7). Glycostaining revealed the same patterns as in the coomaasie stain, while commercial OVA didn't appear to have a detectable amount of carbohydrates attached (Fig. 3.8). In both gels, dextrans of the respective sizes were also loaded as negative control (labeled as 15 kDa, 100 kDa and 450 kDa) and not found on the gels. We used sodium dodecyl sulfate (SDS) to denature and charge proteins. SDS is known to interact with charged or hydrophobic patches of proteins [130], accordingly dextran chains are unable to receive charge. Less bound SDS on glycoconjugates due to dextran chains, also results in reduced migration and a subsequent overestimation of molecular weight. This could also explain the heterogenous bands of 15F2 conjugate, which has the least surface dextran and might be denatured and charged more frequently than 100F2 and 450F2. This shielding effect could also explain the migration pattern of 15F2 and the larger hydrodynamic radius observed in the DLS.

### 3.1.5 OVADex particles remain biologically intact after conjugation


**Figure 3.6:** Surface accessibility predictions as produced by NetSurfP 2.0 algorithm. The OT-I and OT-II peptides (1.3) are framed in red (**A**). Sequence was taken from Uniprot (P01012) - results were validated with sequences from chains A-D of the PDB structure (1OVA). (**B**) shows the 3-D structure of 1OVA A-chain with red colored K-residues. The arrow points to the green framed "SIINFEKL" sequence. 3D structure was processed in chimera [129].


**Figure 3.7:** Coomassie stained SDS-PAGE gels (10 %, Tab. 2.3) with molecular weight standard (Thermo Scientific) size in kDa. Gel photo representative of two independent runs. *Abb.* F1 stands for the large fraction pool, F2 for the smaller ones. The prefix (15, 100, 450) identifies the respective coupled dextrans in kDa (eg. 100F1 = Large particle pool of 100 kDa dextran covalently linked to OVA). 15, 100 and 450 kDa refer to the respective uncoupled dextrans.

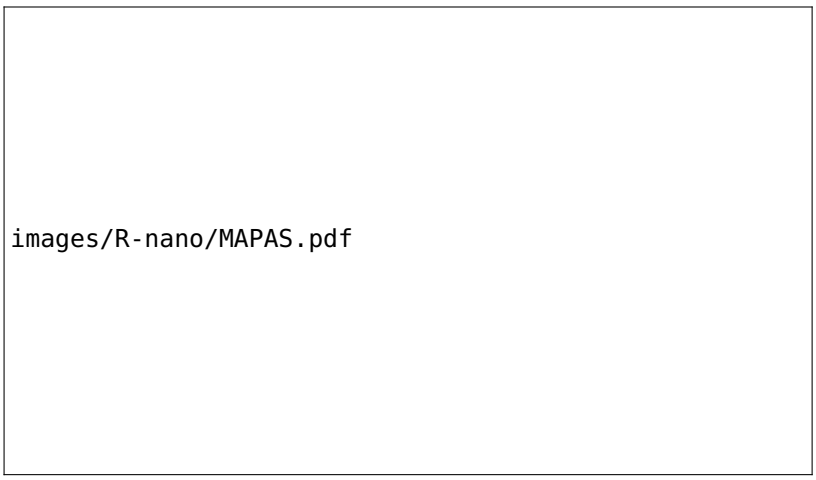


**Figure 3.8:** PAS stained SDS-PAGE gels (10 %, Tab. 2.3) with molecular weight standard (Thermo Scientific) size in kDa. Gel photo representative of two independent runs. *Abb.* PAS = periodic acid-schiff, F1 stands for the large fraction pool, F2 for the smaller ones. The prefix (15, 100, 450) identifies the respective coupled dextrans in kDa (eg. 450F2 = Small particle pool of 450 kDa dextran covalently linked to OVA). 15, 100 and 450 kDa refer to the respective uncoupled dextrans.

To assure binding dextran was still possible after oxidation, we decided to test the binding capabilities of our glycoconjugates

against a known target C-type lectin receptor like SIGN-R1, SIGN-R3 or langerin [11]. Unfortunately, no suitable receptor nor a binding assay was commercially available, so we tested the binding against the soluble, dextran-binding lectin concanavalinA (conA). It is known to bind α-mannose residues and also reported to bind OVA and dextran independently [131, 132]. Consequently we measured the binding activity of the OVADex neoglycoconjugates, uncoupled dextrans and OVA with microscale thermophoresis. Conjugation of OVA to dextran decreases the apparent dissociation constant $K_D$ to conA (Tab. 3.4). In our experiment, OVA binds conA stronger than than the Dextrans, while conjugated OVADex100 and OVADex450 show highest binding capacities overall (Tab. 3.4). Enhanced binding to conA is associated with higher chain length, thereby OVADex15 and 15 kDa Dextran showed the lowest binding strength. However, the OVADex450 and OVADex100 fit has large variations, so the true effect might be less pronounced. Taken together, dextrans showed weaker binding to conA than OVA, therefore differences in binding affinities might be largely due to OVA oligomerization. Furthermore, discussed by Coulibaly and colleagues, polysaccharide binding to conA depends on degree of branching, steric factors, and is determined by OH-groups on the C-3, C-4 and C-6 atoms [133]. The different analytes clearly have distinct conformation, thermophoretic properties and degrees of branching so absolute values should be considered with caution. Nevertheless, we speculate that structure related damage due to the oxidation would render the carbohydrates binding capabilities inactive - so biological activity of dextrans is likely maintained after the conjugation procedure.

images/appendix/MST.pdf

**Figure 3.9:** Binding curves of Ovalbumin-dextran glycoconjugates (OVADex) and their respective dextrans against concanavalinA (conA) using microscale thermophoresis. Tested were 15 OVADex (purple), 100 OVADex (green) and 450 OVADex (blue) and uncoupled OVA (black). OVADex doses were adjusted on antigen content. The figures display normalized fluorescence (Δ Fnorm) against sample concentration. Data is plotted as means and standard deviations (n = 3). *Abb.* F1 stands for the large fraction pool, F2 for the smaller ones. The prefix (15, 100, 450) identifies the respective coupled dextrans in kDa (eg. 455F1 = Large particle pool of 455 kDa dextran covalently linked to OVA).

## 3.2 In vitro assessment of OVADex conjugates

The central goal of vaccine design is to increase immunogenicity and safety of novel formulations. In order to test the immune stimulating potential and the allergenicity of the produced OVADex neoglycoconjugates, we set up adequate cell culture experiments. Therefore, harvested bone marrow cells from mice were stimulated with GM-CSF or FLT3-L in order to generate mixed dendritic cell (DC) suspensions. These DCs were then co-cultured with naive T cells[4] or stimulated in isolation. The cocultures were subsequently treated with antigen adjusted doses of glycoconjugates, then cell proliferation and effector phenotype of the T cells was analyzed after 4-5 days. Isolated DC cultures were stimulated in the same fashion, but analyzed for upregulation of surface markers after 16h. Additionally, the allergenic potential of ovalbumin upon conjugation, was assessed by the degree of β-hexosaminidase release from pre-sensitized rat basophilic leukemia cells. All treatments *in vitro* were equalized on the antigen content of the respective formulations and calculated in weight per volume ($\frac{\mu g}{mL}$).

| | $k_D$app (μM) | | |
|---|---|---|---|
| Dex15 | 14.2 | ± | 4.4 |
| Dex100 | 1.8 | ± | 0.8 |
| Dex450 | 2.1 | ± | 1 |
| OVADex15 | 3.5 | ± | 2.8 |
| OVADex100 | 0.02 | ± | 0.02 |
| OVADex450[1] | 0.02 | ± | 0.05 |
| OVA | 0.9 | ± | 0.3 |

**Table 3.4:** MST measurements were performed to study the binding capabilities of OVADex to conA. $K_D$ values for the unbound Dextrans were based on dextran content (μM), while the OVA and OVADex conjugates were based on protein content (μM). Normalized fluorescence ( Fnorm) is plotted against sample concentration. Graphs show data from three experiments (mean and standard deviation). [1]OVADex450 produced high noise during the measurement, so the $K_D$ is not reported with high confidence. Binding curves are plotted in Figure 3.9.

### 3.2.1 OVADex conjugates are hypoallergenic

Reducing the allergenic potential of therapeutic formulations while increasing immunogenicity is essential for allergen-specific immunotherapy. A subsequent goal is to reduce the long therapy duration as well as the occurrence of adverse events, which both currently result in low patient compliance [134]. High tolerability and effectiveness of glycoconjugated proteins has been demonstrated before, whereby the reduction of allergenicity was attributed to epitope masking of carbohydrate chains [20, 23].

In this work we used a rat basophilic leukemia (RBL) degranulation assay to measure the allergenicity of OVADex constructs *in vitro*. The cultured cells were first loaded with IgE from antiserum of previously OVA sensitized mice. Upon contact with the antigen specific epitopes, Fcε receptor bound IgEs are cross-linked and initiate the degranulation reaction. β-hexosaminidase is one of the released granular compounds, which was measured during this experiment.[5] The level of degranulation was then compared to total cell lysis, as induced by the detergent Triton. OVADex conjugates were compared to uncoupled OVA and a three-parameter Agonist vs. response curves was fitted using GraphPad. Comparison of EC50 is not suitable because OVADex didn't trigger measurable degranulation in our setup. Thus we approximated the degree of degranulation from Figure 3.3. We assessed a twofold lower after 15F2 treatment and threefold lower after treatment with the remaining OVADex particles. The hypoallergenicity is most likely

4: These naive T cells were derived from OVA-specific OT-II mice. These mice have an enriched repertoire of $CD4^+$ T cells with a OVA specific TCR.

contributed allergenic epitope masking of dextran chains. (Fig. 3.3(**B**)). These findings are in line with prior publications [20, 23] of our group and indicate that dextran conjugation could enhance the safety profile of allergen specific immunotherapy. Interestingly, the degree of shielding was less dependent on the hydrodynamic radius, but rather on the molecular weight of the dextrans.

5: As stated, β-hexosaminidase serves as a marker for the degree of degranulation. These terms are therefore used interchangeably.

### 3.2.2 F1 OVADex conjugates induce the highest BMDC activation and CD4$^+$ proliferation *in vitro*

We tested the immunogenicity of our OVADex particles in cell culture, where we either co-cultured FLT3L or GM-CSF derived dendritic cells with naive OT-II T cells, or treated the dendritic cells in isolation. After incubation with the treatments we tracked the activation and proliferation rates using flow cytometry.

Heftl et al. and Brawand et al. characterized the different phenotypes of DCs after the maturation with FLT3L or GM-CSF, whereby former mostly represent a steady-state phenotype and latter comprised a more inflammatory phenotype [62, 135]. Generally, GM-CSF were classified as cDCs which are already pre-inflamed, whereas FLT3 matured BMDCs resemble a naive DC phenotype. Both classes of dendritic cells are involved in skin related immune reactions, therefore we decided to test our glycoconjugates in both culture systems. The activation of these dendritic cells was measured after 16h based on upregulation of surface costimulation molecules CD86, CD80[6] and CD40. $T_H$ cell activation was analyzed by co-incubation of OVA-specific naive T cell from OT-II mice. These T cells have an enriched pools of CD4$^+$ lymphocytes with a distinct TCR with recognizes $OVA_{323\text{-}339}$ (Seq: ISQAVHAAHAEINEAGR). This peptides was subsequently used as a positive control (+C) for coculture experiments, whereas regular T cell medium was used for negative control (-C). CD8$^+$ co-cultures were also set up, with naive T cells from OT-I mice. Similar to OT-II mice, these carry a transgene which drives the expression of a TCR specific for the epitope: $OVA_{257\text{-}264}$ (Seq: SIINFEKL). In those experiments, we observed unspecific proliferation consistently ($n_{total} = 5$) - consequently these results were not included. CD4$^+$ experiments were performed two times with GM-CSF and one time with FLT3L ($n_{total} = 3$).

6: CD80 data is not shown, because the signal was very low and did not show reliable results.

OVADex conjugates show substantial potential to invoke a CD4-Helper response in the cell-culture setting - as observed in both types of dendritic cell suspensions (GM-CSF & FLT3-L). Generally, the larger fractions (F1) generated a higher magnitude of CD$^+$ proliferation than F2 fractions. In contrast, chain length has less impact within the fractions. Surprisingly the 15 kDa conjugate of

the F2 fraction (15F2) outperformed the other F2 fractions in terms of proliferation rate.

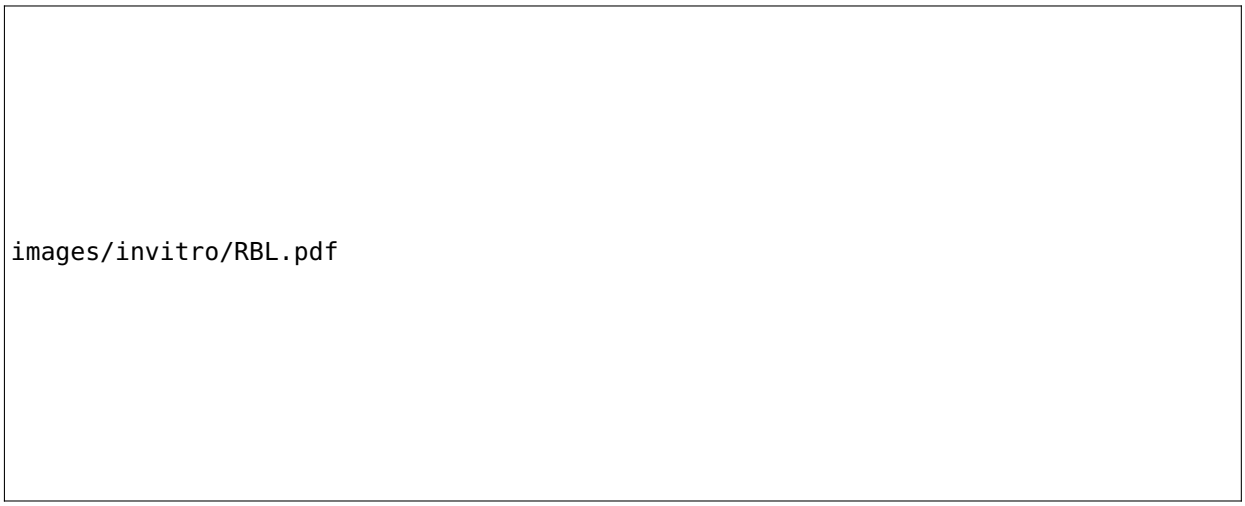


**Figure 3.10:** Percental βhexosaminidase release of antiOVA-IgE sensitized RBL cells compared to total cell lysis induced by triton. Treatments were performed in 10x serial dilutions, the resulting curves were fitted with a three parameter vs. response model in GraphPad Prism. Results are representative of two independent experiments. *Abb.* F1 stands for the large fraction pool, F2 for the smaller ones. The prefix (15, 100, 450) identifies the respective coupled dextran in kDa (eg. 15F1 = Large particle pool of 15 kDa dextran covalently linked to OVA). Note: All treatments *in vitro* were equalized on the antigen content of the respective formulations and calculated in weight per volume ($\frac{\mu g}{mL}$).

**Table 3.5:** Summary statistics naive $CD4^+$ proliferation. Proliferation rate was derived from the GM-CSF-DCs cocultures, treated with in Fig. 3.11 (**A**). Computation was performed using a Dunnett's multiple comparisons test for a simple effect within rows (GrapPad). Shown are only significant results adj. $p < 0.05$. *Abb:* Adj: adjusted, Diff: Difference, F1 stands for the large fraction pool, F2 for the smaller ones. The prefix (15, 100, 450) identifies the respective coupled dextrans in kDa (eg. 15F2 = Smaller particle pool of 15 kDa dextran covalently linked to OVA). All treatments *in vitro* were equalized on the antigen content of the respective formulations and calculated in weight per volume ($\frac{\mu g}{mL}$).

| Groups | Mean Diff | Adj P | Groups | Mean Diff | Adj P |
|---|---|---|---|---|---|
| **20 µg/ml** | | | **4 µ/ml** | | |
| OVA vs. 15F1 | -14436 | <0,0001 | OVA vs. 15F1 | -17956 | <0,0001 |
| OVA vs. 100F1 | -9834 | <0,0001 | OVA vs. 100F1 | -13044 | <0,0001 |
| OVA vs. 100F2 | 7471 | 0.0014 | OVA vs. 450F1 | -16016 | <0,0001 |
| OVA vs. 450F1 | -18629 | <0,0001 | **0.8 µg/ml** | | |
| OVA vs. 450F2 | 10398 | <0,0001 | OVA vs. 15F1 | -11700 | <0,0001 |

**Table 3.6:** Summary statistics naive $CD4^+$ proliferation. Proliferation rate was derived from the FLT3-DCs cocultures, treated with . as displayed in Fig. 3.11 (**B**). Computation was performed using a Dunnett's multiple comparisons test for a simple effect within rows (GrapPad). Shown are only significant results adj. $p < 0.05$ *Abb:* Adj: adjusted, Diff: Difference, F1 stands for the large fraction pool, F2 for the smaller ones. The prefix (15, 100, 450) identifies the respective coupled dextrans in kDa (eg. 450F1 = Large particle pool of 450 kDa dextran covalently linked to OVA).All treatments *in vitro* were equalized on the antigen content of the respective formulations and calculated in weight per volume ($\frac{\mu g}{mL}$).

| Groups | Mean Diff | Adj P | Groups | Mean Diff | Adj P |
|---|---|---|---|---|---|
| **10 µg/ml** | | | **2 µg/ml** | | |
| OVA vs. 15 F1 | -687.3 | <0,0001 | OVA vs. 20 | -411.7 | 0.0058 |
| OVA vs. 15 F2 | -780.7 | <0,0001 | OVA vs. 100 | -608.3 | <0,0001 |
| OVA vs. 100 F1 | -532 | 0.0002 | OVA vs. 15 F1 | -503 | 0.0004 |
| OVA vs. 450 F1 | -882.7 | <0,0001 | | | |

CD44 and CD62L were used to determine effector or central memory phenotypes of the T cells. These two surface markers are

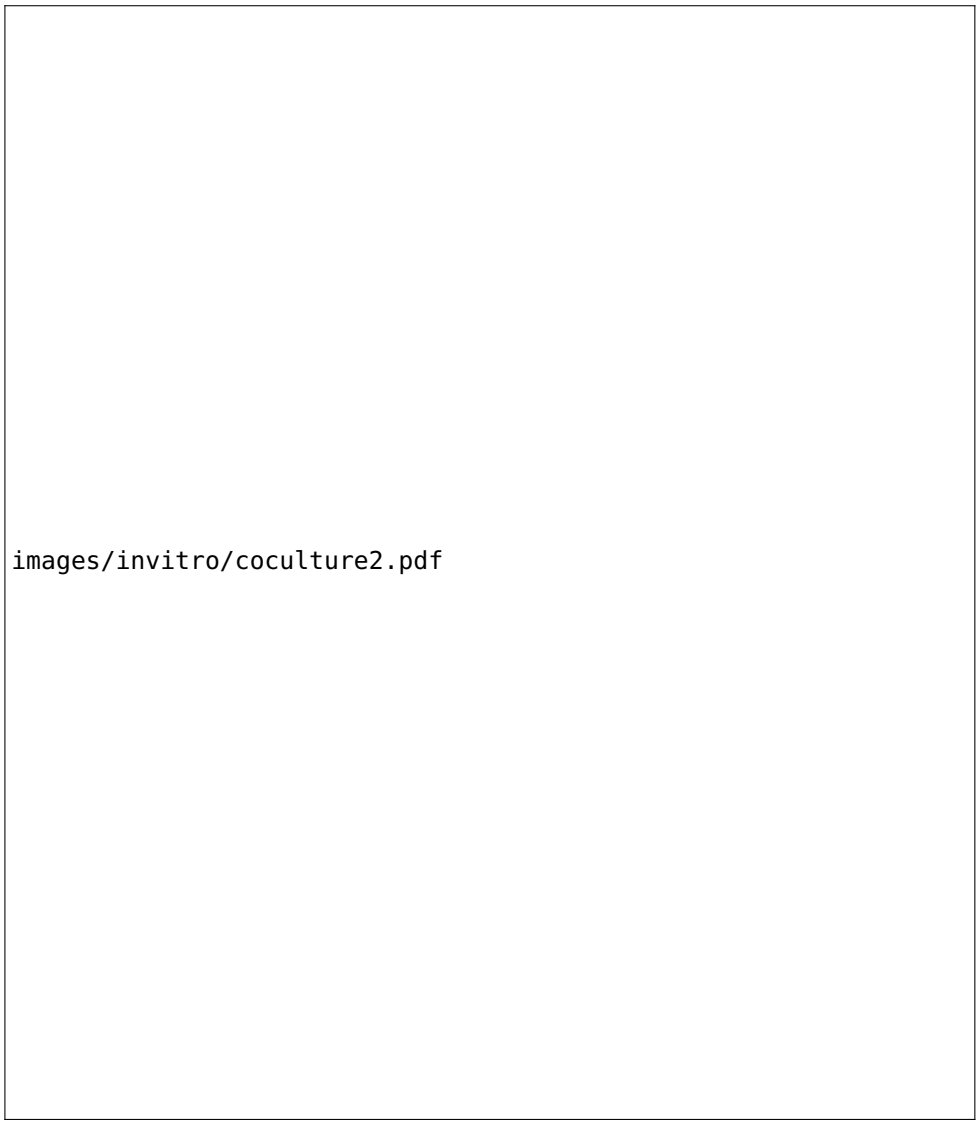


**Figure 3.11:** Proliferating $CD4^+$ T cells after BMDC stimulation with neoglycoconjugates or OVA (three technical replicates). (**A**) represents coculture with GM-CSF derived BMDCs (20 - 0.8 $\frac{\mu g}{mL}$) while (**B**) shows co-culture data for FLT3-L derived BMDCs (10 - 0.4 $\frac{\mu g}{mL}$). Data is shown as individual points, means are marked with a black bar, colored bars show the standard deviation. All significant results ($p < 0.05$) are shown in Tab. 3.6 and 3.5.*Abb.* OT-II peptide was used as positive control, T cell medium as negative control (-C) (Left side in the plots). F1 stands for the large fraction pool, F2 for the smaller ones. The prefix (15, 100, 450) identifies the respective coupled dextrans in kDa (eg. 100F1 = Large particle pool of 100 kDa dextran covalently linked to OVA).All treatments *in vitro* were equalized on the antigen content of the respective formulations and calculated in weight per volume ($\frac{\mu g}{mL}$).

adhesion molecules, which are differently expressed, based on the activation of the T lymphocytes. L-selectin (CD62L) is responsible to keep naive T cells in the seocndary lymphoid organs, where they wait to be activated by mature APCs. In contrast CD44 bind to molecules in extracellular matrix like hyaluronan and is therefore down-regulated upon activation [42]. Based on relative expression of these markers ($\frac{\text{High}}{\text{Low}}$) we inferred the maturation state of the T cells.

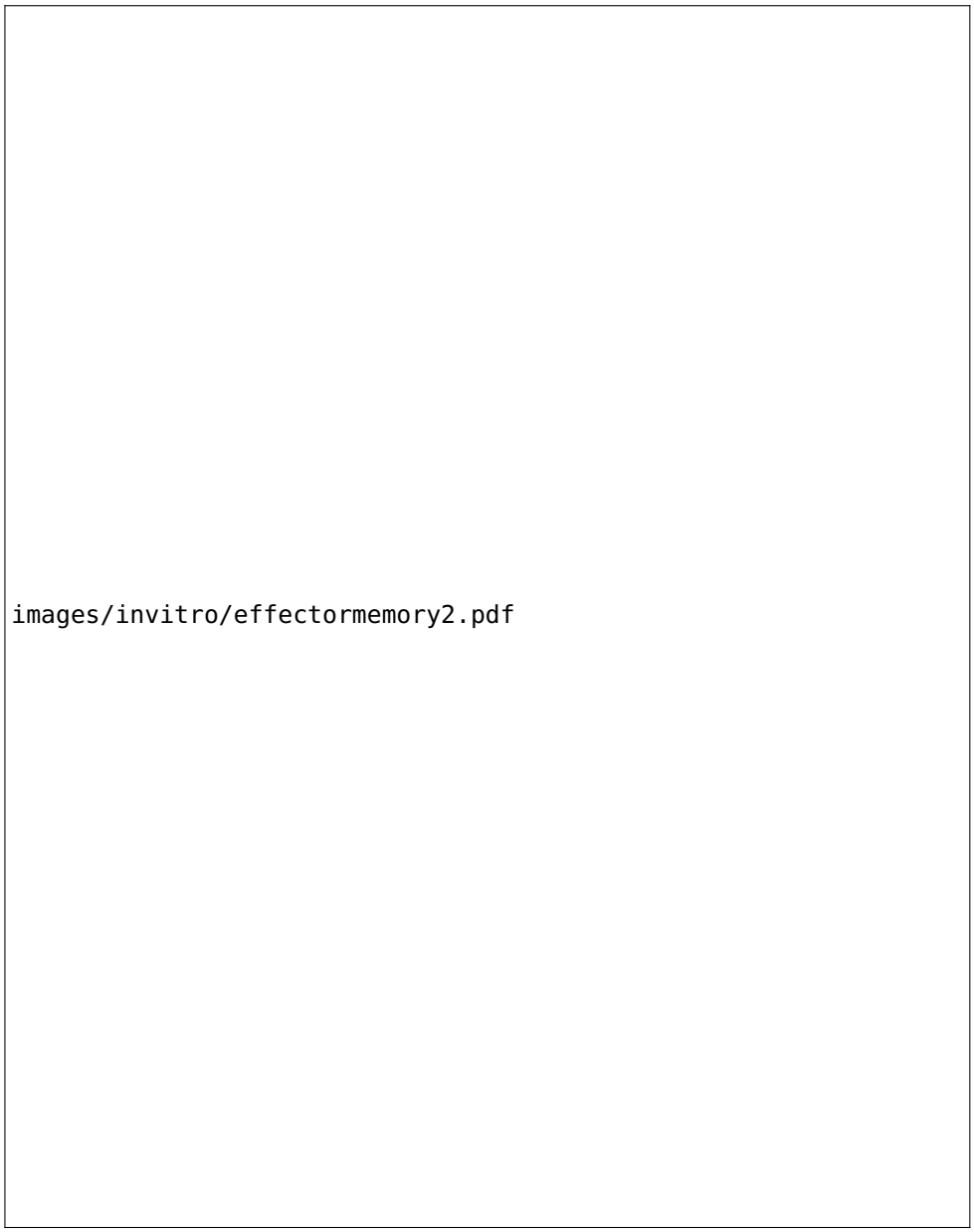


**Figure 3.12:** Flow cytometry data for Naive CD4$^+$ T cell activation experiment (GM-CSF derived BMDCs, see. Fig. 3.11(A)). Figure (**A**) shows T cells with an effector phenotype (CD44$^{high}$ CD62L$^{low}$) - (**B**) displays cell counts for central memory T cells (CD44$^{high}$ CD62L$^{high}$. Naive T cells (both markers low) were barely found at all (not shown). Data is shown as individual points (three technical replicates), means are marked with a black bar, colored bars show the standard deviation. No statistical layer was added. *Abb.* OT-II peptide was used as positive control, T cell medium as negative control (-C) (Left side in the plots). F1 stands for the large fraction pool, F2 for the smaller ones. The prefix (15, 100, 450) identifies the respective coupled dextrans in kDa (eg. 15F1 = Large particle pool of 15 kDa dextran covalently linked to OVA).All treatments *in vitro* were equalized on the antigen content of the respective formulations and calculated in weight per volume ($\frac{\mu g}{mL}$).

No detectable increase in central effector T cell was found compared to OVA treated cells (Fig. 3.12(A)) - while central memory cell counts were heightened in OVADex treated wells. Largest effect size was found for the F1 OVADex fractions (15kDa - 3693, 100kDa - 5300, 450kDa - 5593 - Comparisons at 20 $\frac{\mu g}{mL}$ - 95 % confidence interval deviation of 1759 (15F1). Dunnett's multiple comparisons test was performed on simple effect within rows using GraphPad.)


**Figure 3.13:** Activation of GM-CSF (**A,C**) or FLT3 (**B,D**) derived BMDCs based on the surface markers CD86 (**A-B**) and CD40 (**C-D**) after 16h of stimulation. Intensity of activation is displayed as median fluorescent intensity against the stimulation dosage of the treatments (10 $\frac{\mu g}{mL}$ - 0.4 $\frac{\mu g}{mL}$). *Abb.* Lipopolysaccharide (LPS) was used as positive control, BMDC medium as negative control (-C) (Left side in the plots). F1 stands for the large fraction pool, F2 for the smaller ones. The prefix (15, 100, 450) identifies the respective coupled dextrans in kDa (eg. 100F2 = Small particle pool of 100 kDa dextran covalently linked to OVA). All treatments *in vitro* were equalized on the antigen content of the respective formulations and calculated in weight per volume ($\frac{\mu g}{mL}$).

T lymphocyte maturation was only reported for GM-CSF, because cell counts in the FLT3L experiment were too low. Potent GM-CSF BMDC activation, in terms of CD86 upregulation was only found for the highest treatment doses (10 $\frac{\mu g}{mL}$) of the large 15 kDa functionalized ovalbumin (15F1) (see. Fig. 3.13(**A**)). In contrast, FLT3L derived BMDCs showed a high upregulation of CD86 among treatment of all F1 particles (15 kDa, 100 kDa and 450 kDa) (see. Fig. 3.13(**B**)). CD40 upregulation seemed to correlate well with CD86 upregulation, but had a smaller magnitude in both culture systems (FLT3-L/ GM-CSF) (see. Fig. 3.13(**C,D**)). In summary, FLT3L DCs were more readily activated upon treatment with the F1 OVADex fraction pools, but were poor at stimulating absolute T cell proliferation. This is consistent with the literature, where Korotchenko et al. and Brawand et al. reported a poor T cell stimulating potential but a high capacity for activation [20, 135].

## 3.3 In vivo vaccination with OVADex F2

After assessing the effectiveness of our ovalbumin-dextran neoglycoconjugates in cell culture, we proceeded to test the particles in living model organisms. In the first protocol, we immunized three C57BL/6 mice with unconjugated OVA and all OVADex conjugates. This preliminary protocol consisted of two immunizations in a 14 day interval. We were mainly interested in observing changes in ova specific $T_H1$ and $T_H2$ mediated cellular and humoral immunity. Therefore, we tracked immunocyte activation and IgG production via flow cytometry, ELISpot assay and ELISA. Unfortunately, no induction of cellular immunity was found using flow cytometry or ELISpot assay. Only OVA-specific ELISA titers could be detected in very low dilutions (up to 1:50). As shown in Figure 3.14, deviations between biological replicates were also very high, moreover no antibodies were detected for individuals immunized with 15F2. The antibody levels of the remaining neoglycoconjugates appeared comparable.
Unfortunately, due to the low yield of F1 particles, we had insufficient amounts for a seconds immunization procedure. Since antibody levels appeared relatively similar between F1 and F2 conjugates (except for 15F2), we decided to continue with F2 particles. For the second immunization, we decided to include an *in vivo* cytotoxicity assay, to measure peptide specific target lysis. The generation of a potent $CD8^+$ response is not pivotal for allergen specific vaccination, but is the cornerstone of tumor vaccines. Dendritic cell targeting has been used as a cancer treatment strategy for a long time. Clinical trials with *ex vivo* loaded dendritic cells have been conducted for over a decade [66]. Generally, these therapies were tolerated well and are able to increase cancer specific T lymphocytes, yet tumor control or remission was induced only rarely. Effective reduction in tumor load requires a potent $T_H1$ response, which can be stimulated in mouse models by co-administration of CpG-ODN (TLR9 agonist) [73]. So, we decided immunize the mice three times at 14 day intervals, with the addition of CpG-ODN as an adjuvant.

### 3.3.1 OVADex constructs stimulate potent IgG2c production

Production of specific murine IgG sub-classes is dependent on the surrounding cytokine milieu. IFN-γ is linked to a IgG2c, and IL-4 to a IgG1 dominant antibody response.Consequently, concentration levels of these antibody sub-classes correlate with the corresponding T helper type[7] [136]. To examine total IgG content and antibody polarization in $T_H1$ or $T_H2$ direction, we measured

$IgG_{total}$, IgG2c and IgG1 respectively. Total, circulating IgG only significantly higher at a 1:10000 dilution in the 100F2 and 450F2 treatment groups (Fig. 3.15**A**). Similarly, IgG1 responses between OVA and OVADex were comparably high (Fig. 3.15**B**). In contrast, OVADex conjugates induced potent IgG2c significantly higher with similar responses to OVA with tenfold higher titers compared to OVA. As expected, these results demonstrate a strong $T_H1$ polarization, due to the CpG-ODN administration[8] Interestingly, OVADex conjugates elicited a higher response in IgG2c responses compared to OVA, while total and IgG1 levels were largely similar between the groups. This is consistent with the literature, where Lai et al. found a synergistic effect of mannan and CpG-ODN loaded liposome nanoparticles. They observed a high anti tumor specific response in a melanoma mouse model *in vivo*, compared to the singular use of the respective adjuvants [137].

7: $T_H1$ polarization is associated with potent IFN-γ production, whereas a $T_H2$ response is linked to high IL-4 secretion.

### 3.3.2 High molecular weight dextrans boost OVA-specific IFN-γ production upon immunization

In addition to the $T_H$ specific antibody levels, we measured direct polarization of helper T cells. Thereby, we analyzed the number of IFN-γ and IL-4 spot forming units (SFU) upon stimulation with SIINFEKL, OVA or untreated cell culture medium over night.In addition to the $T_H$ specific antibody levels, we measured direct polarization of helper T cells. Thereby, we analyzed the number of IFN-γ and IL-4 spot forming units (SFU) upon stimulation with SIINFEKL, OVA or untreated cell culture medium over night. SIINFEKL stimulation was performed to examine cytokine production of target specific $CD8^+$ cells. Since SIINFEKL is the dominant cytotoxic epitope of OVA, the presence of specific CTLs would be detected. Unsurprisingly, IL-4 and IFN-γ spot forming units differed strongly in number. As expected for a CpG boosted vaccination, IFN-γ responses were potent, compared to IL-4. The ELISpot assay is a useful tool to differentiate type 1 and type 2 responses, since it has a high sensitivity and is able to detect cytokine secreting cells. This is essential for comparability, since IL-4 is very quickly consumed due to high expression of IL-4R. Moreover biologically active levels are 1000 fold lower than IFN-γ which makes it harder to detect [138]. In summary, ELISpot is an appropriate tool to detect helper polarization, which allows for direct comparisons.

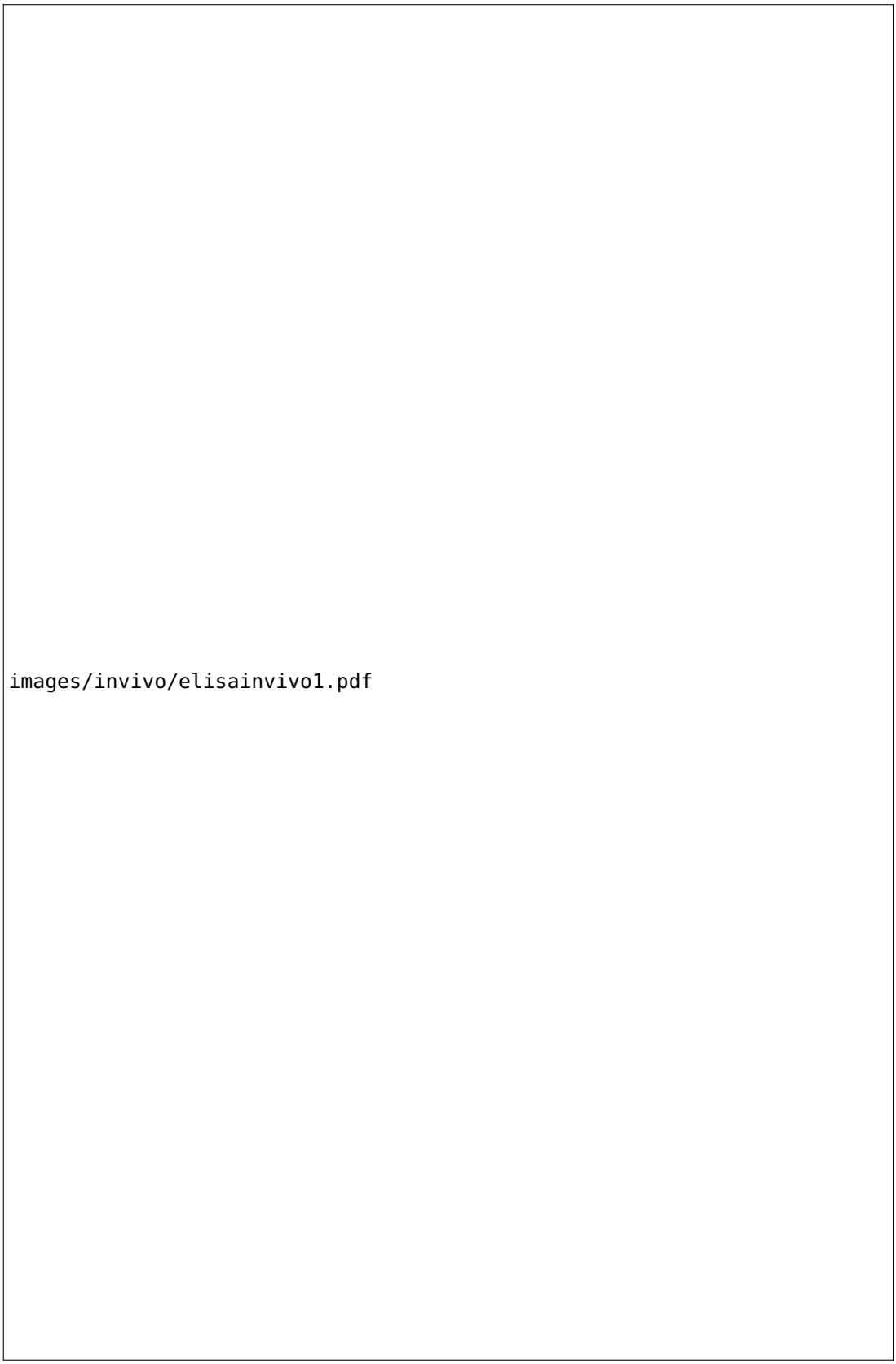


**Figure 3.14:** Anti-OVA ELISA of $IgG_{total}$ (**A**), IgG1 (**B**) and IgG2c (**C**) of the first immunization procedure. Data is pooled from two independent ELISA assays (Dilution: 1000 - 100000) and (Dilution: 50 - 800). The graphs show luminescence intensity over serum dilutions on y-axis (1:50, 1:200, 1:800, 1:1000, 1:10000 to 1:100000). During the first immunization, no adjuvant was used and only two immunizations were performed. *Abb*: RLU: relative luminescence units, Naive mice were used as negative control (naive). F1 stands for the large fraction pool, F2 for the smaller ones. The prefix (15, 100, 450) identifies the respective coupled dextrans in kDa (eg. 100F1 = Large particle pool of 100 kDa dextran covalently linked to OVA).

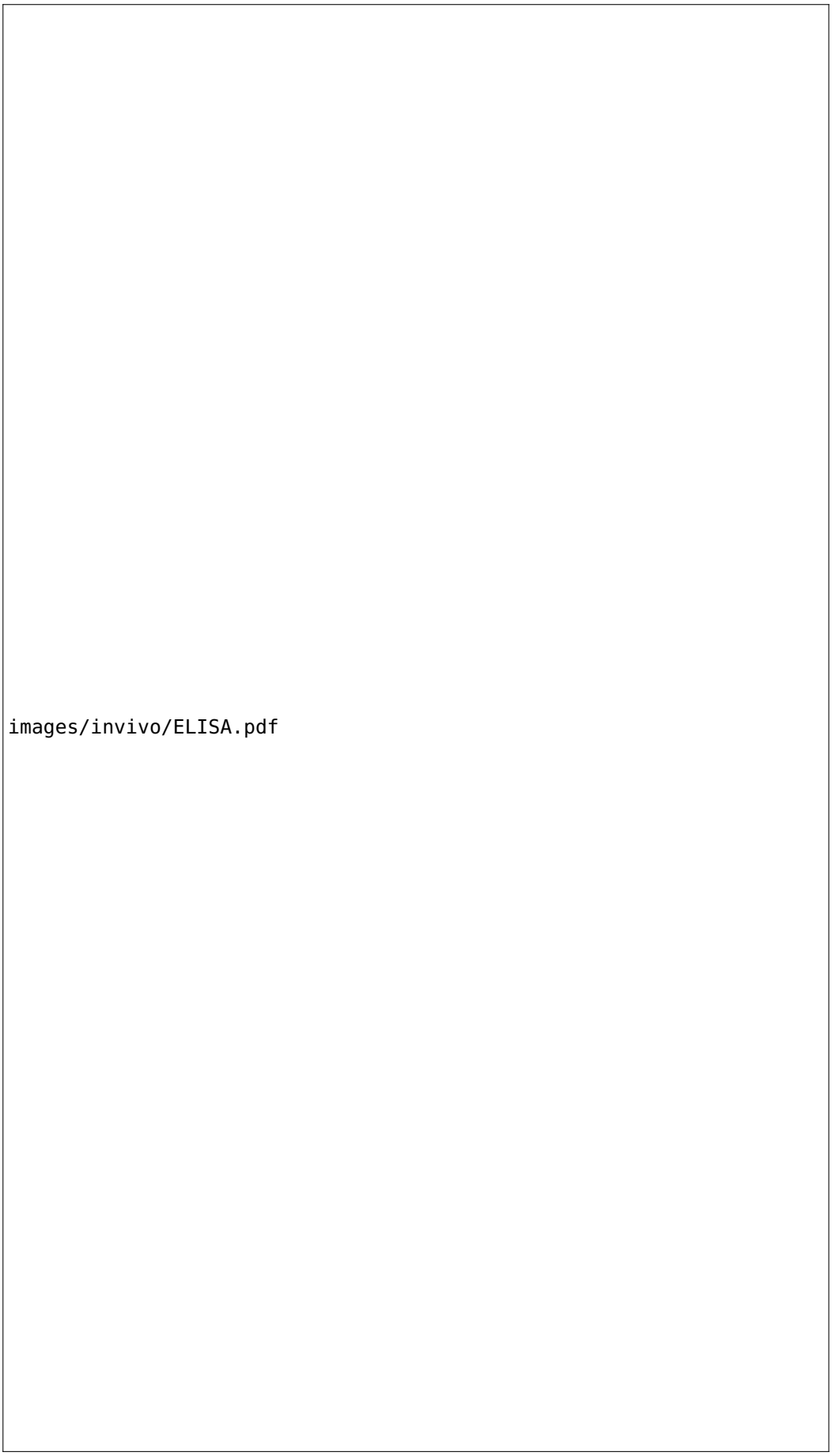


**Figure 3.15:** Anti-OVA ELISA of $IgG_{total}$ (**A**), IgG1 (**B**) and IgG2c (**C**) of the second immunization procedure. Relative luminescence units are on the y-axis and dilution factors on the x-axis. (**A**) shows $IgG_{total}$ levels, (**B**) IgG1 and (**C**) IgG2c. Dunnett's multiple comparisons test was performed on simple effect within rows using GraphPad.*Abb*: RLU: relative luminescence units

Figure 3.16(**B**) Detection of OVA-specific cells in lymph nodes was significantly increased in all treatment groups[9] with large 95% CIs ranging from 56 - 8.5 (OVA) 52 - 9.5 (15F2) 55.3 to 12.7 (100F2) and 52.7 to 10.1 (450F2). Spleenocytes were largely unaffected by OVA stimulation, with one high responder animal in the OVA and 15F2 group (Tab. 3.7(**A**)). Interestingly, stimulation with SIINFEKL did not activate IFN-γ secreting T cells in 100F2 and 450F2 groups. However, OVA and 15F2 vaccinated groups had a higher IFN- response, which was statistically significant between OVA vs. 100F2 and OVA vs. 450F2 in the spleen but not in the lymph nodes. Generally, the highest effect size upon OVA stimulation was found in the lymph nodes, but the highest amount of SIINFEKL specific T lymphocytes were found in the spleens of OVA and 15F2 groups. As expected the $T_H$ 2 signature cytokine IL-4 was barley found on our plates with low absolute counts of 0 - 10 $\frac{\text{spots}}{\text{well}}$.[10] Even though IL-4 is harder to detect, ELISpot data additionally affirms a $T_H1$ biased response. In addition to the ELISpot assay, we examined cytokine levels in the supernatants of four day OVA stimulated lymphocytes from spleen and lymph nodes. The Cytokine profiling using LEGENDPlex showed an significant IFN-γ increase in the spleen and lymph node for 100F2 and 450F2 immunized individuals compared to OVA. Also, an increase in IL-2, IL-17, TNF-α and IL-22 was observed, yet no significance was detected (Fig. 3.16(**E,F**)). Notably, OVA and 15F2 profiles appear relatively similar in the spleen resident immunocytes but not in lymph nodes. In these supernatants only a very low concentration of IFN-γ was found in the 15F2 treatment group.

Taken together 100F2 and 450F2 immunization stimulated comparable numbers of ova-dependent IFN-γ producing cells after 16 hours. Yet, higher absolute levels were recovered after stimulating for four days, with a tendency of increased TNF-α IL-17 and IL-22 levels[11] . 100F2 and 450F2 don't appear to produce a SIINFEKL directed response, thereby other OVA-specific epitopes must be involved in the immune response.

| Groups | P. Diff | Adj P Value |
|---|---|---|
| Lymph node: | | |
| OVA vs. 15F2 | 6791 | <0,0001 |
| OVA vs. 100F2 | -3933 | 0.9973 |
| OVA vs. 450F2 | -7122 | <0,0001 |
| Spleen: | | |
| OVA vs. 100F2 | -26564 | <0,0001 |
| OVA vs. 450F2 | -28356 | <0,0001 |

**Table 3.7:** Summary statistics for cytokine profiles of OVA stimulated supernatants (Lymph node and spleen derived). Computation was performed using a Dunnett's multiple comparisons test for a simple effect within columns (GrapPad). Results are considered significant when adj. $p < 0.05$ *Abb:* Adj: adjusted, P. Diff: Predicted Difference

9: (Medium vs. OVA, adj. p [0.0062-0.0012])

10: In comparison, IFN-γ plates had up 90 $\frac{\text{spots}}{\text{well}}$.

11: IL-17 and IL-22 are signature cytokines of the $T_H17$ helper type pool.

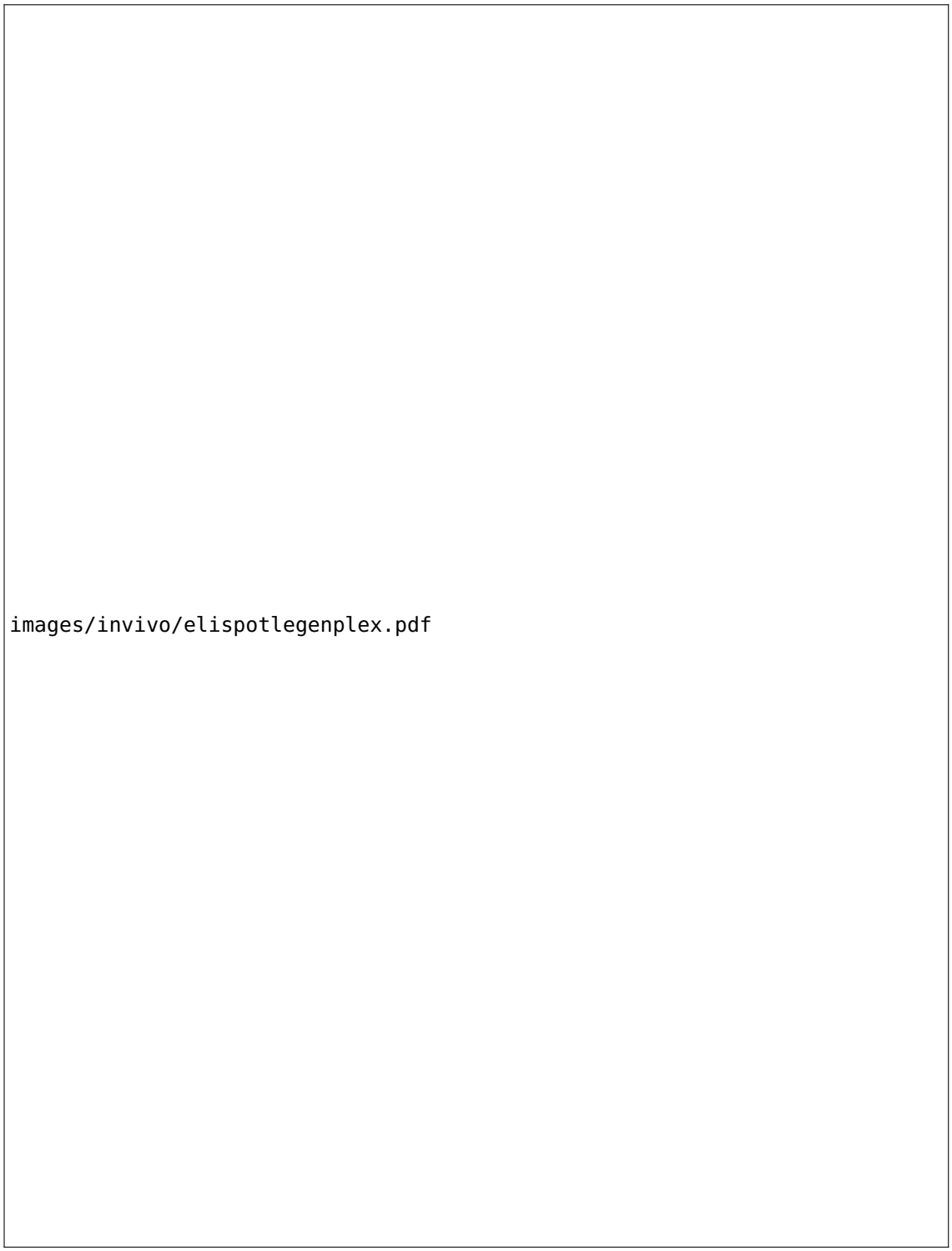


**Figure 3.16:** ELISpot assay and LEGENDplex of pro-inflammatory cytokines of spleen (**A,C,E**) and lymph node resident cells(**B,D,F**). ELISpot cells (**A-D**) were stimulated over night, with regular T cell medium, OVA or the OT-I peptide SIINFEKL. Spot forming units were measured against IFN-γ (**A-B**) and IL-4 (**C-D**). Proinflammatory cytokines measured in supernatants of OVA restimulated (five days) spleen and lymph node resident cells. Dunnett's and Tukey's multiple comparisons test were performed on simple effect within columns using GraphPad. For **E,F** untransformed MFI values were compared statistically and then $\log_{10}$ transformed for enhanced visual discriminability. *Abb.* MFI = median fluorescent intensity, F1 stands for the large fraction pool, F2 for the smaller ones. The prefix (15, 100, 450) identifies the respective coupled dextrans in kDa (eg. 450F2 = Small particle pool of 450 kDa dextran covalently linked to OVA)

### 3.3.3 Higher molecular weight Dextran induces immunocyte proliferation but weak SIINFEKL specific lysis

After re-stimulation of lymph node and spleen derived cells with OVA for four days, we examined the proliferation and maturation of T lymphocytes with flow cytometry. We labeled proliferating cells with Ki67 while effector cells were classified as $CD62^+/CD44^+$. Furthermore we stained for the transcription factor FoxP3, to analyze the presence of regulatory T cells. Activation through OVA and SIINFEKL spiked medium compared to regular T cell medium, was analyzed by Dunnett's multiple comparisons test with matched values - differences were reported when $p < 0.01$. Lymph nodes resident $T_{regs}$ were largely unaffected by antigen stimulation. However, percental spleen resident $T_{regs}$ were significantly reduced upon treatment with SIINFEKL in all groups. Less $T_{regs}$ were also found in OVA treated medium in 100F2, 450F2 and the PBS group. (Fig. 3.18, 3.17 (**B**), Tab. A.1 on page 83).

In lymph node samples, OVA specific increase in proliferating CD8 ($Ki67^+$) cells was observed in for 15F2, 100F2 and 450F2 groups,[12] while specific $CD8^+$ effectors were only increased in 450F2.[13] On the T-helper side ($CD4^+$) 15F2, 100F2 and 450F2 vaccinated effectors increased significantly in OVA stimulated medium.[14] , but no increased proliferation was seen. SIINFEKL stimulation was not followed by a solid expansion of effector or $Ki67^+$ $CD8^+$ cells.

12: (medium vs. OVA, adj. $p < 0.0293$)

13: (medium vs. OVA, adj. $p < 0.0034$)

14: (medium vs. OVA, adj. $p < 0.0292$)

Similar patterns, however clearer effects were observed in the spleen. OVA specific increase in effector CD8 cells were found for the 450F2 group.[15] Moreover, OVA stimulated $Ki67^+$ CD8 cells were increased in 100F2 and 450F2 samples.[16] SIINFEKL triggered effector proliferation in the 15F2, 100F2 and 450F2 groups[17] . OVA specific increase in proliferating $CD4^+$ cells was observed in 15F2, 100F2, 450F2 and PBS immunized groups.[18] 450F2 $CD4^+$ effectors were increased in OVA spiked medium.[19] Generally, the highest effect size in response to OVA medium was observed in spleens of 450F2 vaccinated individuals, also tabulated in Tab. A.2 on page 83. Notably, $Ki67^+$ $CD8^+$ cells were completely abolished upon stimulation with OVA. Furthermore, $CD4^+$ proliferation was highest in OVA and 15F2 groups after SIINFEKL stimulation, yet effector $CD8^+$ cells were activated similarly in all groups. Taken together, we found evidence for a stronger CD4 and CD8 response in 100F2 and 450F2 treated animals compared to OVA. 15F2, on the other hand, produced similar results to uncoupled OVA in our experiments.

15: (medium vs. OVA, adj. $p < 0.0033$)

16: (medium vs. OVA, adj. $p < 0.0068$)

17: (medium vs. SIINFEKL, adj. $p < 0.0095$)

18: (medium vs. OVA, adj. $p < 0.0061$)

19: (medium vs. OVA, adj. $p < 0.0034$)

We were also interested in a dendritic cell mediated, tumor specific response. A successful elimination of malignant cells requires recognition of the cancer specific altered-self antigens[20] and target specific cell lysis. Cross presenting dendritic cells are therefore an attractive and tested target for cancer based vaccine approaches. Over 200 clinical trials[21] on DC targeting have proven a high safety and ability to stimulate an immune response [140], therefore we decided to included an *in vivo* CTL assay. For quantification of specific lysis, donor cells from syngeneic donor mice were pulsed with OT-I peptide (SIINFEKL) and adjusted to a 50/50 ratio with untreated control cells. This suspension was injected into the immunized animals and analyzed after 16 hours. Specific lysis was calculated based on the ratio of recovered control to target cells. Chain length (15 kDa - 450 kDa) dependent decrease in target specific killing was observed in the spleen and lymph nodes of vaccinated mice . This finding is in line with ELISpot data, where 100F2 and 450F2 vaccinated animals only had a weak response to SIINFEKL compared to OVA and 15F2 treatments. However, the flow cytometry analysis of SIINFEKL restimulated $CD8^+$ did not yield a distinct response between the treatment groups.

20: To be exact, this is not the only mechanism for anti-tumor immunity. In addition to the expression of these so called *neoantigens*, genetic instability of the tumor can lead to copy number variations, frame shifts or indels which lead to the presentation of tumor associated antigens. These can be derived from silenced viral proteins, germline antigens, tissue differentiation antigen. Moreover, overexpression of self antigens can also lead to recognition via the immune system [139]

21: State in the year 2018, whereby a large proportion was focused on *ex vivo* loading of dendritic cells


**Figure 3.17:** Flow cytometry data of lymph node resident immunocytes after four days of re-stimulation with medium, OVA or SIINFEKL (**B-F**) or target specific lysis after challenge with SIINFEKL-pulsed cells (**A**). Lymph nodes were harvested after the mice (C57BL/6) were immunized with OVA (black) and OVADex 15F2 (purple), 100F2 (green) and 450F2 (blue) as described in Section 2.3.1. The figures show percentage of FoxP3$^+$ $T_{regs}$ (**B**), CD4$^+$ or CD8$^+$ T-cells with effector phenotype (CD44$^+$ CD62L$^-$) (**C-B**) and percent of proliferating (Ki67$^+$) CD8$^+$ or CD4$^+$ T cells (**C-B**). All cells were gated to live singlets before the percentual fraction was determined. Target cells were pulsed with SIINFEKL and mixed 50/50 with control cells before injection into immunized mice. Target specific lysis was determined after 16h, as the ratio of target/control cell recovery **A**. Dunnett's multiple comparisons test was performed with GraphPad. *Abb.* All treatments were from the smaller F2 fraction pool, the number prefix shows the respective dextran used for conjugation (15 kDa, 100 kDa and 450 kDa)

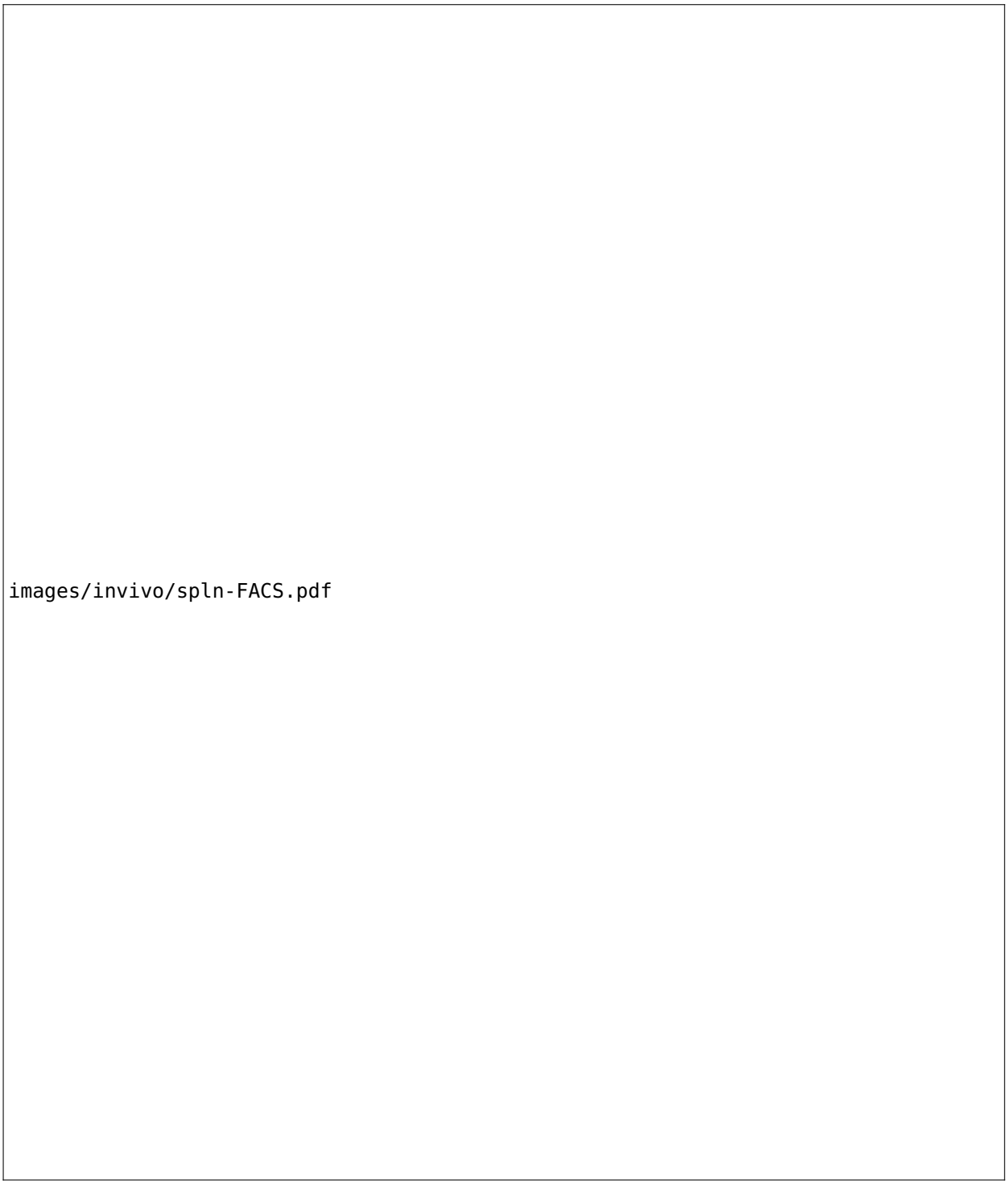


**Figure 3.18:** Flow cytometry data of spleen resident immunocytes after four days of re-stimulation with medium, OVA or SIINFEKL (**B-F**) or target specific lysis after challenge with SIINFEKL-pulsed cells (**A**). Lymph nodes were harvested after the mice (C57BL/6) were immunized with OVA (black) and OVADex 15F2 (purple), 100F2 (green) and 450F2 (blue) as described in Section 2.3.1. The figures show percentage of FoxP3$^+$ $T_{regs}$ (**B**), CD4$^+$ or CD8$^+$ T-cells with effector phenotype (CD44$^+$ CD62L$^-$) (**C-B**) and percent of proliferating (Ki67$^+$) CD8$^+$ or CD4$^+$ T cells (**C-B**). All cells were gated to live singlets before the percentual fraction was determined. Target cells were pulsed with SIINFEKL and mixed 50/50 with control cells before injection into immunized mice. Target specific lysis was determined after 16h, as the ratio of target/control cell recovery **A**. Dunnett's multiple comparisons test was performed with GraphPad. *Abb.* All treatments were from the smaller F2 fraction pool, the number prefix shows the respective dextran used for conjugation (15 kDa, 100 kDa and 450 kDa)

# 4 Discussion



Traditionally, vaccines were successfully deployed against transmission and malady of infectious diseases. Rooted in deeper understanding and an uprise of non-communicable diseases, more and more sophisticated types of vaccines against non-infectious illnesses are developed [46]. Emerging targets are diseases that are immune-modulated and have a high burden on public health. Among the researched areas, allergy and cancer-related therapies show promising results, with increasing safety and efficacy over the years [141, 142]. Allergic diseases have high prevalences, which range from 1 - 20 % in different countries[1] , thus affecting many people over the globe. Most allergies don't result in the death of the affected person, yet they can severely impact quality of life and cause high costs in the health sector [143]. Cancer also poses a large burden on human well-being and is the second leading cause of death worldwide. To make things worse, cancer cases are also rising, with an 33 % increase between 2005 and 2015 [144]. Therefore, potent immunizing therapeutics targeted against allergy and cancer are highly researched. The underlying molecular mechanisms are inherently similar, in that they both aim to activate an adaptive immune response. But due to the different nature of the diseases, application-specific intricacies must be considered when designing a novel formulation. For developing an effective allergy vaccine, minimizing the allergenic potential of the compound is critical, while cancer-targeting approaches aim to evoke a robust $T_H1$ driven cytotoxic response.

1: In western countries, the prevalence of type I allergies is sometimes up to 30 % [47].

To maximize the benefit of an acute type allergy therapeutic, the production of high amounts of blocking antibodies is desired. These IgG antibodies down-regulate the degranulation of IgE loaded mast cells and eosinophils, thus lowering the level of suffering for the patient. Successful therapy is also manifested in a reduction of $T_H2$ polarization. Signature cytokines from type 2 helpers, [2] are responsible for IgE isotype switching of B cells and thus for loading of Fcε receptors on mast cells and eosinophils. Induction of blocking IgG-antibodies can reprogram these loaded granulocytes. Thereby, mast cells and granulocytes switch away from producing IL-4, thus shifting the immune system back towards homeostasis [145, 146]. Moreover, a response is thought to be linked to the induction of a $T_H1$ helpers and $T_{regs}$ [147]. A promising candidate can therefore be considered immunogenic and hypoallergenic.

2: Most prominently IL-4, IL-5 and IL-13.

In essence, malignant transformations cause an altered (non-self)

phenotype of cancer cells, often discernible by the expression of neoantigens [3] . Due to rapid proliferation in an environment with selective pressure, tumor cells often develop a complex line of immune subversion strategies. Hence, therapeutic tumor-specific immunotherapy aims to evoke a strong activation of cytotoxic T lymphocytes, preferably against specific neoantigens of the malignant cells. Depending on the molecular dynamics of the tumor environment, these CTLs can then infiltrate the cancerous tissue and induce target specific lysis [148]. Successful cancer vaccines must therefore be immunogenic, with a bias towards a $T_H1$ response

3: These are novel antigen variants, caused by the mutated genotype of the tumor. Thereby, DNA mutations are translated into altered protein variants with new epitopes that appear foreign to the immune system

Since dendritic cells are the major mediators between innate and adaptive immunity and the dominant initiator of antigen-specific immune responses, they are regarded as highly attractive targets for immunotherapies. The expression of a broad range of danger and pathogen sensing receptors has encouraged many immunologists to develop targeted therapeutics, specifically tailored to these receptors. In this study, we created neoglycoconjugates in order to target carbohydrate specific C-type lectin receptors on dendritic cells. This strategy has been demonstrated before and showed high tolerability and immunogenicity [20, 23, 24, 113]. Here, we created glycoprotein conjugates consisting of ovalbumin and dextran (OVADex) and investigated their immunogenic and allergenic potentials *in vitro* and *in vivo*. In that, we studied the activation of dendritic cells in isolation and their potential to stimulate $CD4^+$ T cell proliferation, as well as the degranulation of pre-sensitized basophils in cell culture. Furthermore, we studied the immune response to OVADex immunization in C57BL/6 mice. In this chapter, I want to discuss the production process of OVADex first and then critically debate the results of the *in vivo* and *in vitro* experiments.

## 4.1 OVADex preparation

Coupling of variable chain-length Dextrans to OVA was a multi-step process, which is apart from testing and subsequent validation, achievable in a short time (Tab. 4.1). Testing and validation can demand grand timely investments - therefore, multiple preparations in parallel are highly recommended. High throughput was not achievable with our setup, especially concerning the F1 fractions, protein recovery was < 10 % (Tab. 4.2). Low mass yield of F1 fractions ultimately obstructed us from testing the potency *in vivo*, therefore conscious planning, considering our yield, should be implemented. Similarly, Weinberger et al. generated mannan

| Step | Duration |
|---|---|
| Triton method | ≈ 1d |
| Oxidation of Dextrans | ≈ 1.5d |
| One-pot conjugation | ≈ 2d |
| Size exclusion chromatography | ≈ 2d |

**Table 4.1:** Very rough outline of the preparation workflow. Clearly concentration measurements have to be performed in between - those assays are usually not too time consuming though. Oxidation duration depends mainly on dialysis time, conjugation duration depends on incubation time (typically 24h - 72h) and purification depends on heavily on sample quantity and total fractionized volume.

| Fraction | Abs. yield | % of total |
|---|---|---|
| 15F1 | ≈ 420 µg | 4.2 % |
| 15F2 | ≈ 2.5 mg | 25 % |
| 100F1 | ≈ 585 µg | 5.89 % |
| 100F2 | ≈ 2.3 mg | 23 % |
| 450F1 | ≈ 630 µg | 6.3 % |
| 450F2 | ≈ 2 mg | 20 % |

**Table 4.2:** Yield of nanoparticles based on protein concentration - as assessed by Amino acid analysis. Percent/total was calculated according to the 10 mg OVA used for each dextran.

and dextran glycoconjugates, but only yielded sufficient amounts of mannan particles for *in vitro* and *in vivo* testing.

The largest average size differences were observed between Fractions (F1 vs. F2) rather than between relative dextran lengths (15kDa vs. 100kDa vs. 450kDa) - less polydispersity would also be desirable to make size-dependent predictions more robust. The most heterogeneous construct was 450F2, which had two distinct peaks in the size distribution (Fig. 3.3). We can speculate that this additional peak might be due to a higher degree of freedom for binding. Thereby, a longer dextran chain has more conformational degrees of freedom because the possible distance between aldehyde groups is larger. On the other hand, it is also important to consider that the individual dextrans did not have a homogeneous molecular weight. We only referred to them as 15 kDa, 100 kDa and 450 kDa for enhanced readability and interpretability. What we referred to as 15 kDa dextran has a declared range of 15 - 25 kDa, while 450 kDa dextran is labeled with 450 - 650 kDa. Only 100 kDa dextran was precisely labeled with 100 kDa by the manufacturer (Sigma-Aldrich). Hence, the large molecular weight distribution (200 kDa) for 450 kDa dextran might be responsible for heterogeneous size distribution of the F2 fraction pool. In contrast, the absolute molecular weight distribution of 15 kDa is very small (5 %) compared to 450 kDa dextran (10 kDa vs. 200 kDa). This might also be a reason why 15F2 OVADex appeared homogeneous compared to 450F2. These presumed steric effects were not observed in F1 fraction pools. This can be explained by cross-linking of multiple OVA molecules by individual dextran chains. Due to the large size of these multimeric OVA fractions, variations in conformational arrangements would be hard to detect.

Binding to conA during MST confirmed the biological integrity of the dextrans after oxidation and conjugation. Interestingly, conjugation of OVA to dextran decreased binding strength in the 15 kDa particles (Fig. 3.9). In contrast, 100 and 450 kDa dextran particles showed higher binding affinities, but are reported with caution due to the high standard deviations. In general OVA had higher affinity to conA, therefore the differences in binding strength might be due to di- or oligomerization of OVA. For precise conclusions, it would have been more relevant to test the binding capacities to the actual receptors. Unfortunately, no receptor binding assay commercially available, therefore we decided to test for conA binding ability. Takahara and colleagues observed size dependent binding of dextran to SIGNR1 and SIGNR3 and Langerin, which all contain an EPN binding motif in their carbohydrate recognition domain [11]. In contrast, carbohydrate binding to conA is mainly mediated through the hydroxyl groups on C-6, C-4 and C-3 carbons. Nevertheless, Coulibaly and colleagues speculated that binding

affinities of conA are size dependent. In their study, they measured glycogen and mannan binding, whereby glycogen had a lower apparent dissociation constant. These findings were surprising and best explained by the differences in molecular weight, branching patterns and steric effects [133]. Even though, no receptors were available conA was useful for assessing binding capabilities of OVADex conjugates. Because conA also binds OVA independently, we were able to compare binding strength of the conjugates to uncoupled OVA.

Strikingly, the mass ratio of OVA to Dextran was inversed between F1 and F2 fractions (see. 3.1.4 on page 42) - whereby the larger fractions had high protein and F2 had high carbohydrate content. Generally, a higher molecular weight was associated with higher Dextran content. Glycostaining of the polyacrylamide gels confirmed these results as bands appeared dimmer in 15F2 than 100F2/450F2. Control runs of uncoupled Dextrans in the SE-FPLC yielded carbohydrates after ≈ 150 mL (Fig. A.4**(B))** as determined by Anthrone assay - thus unbound Dextrans in the F2 pools could be thinkable. As expected due to the lack of charge from SDS, negative controls,[4] were not detectable on the PAGE gels (Fig. 3.8). This illustrates the presence of Dextran covalently bound to OVA, otherwise no visible carbohydrate stain would have been present. However, gel eletrophoresis does also not rule out residual contaminations with uncoupled dextran, because it might have been co-migrating with the OVADex particles. Based on hydrodynamic radii of the individual dextrans and OVA we deduced that cross-linking of multiple OVAs with dextran chains occurred in all F1 constructs, whereas F2 pools were likely mono/oligomeric protein fractions. Interestingly, monomeric[5] F2 fractions of our nanoparticles were lower in size than comparable laminarin-ovalbumin glycoconjugates generated by Korotchenko et al. [20]. In their study they measured an average size of 8.3 nm for their conjugates, although laminarin has a lower molecular weight (4.5 kDa) than the dextrans in the present study (15 kDa - 450 kDa). Models of flexibility and conformation of various polysaccharides indicate steric and mechanical variations between the glycosidic binding modalities [127, 149]. Therefore, we hypothesize that the different rigidness of glycosidic linkages between dextran and laminarin [6] might cause the variation in hydrodynamic sizes. The authors also reported a different coupling rate than we found in our setup. While an average of 6 Lysine residues was coupled to ovalbumin in their experiment, we measured 6 - 10 coupled Lys. The additional coupling of 4 Lysine residues might also be explained by different degrees of branching between dextran and laminarin.[7] Weinberger et al. tested glycoconjugation of dextran to OVA and papain[8] before. In their study, they compared coupling of 46 kDa mannan[9] to 40 kDa and 6 kDa dextran. Unfortunately, their

4: Non conjugated dextrans (15 kDa, 100 kDa and 450 kDa)

5: Based on the number of ovalbumin molecules

6: Dextran consists predominantly of α-1↦6 bonds, while laminarin is mainly linked via(1 ↦ 3)-β-bonds

7: Inaccuracies of the measurement method might contribute to some variation, as seen for the 22 measured Lysines instead of 20 Lys during the ovalbumin run. Yet, consistent deviations of 4 amino acids for multiple OVADex conjugates are highly unlikely and therefore not discussed.

8: A plant protease naturally occurring in papaya [150].

9: Mannan is a broadly used term applicable to linear polymers of mannose residues and cell wall constituents of yeast cell walls [147]

OVA-dextran constructs precipitated after conjugation and were therefore not further tested for immunogenicity and allergenicity in their publication. Dynamic light scattering measurements showed an average hydrodynamic radius of 4.7 nm for 40 kDa coupled dextran, which is in good agreement with our data (15F2 = 5.6nm, 100F2 = 4.1 nm). In contrast to the publication, our procedure yielded two distinct fraction pools, while Weinberger et al. saw a heterogenous band, spanning the whole range of their denaturing PAGE gels (> 250 kDa to > 25 kDa). The authors also mentioned a different efficiency rate of carbohydrate coupling to papain and ovalbumin respectively. Thereby, papain was more efficiently coupled to carbohydrates, yet resulted in more heterogeneity and more complex particles. This was attributed to the higher number of disulifide bridges in papain compared to OVA.

In summary, our study is is line with previous glycoconjugation studies in which demonstrated successful carbohydrate to protein linkage via reductive amination [20, 23, 24]. In the following sections, I outline the immunological testing procedures and draw comparison to the current literature.

## 4.2 Immune responses to OVADex

Helft et al. showed that GM-CSF derived murine BMDCs comprise a heterogenous population of macrophages, dendritic cells and granulocytes *in vitro*. Generally, the population of interest for many immunological researcher has a $CD11c^{+}MHC\text{-}II^{+}$ phenotype, and is often regarded as pure DC population. Yet, even this population is heterogenous and divisible into dendritic cells[10] and monocyte derived macrophages. Although both have a similar phenotype, each cell type has distinct transcription programs and evoke specific immune responses upon stimulation [62]. In contrast, FLT3-L derived murine BMDCs are a mixture of myeloid and plasmacytoid DC ($CD11c^{+}B220^{+}$) in cell culture. These DCs showed non-overlapping TLR expression, were poor at T cell induction and were classified as immature by the authors [135]. Xu and colleagues compared both DC culture systems[11] functionally and phenotypically. They concluded that FLT3L derived DCs represent steady-state DCs, whereas GM-CSF BMDCs represent inflammatory DCs [61]. Those findings were also confirmed in our laboratory (unpublished).

Since the dynamic skin landscape comprises a large palette of professional antigen presenting cells,[12] we decided to generate both, GM-CSF and FLT3-L dendritic cell cultures, in order to model the activation of as many *in vivo* APC subclasses as possible. We also considered to cultivate Langerhans cells *ex vivo*, unfortunately

10: These dendritic cells develop in the expected manner, namely from a common DC precursor to a pre-DC before fully developing to a naive DC.

11: They supplemented GM-CSF cultures with IL-4.

12: The murine skin APC repertoire consists of: classical DCs, Langerhans cells, dermal DCs, monocyte derived DCs and macrophages. Additionally, circulating plasmacytoid DCs can rapidly infiltrate skin tissue upon injury by sensing nucleic acids [151, 152].

no established protocol was available at that time and we decided to omit this cell culture experiment.

Our *in vitro* GM-CSF or FLT3-L - BMDC cocultures with naive T cells, demonstrated the potential of OVADex to dose-dependently stimulate an APC mediated MHC-II dependent $CD4^+$ activation - by increase in cell number and effector maturation. No direct comparison between the two culture systems was set-up, therefore no statistical comparison between the two methods was performed. Generally, the patterns of activation were largely similar. Additionally, the analysis of cytokine secretion did not produce analyzable results with one technical replicate and high noise. Further limitations were the lack of a replicate for the FLT3-L culture, moreover the low number of live cells in the experiment did not enable a reliable analysis of effector status. The larger F1 fractions, continuously showed highest immunogenicity in co-cultures with GM-CSF or FLT3L derived BMDCs (see. Fig. 3.11). As expected from the literature, we observed a lower absolute proliferation rate of OVA-specific $CD4^+$ T lymphocytes in FLT3L DC cocultures than in GM-CSF. FLT3 derived DCs closely resemble a immature DC phenotype, which are known to be poor at in inducing T cell activation [135]. This has also been validated by Korotchenko and colleagues, where GM-CSF derived BMDCs were more effective at mounting T cell proliferation [20].

Activation of both BMDC populations (GM-CSF / FLT3L) showed an upregulation of CD86 at the highest administered doses. But FLT3L DCs seemed to be triggered stronger upon treatment than GM-CSF DCs. This is clearly seen by the high CD86 upregulation of FLT3L DCs after treatment with F1 glycoconjugates (15F1, 100F1 and 450F1) at 10 $\frac{\mu g}{mL}$. In contrast, only OVADex 15F1 was able to stimulate CD86 upregulation of GM-CSF DCs (see. Fig. 2.2.4(**A**,**B**)). CD40 upregulation followed a similar trend in both DC cultures, yet the effect size was smaller than in CD86. These observations were expected, since FLT3 derived DCs have a lower degree of pre-activation, they can be activated more strongly than GM-CSF DCs. Surprisingly though, LPS induced strong upregulation of CD86 in FLT3L BMDCs, which is not consistent with data from previous publications [20, 135], where FLT3L showed lower expression of TLR4 and a weaker response to endotoxin than GM-CSF BMDCs. Since we performed independent experiments with GM-CSF and FLT3L DCs, we can not rule out concentration variations in LPS aliquots, therefore the absolute response to LPS should be considered with caution.

No dose-escalation experiment was performed, where the maximum tolerable dose could have been determined. Co-culture and activation experiments might subsequently show different effects or stronger patterns at higher doses. Additionally, higher

doses might have enabled conclusions from cytokine profiling experiments. Korotchenko et al. used laminarin-ovalbumin glycoconjugates at concentrations up to 50 $\frac{\mu g}{mL}$, which might have lead to more reliable effects in our study as well [20]. OT-I co-cultures were also set up, but consistently showed high cell counts in sham treated wells (T cell medium) compared to the treated wells and the positive control (SIINFEKL). Unfortunately no cause could be elucidated with subsequent experiments[13] One untested difference to the literature, is the lack of DC pulsing. As presented by Helft et al. [62], APCs in their $CD8^+$ cell culture experiments were pulsed with antigen and washed before culturing them with naive OT-I cells. Excess peptide-antigen in the medium could have led to auto-reactive CTL clones, resulting in low viable cell counts. These concerns were not tested experimentally, thus - mistakes, contaminations or other experimental flaws could not be excluded - subsequently the OT-I data is not presented in this thesis.

13: We also tested naive OT-I cells from $RAG^{-/-}$ mice, in order to exclude proliferation from other antigens. We also treated whole spleen cell suspensions to exclude problems with DC cultures. Unfortunately all strategies were unsuccessful, so OT-I cocultures were omitted.

Even though no phenotyping of the antigen presenting cells in culture was carried out, these experiments support the notion of effective targeting *in vivo*- based on publications from our group [20, 23, 24]. As mentioned in the chapter 1.4.3.3, our group demonstrated the role of active transport to the draining lymph node via FITC-dextran before. Compared to s.c injection of the analyte, no or low amounts of circulating dextran was found in subcapsular sinus, indicating the role of active transport - especially by $CD207^-/CD11b^+$ DCs. Both, GM-CSF and FLT3L derived BMDCs, comprise $CD11b^{high}$ DCs [61] thus effective targeting in culture might be linked to a higher active transport *in vivo*, but is not experimentally verified in this study.

In the present thesis, we were able to validate the allergenic reduction of OVA by carbohydrate coupling shown before. The RBL assay indicates a stronger shielding of allergenic epitopes for the larger particles, based the highest maximum effect in 15F2. This particle has a larger hydrodynamic radius than 100 and 450 kDa OVADex conjugates from the F2 fraction pool, but apparently provided less effective shielding of allergenic epitopes. Based on our assumptions, the longer chains of 100 kDa and 450 kDa dextrans might be wrapped around OVA more easily and subsequently cover more epitopes. More data with higher antigen doses would be desirable, in order to validate or falsify these assumptions in the future. The collective findings of our cell culture experiments is inconsistent with our $Hypothesis_{1+4}$.[14] . As shown in Figures 3.11 on page 50 and 3.12 on page 51, conjugation alone did not potentiate the immuno-stimulatory effects of OVA. F2 OVADex particles were often comparable or worse than uncoupled OVA in our setup. [15] Furthermore, in our experiments hypoallergenicity was rather dependent on chain length than on particle size. As

14: $H_1$: "Conjugated ovalbumin-dextran particles have a higher immunogenic potential than ovalbumin alone"
$H_4$: "Allergenicity of OVADex particles decrease with size"

15: With the exception of 15F2 in the FLT3L experiment.

shown in Figure 3.10 on page 49 the 15F2 particle elicited the strongest degranulation reaction overall. The residual F2 particles, 100 and 450 conjugates were smaller in radius[16] than 15F2 which led to the assumption that enhanced allergenic epitope shielding is provided by longer glucan chains rather than size. In that, only one of five IgE dominant ovalbumin epitopes identified by Mine et al. contains a Lysine residue (see. Tab. 4.3 [153]. Therefore coupling related epitope alterations are not critical for allergenic shielding. It is plausible that higher molecular weight is relevant for the steric hindrance of interaction between IgE and allergenic epitopes. This is also reflected in the studies with laminarin and mannan coupling to allergens. Compared to their respective uncoupled controls, 4.5 kDa laminarin-ovalbumin conjugates were 5fold less allergenic [20], while allergenic reduction of 46 kDa mannan-papain conjugates was over 1600fold higher. Interestingly Weinberger et al. also conjugated mannan to ovalbumin, where they found no difference in degranulation to the uncoupled control. In the same study, the authors produced papain glycoconjugates with 40 kDa dextran. These particles were 105fold less immunogenic than papain [23]. These results show a lower efficiency of allergenic shielding upon conjugation with OVA compared papain. Therefore, our results of approximately 2 - 3 fold increased hypoallergenicity upon conjugation, also fall in line with their observations.

16: 100F2: 4.1 nm, 450F2: 4.8 nm, 15F2: 5.8 nm

Pre-clinical research with laser-facilitated delivery of glycoconjugates has already been demonstrated to be effective and safe in allergen models. Weinberger et al. investigated the immune responses to a common birch pollen allergen "Bet v 1" upon coupling to mannan. They found high blocking antibody levels after two immunizations with the neoglycoconjugates but not with uncoupled allergen administered with mannan. [24]. Furthermore Korotchenko and colleagues have observed high production of blocking antibodies upon administration of laminarin-ovalbumin conjugates without generating a strong shift towards $T_H1$ / $T_H17$ [20]. Similarly, our neoglycoconjugates induced a boost in antibody production compared to uncoupled OVA. In contrast to these publications, we did co-administer CpG-ODN as an adjuvant, thus we did observe a potent polarization towards the IgG2c compared to IgG1. In that, our immunization experiment showed a rise in $T_H1$ polarized humoral immunity by conjugation of dextran, demonstrated by ≈10x higher IgG2c titers. Subsequently, Korotchenko and colleagues did not observe $CD4^+$ T cell activation *in vivo*, whereas the higher molecular weight OVADex conjugates 100F2 and 450F2 stimulated a T cell response. Shifts in cellular phenotypes showed a a similar pattern in spleens and lymph nodes. 100F2 and 450F2 immunized animals, had higher occurrence of OVA specific proliferating $CD4^+$ and $CD8^+$ lymphocytes and more cells with effector phenotypes. Kumar and colleagues studied different combinations

| AA code | SequenceID |
|---|---|
| LAMVYLGAKDST | 38–49 |
| DVYSFSLA | 95–102 |
| EDTQAMPFRV | 191–200 |
| VLLPDE | 243–248 |
| GLEQLESIIN | 251–260 height |

**Table 4.3:** Amino acids and their sequence position of ovalbumin IgE epitopes

| SequenceID | AA code |
|---|---|
| $OVA_{27–35}$ | IFYCPIAIM |
| $OVA_{97–105}$ | YSFSLASR |
| $OVA_{208–216}$ | VQMMYQIG |

**Table 4.4:** List of non-Lys containing epitopes, shown to induce IFN-γ–secreting, $CD44^{high}$, $CD8^+$ T cells. *Abb:* AA: amino acid

of adjuvants for treatment of OVA-sensitized BALB/c mice upon ablative laser microporation. They combined calcipotriol (VD3) and CpG-ODN adjuvants to generate $T_{reg}$ expansion via IL-10 and TGF-β while also producing high levels IL-12 and $T_H1$ associated IgG2a. In contrast, administration of CpG-ODN alone, produced higher levels of IgG2a and IgG1 but lower levels of OVA-specific $T_{regs}$[154]. Those findings are similar to our results, with the exception of the high IgG1 titers. This might be explained in the genetic differences between C57BL/6 and BALB/c mice. It has been shown before that C57BL/6 are more prone to a Type 1 response, whereas BALB/c mice more towards a $T_H2$ polarization [155].

Surprisingly, SIINFEKL stimulation did not induce major differences in cell proliferation between the treatment groups. Using an ELISpot assay, we found a difference between OVA immunized and 100F2/450F2 spleen resident immunocytes stimulated with SIINFEKL. Interestingly, these results could be explained by the presence of non-SIINFEKL specific CD8 effectors. As shown in Figure 3.16**A**, counts of SIINFEKL specific IFN-γ producing spleenocytes were significantly lower in the 100F2 and 450F2 groups compared to OVA. In contrast, OVA specific IFN-γ producers were found in these OVADex treatment groups, thus indicating the existence of alternative immunogenic epitopes. During the reductive amination reaction, the surface accessible Lys residue (see. Fig. 3.6(**C**)) of OVA might have been coupled to an aldehyde group of the present dextran. We speculate that these covalent bonds might be resistant to cytosol and vacuolar degradation processes necessary for antigen cross-presentation, because both pathways cleave peptide bonds [156]. Interestingly, Karandikar et al. found additional subdominant, epitypic CTL sequences, namely, $OVA_{27–35}$, $OVA_{97–105}$ and $OVA_{208–216}$ which commonly lack a Lys residue (Tab. 4.4) [157]. We suspect that these epitopes might be immunodominant in our 100F2 and 450F2 treatment groups, yet we don't have experimental evidence for it. As expected from these findings, SIINFEKL pulsed target cells in our experiment were not lysed in 100F2 and 450F2 but in OVA and 15F2 treatment groups. Interestingly, Braders et al. studied degradation rates of dextran complexed biomolecules for immunotherapies. They created acetalated dextran which is insoluble in water and readily dissociated under acidic conditions. Their particles were consequently loaded with ovalbumin and showed hydrodynamic radii of 150 - 385 nm. The authors also compared dextrans of different molecular weights and found different degradation rates which in turn dictated presentation efficiency[17] [158]. As explained above, we suspect that alternative immunogenic OVA-epitopes were processed in 100F2 and 450F2 vaccinated mice. Due to the lack of experimental evidence the lack of SIINFEKL specific target lysis might also be caused by impaired processing and presentation of these particles

17: Generally, smaller dextrans resulted in faster degradation rates and thereby induced stronger MHC presentation. This was not true for 5 kDa Dextran which caused ≈ 75% less presentation than 10 kDa dextran. The latter, was the best performing candidate in their study overall.

in the MHC-I pathway. Based on this assumption, the high IFN-γ production must be caused by non CTL-T cells, like $CD4^+$ T cells or NK cells [93].

Taken together, *in vivo* data concerning $Hypothesis_1$ largely contradicts the cell culture studies, in that F2 fractions elicited stronger immune responses than uncoupled OVA. We recommend to carefully examine immunodominat epitopes for their lysine residues and surface accessibility in order to preserve the maximum number of peptides for MHC presentation. We were not able to make strong deductions for $Hypothesis_2$, since F2 fractions were relatively similar in size. We were only able to test the multimeric OVADex particles in the preliminary *in vivo* experiment, which produced results with high standard deviations. Nevertheless, as shown in Figure 3.14 a $T_H1$ driven IgG2c production was almost completely absent in OVA and F2 treated groups, whereas 15F1 and 100F1 groups had comprised some high responder animals. Furthermore *in vitro* data provides strong indications that larger, multimeric constructs stimulate a higher degree of immune activation. This prediction would fall in line with reports from the literature. Amy Rosenberg reviewed the effect of protein aggregation on immune responses. She concluded that protein multimers are generally more immunogenic than their non-aggregated variants [159]. Therefore we would also predict a stronger immune response of the multimeric OVADex particles (F1) compared to the smaller mono- or oligo-meric conjugates (F2) *in vivo*.

## 4.3 Limitations

As criticized above, no dose escalation tests were performed, thereby no upper tolerable limits can be reported. Yet, immunization of C57BL/6 mice was not associated with any adverse reactions upon visual inspection. The heterogenous antigen presenting cells were not phenotyped, nor the specific receptors used for testing binding capabilities. MHC-I dependent activation was not shown *in vitro*, because naive CD8 cell proliferated unspecifically. Moreover, the *in vivo* experiment did not allow for a wholesome conclusion because we were unable to immunize with multimeric F1 particles. Lastly, we did not proof the existence of alternative immunogenic non-SIINFEKL epitopes. Unsuccessful experiments or conflicting data was reported transparently, to ensure maximal reproducibility and scientific value of the study. Despite our limitations, most of the generated data falls in line with currently available literature. Whenever we were not able to make unambiguous conclusions from our readouts we tried to discuss issues critically and want

to encourage readers to examine our provided resources on their own.

## 4.4 Final thoughts

In summary, production of novel glycoproteins has been described before and is a feasible approach to tackle problems in immunological research - mainly with the goal of enhancing antigenic immunogenicity and tolerability. Coupling of laminarin and mannan has shown promising results for allergen-specific immunotherapy in a murine model of allergic asthma [20, 24]. Moreover, skin immunization is of increasing interest due to the specialized immune landscape associated with favorable immune responses. Epicutaneous laser facilitated immunization with dextran is sensible, yet a direct comparison of immunogenicity and allergenicity against other polysaccharides would help to identify the most promising candidates for future therapy designs.

Another possible direction would be additional chemical modifications, like antigen coupling via a pH-sensitive linker, or a direct incorporation of adjuvant into a dextran-based matrix. Acetalation of dextran can enhance the efficiency of MHC-I restricted presentation pathways [158]. Furthermore, a microparticle structure generated via acetalated Dex, was shown to reliably transport the TLR7 agonist imiquimod [160]. While OVA was cleaned manually in this work, prior formulations relied on Endofit® OVA (sterile, free of endotoxins). Dextran mediated stimulation did evoke immune responses *in vitro* and *in vivo*. As discussed above, it could still be worthwhile to explore the immunogenicity of Dextran in the future. It might be wise to seek an approach with modified Dextran to enhance intracellular processing and subsequent antigen presentation - or boost its interaction with PRRs. Yet, this raises the question whether such an approach is worth the resources. The literature comprises a repertoire of pathogen associated polysaccharides - especially β-Glucans - which have more detailed reports on the interaction with CLRs on APCs. However, dextran is commercially available in many different sizes, which makes it attractive for fine tuning nanoparticle design. Dextran is also convenient because of it's high solubility in water and high safety profiles. If further studies show a weaker immunogenic profile of dextran compared to other polysaccharides, the chemical flexibility and safety might still be a good reason to further create novel nanoparticle-based vaccines.

As shown before, mannan or fucose residues are usually the natural ligands of CLRs and thereby show higher binding affinities than dextran [11, 161]. Therefore, mannose- or fucosylation of dextran

polymers is a interesting approach for the design of future nano-vaccines. Especially multivalent synthetic carbohydrates can be modified for improved binding affinities. Kiran and colleagues have demonstrated strong binding affinities of synthesized linear and hyper-branched mannan and fucose glycol-polymers against DC-SIGN and MBL. Interestingly, they saw a binding preference for branched conjugates with MBL, while DC-SIGN had clear binding preferences for the linear carbohydrate polymers [162]. The authors used polyethylene glycol as a backbone for carbohydrate functionalization. They used unconjugated PEG in their control experiments and observed no binding to either one of the receptors. As shown by Cui et al. dextran based pH-sensitive polymers can also be mannosylated and used for potent MHC-I dependent antigen presentation [163]. PEG coating on $FeO_3$ nanoparticles was linked to the same decrease in cytotoxicity as dextran in a cell culture experiment, demonstrating high bio-compatibility of both substances [164]. Based on the current literature I hypothesize that dextran based polymers might have intrinsically higher CLR binding affinities and increase the efficiency of dendritic cell targeting compared to PEG-nanoparticles. To investigate this issue, studies which directly compare the safety and immunogenicity of dextran and PEG as polymers for nanoparticle construction are needed.

This work helped to explore the topic of carbohydrate adjuvants in combination with dermal targeted delivery strategies. Hopefully, we can further expand the knowledge and possibly enrich the repertoire of safe immuno-stimulants in the future.

# Acknowledgement

I am incredibly thankful for the constant support from my supervisors and my personal environment. Without you, this work would never have been possible.

Richard and Sandra always had an open ear and patiently taught me their scientific craft and problem oriented thinking. During the time in the Lab, I learned a lot from you and I admire the energy and focus you put into your research. I am sure that your studies will benefit humanity in the future and might pave the way to successful, novel immunotherapies.

My lab colleagues Evgeniia, Helen and Tanja are amazing. We had a great time together that I will never forget.

My family and friends have always had my back and motivated me when I needed it. I am deeply grateful to you for always believing in me and for giving me valuable advice. Even though no one of you knows what I am studying exactly, you are always interested and listen to my babbling.
I wanna thank my parents for inspiring me to stay curious and question everything - your support throughout my life made all of this possible.
My closest friends have always been like family to me - without you I wouldn't be who I am today.
Thank you Sarah for walking this path with me for the last years. You are a central pillar in my life and certainly my best consultant. With you, time really flies by.

I am also grateful for having the privilege of studying in this innovative and promising scientific field. I am convinced that molecular biology will become increasingly important for the future of mankind. There is a lot to be discovered and we will have to work hard to untangle the delicate and beautiful intricacies of nature.

# Appendix

# Appendix A

### A.0.1 Code

#### A.0.1.1 Code for ImageJ macro

```
macro "ELISPOT [f2]" {
    run("Paste");
        run("Make Binary");
    run("Analyze Particles...", "size=4-200 circularity
    =0.70-1.00 show=Nothing exclude summarize");
    close();
    }
```

**Listing A.1**: Macro for counting ELISpot plates in ImageJ

#### A.0.1.2 R code for: Coupling control via SE-HPLC

```
HPLC_21_01 %>%
  filter(‘Time (min)‘ < 13) %>%  #exclude pic-peak
  select(‘OVA SIGMA‘,           #choose cols of interest
         ‘OVA-DEX15 1:10 0%‘,
         ‘OVA-DEX15 1:10 20%‘,
         ‘OVA-DEX15 1:10 40%‘,
         ‘OVA-DEX15 1:20 0%‘,
         ‘OVA-DEX15 1:20 20%‘,
         ‘OVA-DEX15 1:20 40%‘) %>%
  scale() %>%                   #for normalization
  as_tibble() %>%              #matrix to DT
  gather("id","value", 1:6) %>%  #for rowwise comparisons (
    exclude time)
  cbind(HPLC_21_01 %>%           #get time back after
    normalization
         filter(‘Time (min)‘ < 13) %>%
         select(‘Time (min)‘)) %>%
  rename(time = ‘Time (min)‘) %>%
  ggplot() +
  geom_path(aes(time,
                value,
                color=id,
               ),
            size = 1.2) +
  geom_vline(xintercept = 2 )+   #left area marker
  geom_vline(xintercept = 6 ) +   #right area marker
  theme_borstus() +
  labs(title = "Testing - Chromatogram OVADex 15",
       y = "OD280",
       x = "Time (min)",
       color = "Sample") +
```

**Listing A.2**: Exemplary plot for OVADex 15kDa. 100 and 450 kDa were created analogously using the "tidyverse" package. The three plots were arranged with ggarrange() from "ggpubr" package. Coding steps are explained in the comments (after "#").

```
  scale_color_brewer(palette="Purples")+
  theme(legend.title = element_blank())
```

### A.0.1.3 R code for: SEC control data

```

# Chunk 1
merge3 %>%  #Variable name for the the 15 kDa combined data
  tidyr::gather("id", "value", 2:4) %>%
  ggplot(., aes(Time/60, value, color=id))+ #time /60 yield
     flow in mL
  geom_line()+
  theme_borstus()+
  theme(legend.position = c(0.2,0.8),
        legend.direction = "vertical",
         legend.title = element_text(size = 13))+
  labs(title = "Chromatogram of OVADex",
       y = "OD280",
       x = "Flow (ml)",
       color = "Sample") +
  scale_color_manual(values = c("black","grey","purple")) #
    colpr code for the plots

# Chunk 2
DexcontrolsAn %>% #Variable name for all Dextran controls
  gather("id","value",2:4) %>%
  ggplot(., aes(fraction*2, value, color=id))+ #fraction x2
     yields flow in mL
  geom_line()+
  theme_borstus()+
  theme(legend.position = c(0.2,0.8),
        legend.direction = "vertical",
        legend.title = element_text(size = 13))+
  labs(title = "Anthrone assay of Dextran controls",
       y = "OD620",
       x = "Flow (ml)",
       color = "Sample")
```

**Listing A.3**: Exemplary plot for OVADex 15kDa (**A**) was created "tidyverse" package and explained in the first code chunk. Plot (**B**) was created with the second chunk - code was data import was excluded. Coding steps are explained in the comments (after "#").

### A.0.1.4 SessionInfo

```
sessionInfo()
R version 4.0.3 (2020-10-10)
Platform: x86_64-w64-mingw32/x64 (64-bit)
Running under: Windows 10 x64 (build 18363)

Matrix products: default

locale:
[1] LC_COLLATE=German_Germany.1252  LC_CTYPE=German_Germany
    .1252
[3] LC_MONETARY=German_Germany.1252 LC_NUMERIC=C
[5] LC_TIME=German_Germany.1252

```

**Listing A.4**: Representative SessionInfo() from Rstudio() used for analysis. Updates were released and installed during the project - functionality was tested up to 10.2020.

```
attached base packages:
[1] grid      stats     graphics  grDevices utils
    datasets
[7] methods   base

other attached packages:
 [1] readxl_1.3.1      png_0.1-7         knitr_1.30
 [4] ggsci_2.9         ggsignif_0.6.0    ggpubr_0.4.0
 [7] ggthemes_4.2.0    forcats_0.5.0     stringr_1.4.0
[10] dplyr_1.0.2       purrr_0.3.4       readr_1.4.0
[13] tidyr_1.1.2       tibble_3.0.4      ggplot2_3.3.2
[16] tidyverse_1.3.0   data.table_1.13.2

loaded via a namespace (and not attached):
 [1] Rcpp_1.0.5        lubridate_1.7.9.2 utf8_1.1.4
 [4] digest_0.6.27     assertthat_0.2.1  R6_2.5.0
 [7] cellranger_1.1.0  backports_1.1.10  reprex_0.3.0
[10] httr_1.4.2        pillar_1.4.7      rlang_0.4.8
[13] rematch_1.0.1     curl_4.3          rstudioapi_0.13
[16] car_3.0-10        labeling_0.4.2    foreign_0.8-80
[19] munsell_0.5.0     tinytex_0.27      broom_0.7.2
[22] compiler_4.0.3    modelr_0.1.8      xfun_0.19
[25] pkgconfig_2.0.3   tidyselect_1.1.0  rio_0.5.16
[28] fansi_0.4.1       crayon_1.3.4      dbplyr_2.0.0
[31] withr_2.3.0       jsonlite_1.7.1    gtable_0.3.0
[34] lifecycle_0.2.0   DBI_1.1.0         pacman_0.5.1
[37] magrittr_2.0.1    scales_1.1.1      zip_2.1.1
[40] cli_2.2.0         stringi_1.5.3     carData_3.0-4
[43] farver_2.0.3      fs_1.5.0          xml2_1.3.2
[46] ellipsis_0.3.1    generics_0.1.0    vctrs_0.3.4
[49] openxlsx_4.2.3    tools_4.0.3       glue_1.4.2
[52] hms_0.5.3         abind_1.4-5       yaml_2.2.1
[55] colorspace_2.0-0  rstatix_0.6.0     rvest_0.3.6
[58] haven_2.3.1
```

### A.0.2 Visuals

#### A.0.2.1 Triton contamination

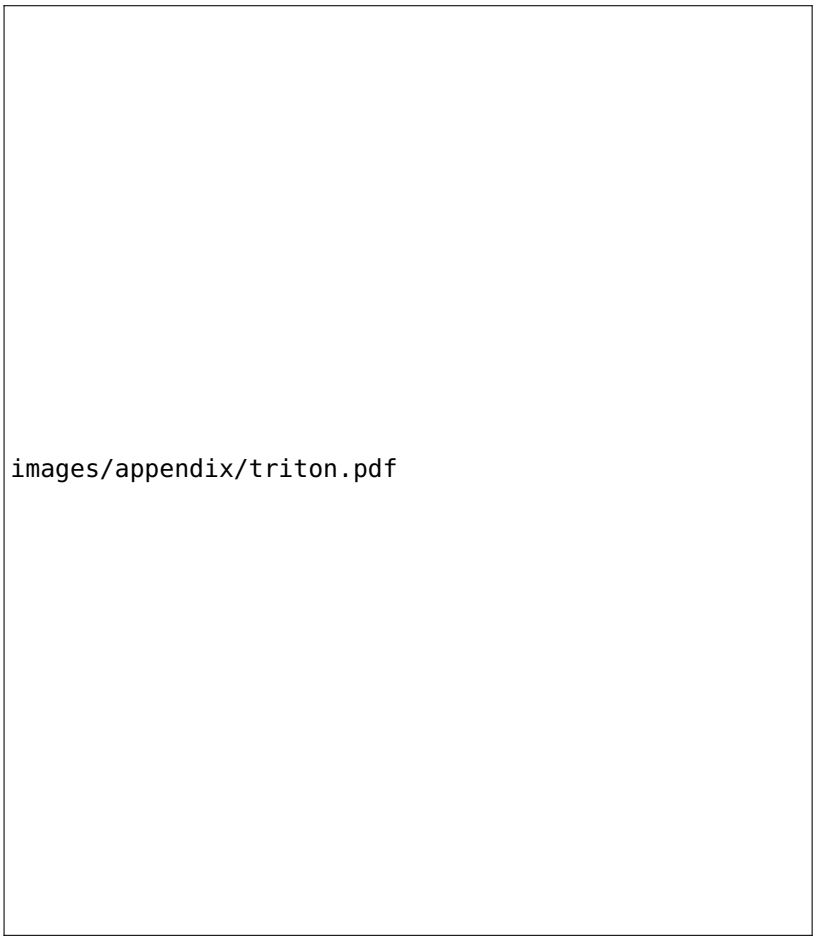


**Figure A.1:** Workflow for determining Triton contamination. (**A**) shows the concentration assessment via Bicinchoninic acid assay. (**B**) for the OD280 concentration measurement. The molar extinction coefficient of OVA (0.74) was experimentally determined on an Eppendorf BioSpectrometer®

#### A.0.2.2 Anthrone assay


**Figure A.2:** Anthrone assay for the Dextrans to be coupled.

### A.0.2.3 Coupling tests - Chromatograms

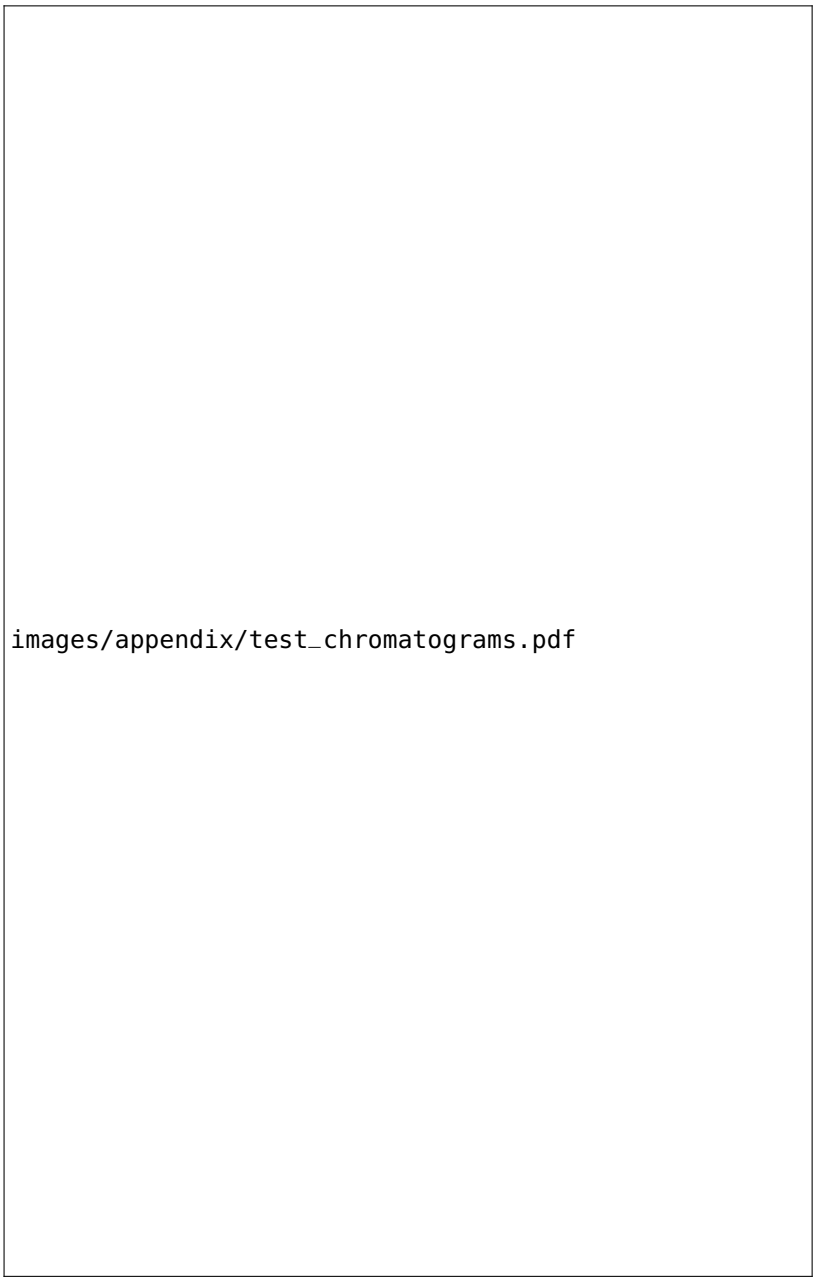


**Figure A.3:** Exemplary chromatograms of coupling pre-testing. OVA from Sigma is displayed as a reference. Differently oxidized Dextrans (15 kDa (**A**), 100 kDa (**B**), 450 kDa (**C**)) were tested in different ratios (0,20,40 %, 1:10, 1:20). The area between the two vertical black lines indicates the area of product formation.

### A.0.2.4 SEC control data


**Figure A.4:** Control data for SEC runs described in 2.1.7.2. (**A**) shows an exemplary chromatogram for OVADex15 (Run A) with the pure OVA and pure DEX 15 kDa as controls. Figure (**B**) shows data from an 2.1.5 of the uncoupled DEX runs.

### A.0.2.5 Recovery Ovalbumin

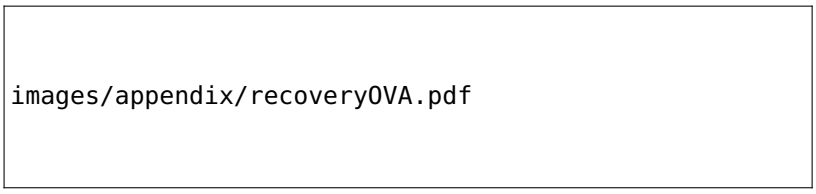


**Figure A.5:** Electrophoretic analysis of OVA (Sigma), cleaned OVA (cOVA, 2.1.1) and lyophilized OVA (L.OVA, also cleaned). Ladder was a Protein Marker from Thermo Fischer (see. 2.1.8, size bands in kDa. The different band intensities were most likely due to the quick dissolving of L.OVA and subsequent heterogenous concentration within the sample.

## A.0.3 Tables

### A.0.3.1 FoxP3$^+$-T$_{regs}$

| Groups | P. mean diff, | Adj P Value |
|---|---|---|
| OVA | | |
| medium vs. OVA | -0.245 | 0.9973 |
| medium vs. SIINFEKL | 8.543 | 0.0697 |
| 15F2 | | |
| medium vs. OVA | 3.22 | 0.576 |
| medium vs. SIINFEKL | 27.27 | <0,0001 |
| 100F2 | | |
| medium vs. OVA | 11.45 | 0.0046 |
| medium vs. SIINFEKL | 27.01 | <0,0001 |
| 450F2 | | |
| medium vs. OVA | 10.77 | 0.0078 |
| medium vs. SIINFEKL | 24.92 | <0,0001 |
| PBS | | |
| medium vs. OVA | 19.62 | <0,0001 |
| medium vs. SIINFEKL | 28.15 | <0,0001 |

**Table A.1:** Counts of spleen resident FoxP3-T$_{regs}$ described in Section 3.3.3 on page 59. Computation was performed using a Dunnett's multiple comparisons test for a simple effect within columns (GrapPad). Results are considered significant when adj. p < 0.05 *Abb:* Adj: adjusted, P. Diff: Predicted Difference

### A.0.3.2 Effector and proliferating CD4$^+$ and CD8$^+$ cells

| Groups | P. Mean diff | Adj. P | Stimulant |
|---|---|---|---|
| Spln CD4 effector | | | |
| OVA vs. 100F2 | -12.87 | <0,0001 | OVA |
| OVA vs. 450F2 | -19.52 | <0,0001 | OVA |
| Spln CD8 effector | | | |
| OVA vs. 450F2 | 9.941 | 0.0051 | medium |
| OVA vs. 450F2 | -13.52 | 0.0001 | OVA |
| Spln KI67 CD4 | | | |
| OVA vs. 100F2 | 14.16 | 0.0003 | SIINFEKL |
| OVA vs. 450F2 | 12.77 | 0.001 | SIINFEKL |
| Spln KI67 CD8 | | | |
| OVA vs. 15F2 | 7.699 | 0.0029 | medium |
| OVA vs. 100F2 | 8.395 | 0.0011 | medium |
| OVA vs. 450F2 | 9.941 | 0.0001 | medium |
| OVA vs. 100F2 | -12.87 | <0,0001 | OVA |
| OVA vs. 450F2 | -19.52 | <0,0001 | OVA |
| LN CD8 effector | | | |
| OVA vs. 100F2 | -4.98 | 0.0008 | OVA |

**Table A.2:** Comparison of spleenic and lymph node resident cells upon incubation in plain Tcell medium /+ OVA /+ SIINFEKL, as assessed by flow cytometry. Group comparisons were performed using a Dunnett's multiple comparisons test for a simple effect within columns (GrapPad). Results are considered significant wehen adj. p < 0.05 *Abb:* Adj: adjusted, P.

# Bibliography

Here are the references in citation order.


[1] Bent Petersen et al. 'A generic method for assignment of reliability scores applied to solvent accessibility predictions'. In: BMC structural biology 9.1 (2009), p. 51 (cited on pages vi, 42).

[2] Michael Schantz Klausen et al. 'NetSurfP-2.0: Improved prediction of protein structural features by integrated deep learning'. In: Proteins: Structure, Function, and Bioinformatics 87.6 (2019), pp. 520–527 (cited on pages vi, 42).

[3] Boriana Marintcheva. 'Chapter 8 - Viruses as Tools for Vaccine Development'. In: (Jan. 2018), pp. 217–242. DOI: 10.1016/B978-0-12-810514-6.00008-8 (cited on pages x, 6).

[4] Steven G Reed, Mark T Orr, and Rhea N Coler. 'Vaccine adjuvants'. In: The Vaccine Book. Elsevier, 2016, pp. 67–76 (cited on pages x, 6, 7).

[5] Roy M Anderson. 'The impact of vaccination on the epidemiology of infectious diseases'. In: The Vaccine Book. Elsevier, 2016, pp. 3–31 (cited on page x).

[6] Stanley Plotkin, Walter Orenstein, and Paul Offit. General aspects of vaccination. Jan. 2015, pp. 1–11 (cited on pages x, 2).

[7] Weidang Li et al. 'Peptide vaccine: progress and challenges'. In: Vaccines 2.3 (2014), pp. 515–536. DOI: 10.3390/vaccines2030515 (cited on pages x, 6).

[8] Peter Michael Moyle and Istvan Toth. 'Modern subunit vaccines: development, components, and research opportunities'. In: ChemMedChem 8.3 (2013), pp. 360–376 (cited on page x).

[9] Teunis BH Geijtenbeek and Sonja I Gringhuis. 'Signalling through C-type lectin receptors: shaping immune responses'. In: Nature Reviews Immunology 9.7 (2009), pp. 465–479 (cited on pages x, 9, 10).

[10] Pilar Garcia-Vello et al. 'Carbohydrate-based adjuvants'. In: Drug Discovery Today: Technologies (2020) (cited on pages x, 11).

[11] Kazuhiko Takahara et al. 'Functional comparison of the mouse DC-SIGN, SIGNR1, SIGNR3 and Langerin, C-type lectins'. In: International immunology 16.6 (2004), pp. 819–829 (cited on pages x, xiv, 11, 46, 65, 73).

[12] Sergey Pustylnikov et al. 'Targeting the C-type lectins-mediated host-pathogen interactions with dextran'. In: Journal of pharmacy & pharmaceutical sciences: a publication of the Canadian Society fo 17.3 (2014), p. 371 (cited on pages x, 8, 11, 12).

[13] R. Kenney et al. 'Dose sparing with intradermal injection of influenza vaccine.' In: The New England journal o 351 22 (2004), pp. 2295–301 (cited on pages xi, 12, 15).

[14] Elena Criscuolo et al. 'Alternative methods of vaccine delivery: an overview of edible and intradermal vaccines'. In: Journal of immunology research 2019 (2019) (cited on pages xi, 12).

[15] Jean-Francois Nicolas and Bruno Guy. 'Intradermal, epidermal and transcutaneous vaccination: from immunology to clinical practice'. In: Expert review of vaccines 7.8 (2008), pp. 1201–1214 (cited on pages xi, 12).

[16] Sandra Scheiblhofer, Josef Thalhamer, and Richard Weiss. 'Laser microporation of the skin: prospects for painless application of protective and therapeutic vaccines'. In: Expert opinion on drug delivery 10.6 (2013), pp. 761–773 (cited on pages xi, 6, 9).

[17] Bruce G Weniger and Mark J Papania. 'Alternative vaccine delivery methods'. In: Vaccines (2013), p. 1200 (cited on pages xi, 15).

[18] Paul Henri Lambert and Philippe E Laurent. 'Intradermal vaccine delivery: will new delivery systems transform vaccine administration?' In: Vaccine 26.26 (2008), pp. 3197–3208 (cited on pages xi, 1, 2).

[19] Ivan FN Hung and Kwok-Yung Yuen. 'Immunogenicity, safety and tolerability of intradermal influenza vaccines'. In: Human vaccines & immunotherapeutics 14.3 (2018), pp. 565–570 (cited on page xi).

[20] Evgeniia Korotchenko et al. 'Laser-facilitated epicutaneous immunotherapy with hypoallergenic beta-glucan neoglycoconjugates suppresses lung inflammation and avoids local side effects in a mouse model of allergic asthma'. In: bioRxiv (2020) (cited on pages xi, xiv, 11, 40, 43, 47, 48, 52, 64, 66–70, 73).

[21] Md Kamal Hossain and Katherine A Wall. 'Use of dendritic cell receptors as targets for enhancing anti-cancer immune responses'. In: Cancers 11.3 (2019), p. 418 (cited on page xi).

[22] Aurélie Durgeau et al. 'Recent advances in targeting CD8 T-cell immunity for more effective cancer immunotherapy'. In: Frontiers in immunology 9 (2018), p. 14 (cited on page xi).

[23] Esther E Weinberger et al. 'Generation of hypoallergenic neoglycoconjugates for dendritic cell targeted vaccination: a novel tool for specific immunotherapy'. In: Journal of controlled release 165.2 (2013), pp. 101–109 (cited on pages xiv, 6, 11, 12, 47, 48, 64, 67, 69, 70).

[24] Yoan Machado et al. 'Synergistic effects of dendritic cell targeting and laser-microporation on enhancing epicutaneous skin vaccination efficacy'. In: Journal of Controlled Release 266 (2017), pp. 87–99 (cited on pages xiv, 11, 17, 64, 67, 69, 70, 73).

[25] Joseph Needham, Lu Gwei-Djen, and Nathan Sivin. Science And Civilization In China. Volume 6 Biology an Cambridge University Press, 2000, pp. 114–127 (cited on pages 1, 2).

[26] Inaya Hajj Hussein et al. 'Vaccines through centuries: major cornerstones of global health'. In: Frontiers in public health 3 (2015), p. 269 (cited on page 1).

[27] Stefan Riedel. 'Edward Jenner and the history of smallpox and vaccination'. In: Baylor University Medical Cen Vol. 18. 1. Taylor & Francis. 2005, pp. 21–25 (cited on page 1).

[28] Edward Jenner. An Inquiry Into the Causes and Effects of the Variolæ Vaccinæ, Or Cow-Pox. author, 1798 (cited on page 2).

[29] Stanley A Plotkin and Susan L Plotkin. 'The development of vaccines: how the past led to the future'. In: Nature Reviews Microbiology 9.12 (2011), pp. 889–893 (cited on pages 2, 3).

[30] Hervé Lecoq. 'Découverte du premier virus, le virus de la mosaıque du tabac: 1892 ou 1898?' In: Comptes Rendus de l'Académie des Sciences-Series III-Sciences de la Vie 324.10 (2001), pp. 929–933 (cited on page 2).

[31] John F Enders, Thomas H Weller, and Frederick C Robbins. 'Cultivation of the Lansing strain of poliomyelitis virus in cultures of various human embryonic tissues'. In: Science 109.2822 (1949), pp. 85–87 (cited on page 2).

[32] Frank DeStefano, Heather Monk Bodenstab, and Paul A Offit. 'Principal controversies in vaccine safety in the United States'. In: Clinical Infectious Diseases 69.4 (2019), pp. 726–731 (cited on page 3).

[33] Difeng Fang and Jinfang Zhu. 'Dynamic balance between master transcription factors determines the fates and functions of CD4 T cell and innate lymphoid cell subsets'. In: Journal of Experimental Medicine 214.7 (2017), pp. 1861–1876 (cited on pages 3, 6).

[34] Marek Wieczorek et al. 'Major histocompatibility complex (MHC) class I and MHC class II proteins: conformational plasticity in antigen presentation'. In: Frontiers in immunology 8 (2017), p. 292 (cited on page 4).

[35] Claire-Anne Siegrist and Paul-Henri Lambert. 'How Vaccines Work'. In: The vaccine book. Second Edition. Elsevier, 2016 (cited on page 4).

[36] M. Oettinger et al. 'RAG-1 and RAG-2, adjacent genes that synergistically activate V(D)J recombination.' In: Science 248 4962 (1990), pp. 1517–23 (cited on page 4).

[37] Abul K. Abbas et al. 'Overview of Humoral Immune Responses'. In: Cellular and molecular immunology. 9th ed. Elsevier, 2018, pp. 252–274 (cited on page 4).

[38] Jason G Cyster and Christopher DC Allen. 'B cell responses: cell interaction dynamics and decisions'. In: Cell 177.3 (2019), pp. 524–540 (cited on page 4).

[39] Balthasar A Heesters, Riley C Myers, and Michael C Carroll. 'Follicular dendritic cells: dynamic antigen libraries'. In: Nature Reviews Immunology 14.7 (2014), pp. 495–504 (cited on pages 4, 11).

[40] Natalia B Pikor et al. 'Remodeling of light and dark zone follicular dendritic cells governs germinal center responses'. In: Nature Immunology (2020), pp. 1–11 (cited on page 4).

[41] Jennifer E Smith-Garvin, Gary A Koretzky, and Martha S Jordan. 'T cell activation'. In: Annual review of immunology 27 (2009), pp. 591–619 (cited on page 5).

[42] Abul K. Abbas et al. 'Activation of T Lymphocytes'. In: Cellular and molecular immunology. 9th ed. Elsevier, 2018, pp. 210–223 (cited on pages 5, 50).

[43] Maria Embgenbroich and Sven Burgdorf. 'Current concepts of antigen cross-presentation'. In: Frontiers in immunology 9 (2018), p. 1643 (cited on pages 5, 9).

[44] Abul K. bbas et al. 'Antigen Presentation to T Lymphocytes and the Functions of Major Histocompatibility Complex Molecules'. In: Cellular and molecular immunology. 9th ed. Elsevier, 2018, pp. 117–142 (cited on page 5).

[45] Nu Zhang and Michael J Bevan. 'CD8+ T cells: foot soldiers of the immune system'. In: Immunity 35.2 (2011), pp. 161–168 (cited on page 5).

[46] Jonathan J Darrow and Aaron S Kesselheim. 'A New Wave of Vaccines for Non-Communicable Diseases'. In: Food and drug law journal 70.2 (2015), pp. 243–258 (cited on pages 6, 63).

[47] Sandra Scheiblhofer, Josef Thalhamer, and Richard Weiss. 'Novel vaccines for type I allergy'. In: Molecular Vaccines. Springer, 2014, pp. 489–501 (cited on pages 6, 63).

[48] Michael M McNeil. 'Vaccine-Associated Anaphylaxis'. In: Current Treatment Options in Allergy 6.3 (2019), pp. 297–308 (cited on page 6).

[49] Niels Peter H Knudsen et al. 'Different human vaccine adjuvants promote distinct antigen-independent immunological signatures tailored to different pathogens'. In: Scientific reports 6.1 (2016), pp. 1–13 (cited on page 6).

[50] Giuseppe Del Giudice, Rino Rappuoli, and Arnaud M Didierlaurent. 'Correlates of adjuvanticity: a review on adjuvants in licensed vaccines'. In: Seminars in immunology. Vol. 39. Elsevier. 2018, pp. 14–21 (cited on pages 6, 7).

[51] Harm HogenEsch, Derek T O'Hagan, and Christopher B Fox. 'Optimizing the utilization of aluminum adjuvants in vaccines: you might just get what you want'. In: npj Vaccines 3.1 (2018), pp. 1–11 (cited on page 7).

[52] Matthias Giese. 'Basic vaccine immunology'. In: Molecular Vaccines. Springer, 2013, pp. 23–58 (cited on page 7).

[53] Amy S McKee and Philippa Marrack. 'Old and new adjuvants'. In: Current opinion in immunology 47 (2017), pp. 44–51 (cited on page 7).

[54] Robert L Coffman, Alan Sher, and Robert A Seder. 'Vaccine adjuvants: putting innate immunity to work'. In: Immunity 33.4 (2010), pp. 492–503 (cited on page 7).

[55] Tyson J Moyer, Andrew C Zmolek, Darrell J Irvine, et al. 'Beyond antigens and adjuvants: formulating future vaccines'. In: The Journal of clinical investigation 126.3 (2016), pp. 799–808 (cited on page 7).

[56] Michael J Bevan. 'The earliest knockouts'. In: The Journal of Immunology 184.9 (2010), pp. 4585–4586 (cited on page 7).

[57] Lisa E Wagar, Robert M DiFazio, and Mark M Davis. 'Advanced model systems and tools for basic and translational human immunology'. In: Genome medicine 10.1 (2018), pp. 1–14 (cited on page 7).

[58] Lili Tao and Tiffany A Reese. 'Making mouse models that reflect human immune responses'. In: Trends in immunology 38.3 (2017), pp. 181–193 (cited on page 8).

[59] Todd M Allen et al. 'Humanized immune system mouse models: progress, challenges and opportunities'. In: Nature immunology 20.7 (2019), pp. 770–774 (cited on page 8).

[60] Christian Thomas Mayer et al. 'Selective and efficient generation of functional Batf3-dependent CD103+ dendritic cells from mouse bone marrow'. In: Blood, The Journal of the American Society 124.20 (2014), pp. 3081–3091 (cited on page 8).

[61] Yuekang Xu et al. 'Differential development of murine dendritic cells by GM-CSF versus Flt3 ligand has implications for inflammation and trafficking'. In: The Journal of Immunology 179.11 (2007), pp. 7577–7584 (cited on pages 8, 67, 69).

[62] Julie Helft et al. 'GM-CSF mouse bone marrow cultures comprise a heterogeneous population of CD11c+ MHCII+ macrophages and dendritic cells'. In: Immunity 42.6 (2015), pp. 1197–1211 (cited on pages 8, 48, 67, 69).

[63] Kristin A Hogquist et al. 'T cell receptor antagonist peptides induce positive selection'. In: Cell 76.1 (1994), pp. 17–27 (cited on page 8).

[64] Megan J Barnden et al. 'Defective TCR expression in transgenic mice constructed using cDNA-based $\alpha$-and $\beta$-chain genes under the control of heterologous regulatory elements'. In: Immunology and cell biology 76.1 (1998), pp. 34–40 (cited on page 8).

[65] James A Huntington and Penelope E Stein. 'Structure and properties of ovalbumin'. In: Journal of Chromatography B: Biomedical Sciences and Applications 756.1-2 (2001), pp. 189–198 (cited on page 8).

[66] Dieke van Dinther et al. 'Targeting C-type lectin receptors: a high-carbohydrate diet for dendritic cells to improve cancer vaccines'. In: Journal of leukocyte biology 102.4 (2017), pp. 1017–1034 (cited on pages 8–10, 13, 53).

[67] V. Apostolopoulos et al. 'Targeting Antigens to Dendritic Cell Receptors for Vaccine Development'. In: Journal of Drug Delivery 2013 (2013) (cited on page 10).

[68] Alex S. Powlesland et al. 'Widely Divergent Biochemical Properties of the Complete Set of Mouse DC-SIGN-related Proteins*'. In: Journal of Biological Chemistry 281 (2006), pp. 20440–20449 (cited on page 10).

[69] Magdalena Eriksson et al. 'The C-Type Lectin Receptor SIGNR3 Binds to Fungi Present in Commensal Microbiota and Influences Immune Regulation in Experimental Colitis'. In: Frontiers in Immunology 4 (2013) (cited on page 10).

[70] Young-Sun Kang et al. 'The C-type lectin SIGN-R1 mediates uptake of the capsular polysaccharide of Streptococcus pneumoniae in the marginal zone of mouse spleen'. In: Proceedings of the National Academy of Sciences of the United States of America 101 (2003), pp. 215–220 (cited on page 10).

[71] I. Caminschi, Simone Meuter, and W. Heath. 'DEC-205 is a cell surface receptor for CpG oligonucleotides'. In: Oncoimmunology 2 (2013) (cited on page 10).

[72] Hitomi Sano et al. 'Analysis of chimeric proteins identifies the regions in the carbohydrate recognition domains of rat lung collectins that are essential for interactions with phospholipids, glycolipids, and alveolar type II cells'. In: Journal of Biological Chemistry 273.8 (1998), pp. 4783–4789 (cited on page 10).

[73] Wolfgang Kastenmüller et al. 'Dendritic cell-targeted vaccines—hope or hype?' In: Nature Reviews Immunolo 14.10 (2014), pp. 705–711 (cited on pages 11, 53).

[74] Amy J Foster et al. 'The ligands of C-type lectins'. In: C-Type Lectin Receptors in Immunity. Springer, 2016, pp. 191–215 (cited on page 11).

[75] SCOGS (Select Committee on GRAS Substances). URL: https://www.fda.gov/food/generally-recognized-safe-gras/gras-substances-scogs-database (cited on page 11).

[76] Luis J Cruz et al. 'Comparison of antibodies and carbohydrates to target vaccines to human dendritic cells via DC-SIGN'. In: Biomaterials 33.16 (2012), pp. 4229–4239 (cited on page 11).

[77] Roy A Dalmo and Jarl Bøgwald. 'ß-glucans as conductors of immune symphonies'. In: Fish & shellfish immunology 25.4 (2008), pp. 384–396 (cited on page 11).

[78] Stuart M Levitz. 'Innate recognition of fungal cell walls'. In: PLoS Pathog 6.4 (2010), e1000758 (cited on page 11).

[79] Suneela S Dhaneshwar et al. 'Dextran: A promising macromolecular drug carrier'. In: Indian journal of pharmaceutical sciences 68.6 (2006), p. 705 (cited on page 11).

[80] Dextran. URL: https://www.sigmaaldrich.com/technical-documents/protocols/biology/dextran.html (cited on page 11).

[81] Jaleh Varshosaz. 'Dextran conjugates in drug delivery'. In: Expert Opinion on Drug Delivery 9.5 (2012), pp. 509–523 (cited on page 11).

[82] Akhilesh Kumar Shakya and Kutty Selva Nandakumar. 'Applications of polymeric adjuvants in studying autoimmune responses and vaccination against infectious diseases'. In: Journal of the Royal Society Interface 10.79 (2013), p. 20120536 (cited on page 11).

[83] Eleonora Altman, Vandana Chandan, and Blair Harrison. 'The potential of dextran-based glycoconjugates for development of Helicobacter pylori vaccine'. In: Glycoconjugate journal 31.1 (2014), pp. 13–24 (cited on page 11).

[84] Emanuela Bartoccioni. 'Why Does an IM Immunization Work?' In: Molecular Vaccines. Springer, 2014, pp. 793–802 (cited on page 12).

[85] Anna Taddio et al. 'Survey of the prevalence of immunization non-compliance due to needle fears in children and adults'. In: Vaccine 30.32 (2012), pp. 4807–4812 (cited on page 12).

[86] M. Shampo, R. Kyle, and D. Steensma. 'Albert Sabin–conqueror of poliomyelitis.' In: Mayo Clinic proceedings 86 7 (2011), e44 (cited on page 12).

[87] N. Carter and M. Curran. 'Live Attenuated Influenza Vaccine (FluMist®; Fluenz™)'. In: Drugs 71 (2012), pp. 1591–1622 (cited on page 12).

[88] J Wayne Streilein. 'Skin-associated lymphoid tissues (SALT): origins and functions.' In: Journal of Investigative Dermatology 80 (1983) (cited on page 12).

[89] Jan D Bos and Martien L Kapsenberg. 'The skin immune system Its cellular constituents and their interactions'. In: Immunology Today 7.7-8 (1986), pp. 235–240 (cited on page 12).

[90] Florence Abdallah, Lily Mijouin, and Chantal Pichon. 'Skin immune landscape: inside and outside the organism'. In: Mediators of inflammation 2017 (2017) (cited on pages 13, 14).

[91] Thomas Doebel, Benjamin Voisin, and Keisuke Nagao. 'Langerhans cells–the macrophage in dendritic cell clothing'. In: Trends in immunology 38.11 (2017), pp. 817–828 (cited on page 13).

[92] M. Guilliams et al. 'Unsupervised High-Dimensional Analysis Aligns Dendritic Cells across Tissues and Species'. In: Immunity 45 (2016), pp. 669–684 (cited on page 13).

[93] Akiko Iwasaki and Ruslan Medzhitov. 'Control of adaptive immunity by the innate immune system'. In: Nature immunology 16.4 (2015), pp. 343–353 (cited on pages 13, 72).

[94] Francisco A Bonilla and Hans C Oettgen. 'Adaptive immunity'. In: Journal of Allergy and Clinical Immunolo 125.2 (2010), S33–S40 (cited on page 13).

[95] Lucie Mondoulet et al. 'Epicutaneous immunotherapy for food allergy as a novel pathway for oral tolerance induction'. In: Immunotherapy 7.12 (2015), pp. 1293–1305 (cited on page 14).

[96] Julie Wang and Hugh A Sampson. 'Safety and efficacy of epicutaneous immunotherapy for food allergy'. In: Pediatric Allergy and Immunology 29.4 (2018), pp. 341–349 (cited on page 14).

[97] Laura Engelke et al. 'Recent insights into cutaneous immunization: how to vaccinate via the skin'. In: Vaccine 33.37 (2015), pp. 4663–4674 (cited on page 14).

[98] Samir Mitragotri. 'Current status and future prospects of needle-free liquid jet injectors'. In: Nature reviews Drug discovery 5.7 (2006), pp. 543–548 (cited on page 15).

[99] Elsa E Kis, Gerhard Winter, and Julia Myschik. 'Devices for intradermal vaccination'. In: Vaccine 30.3 (2012), pp. 523–538 (cited on page 15).

[100] Tuan-Mazlelaa Tuan-Mahmood et al. 'Microneedles for intradermal and transdermal drug delivery'. In: European Journal of Pharmaceutical Sciences 50.5 (2013), pp. 623–637 (cited on page 15).

[101] Babu M Medi, Buddhadev Layek, and Jagdish Singh. 'Electroporation for dermal and transdermal drug delivery'. In: Percutaneous Penetration Enhancers Physical Methods in Penetration Enhancement Springer, 2017, pp. 105–122 (cited on page 16).

[102] HD Liang, J Tang, and M Halliwell. 'Sonoporation, drug delivery, and gene therapy'. In: Proceedings of the Institution of Mechanical Engineers, Part H: Journal of Engineering in Medicine 224.2 (2010), pp. 343–361 (cited on page 16).

[103] Galit Levin. 'Skin Ablation Methods for Transdermal Drug Delivery'. In: Percutaneous Penetration Enhancers Springer, 2017, pp. 233–241 (cited on page 16).

[104] Hiroaki Todo, Wesam R Kadhum, and Kenji Sugibayashi. 'The Synergistic Effect of Iontophoresis or Electroporation and Microneedles on the Skin Permeation of High Molecular Weight Compounds'. In: Percutaneous Penetration Enhancers Physical Methods in Penetration Enhancement. Springer, 2017, pp. 379–387 (cited on page 16).

[105] Sandra Scheiblhofer et al. 'Skin vaccination via fractional infrared laser ablation-Optimization of laser-parameters and adjuvantation'. In: Vaccine 35.14 (2017), pp. 1802–1809 (cited on pages 16, 18).

[106] Satoshi Kashiwagi, Timothy Brauns, and Mark C Poznansky. 'Classification of laser vaccine adjuvants'. In: Journal of vaccines & vaccination 7.1 (2016) (cited on page 16).

[107] Satoshi Kashiwagi et al. 'Laser vaccine adjuvants: History, progress, and potential'. In: Human vaccines & immunotherapeutics 10.7 (2014), pp. 1892–1907 (cited on page 16).

[108] Kaitlyn Morse et al. 'Near-infrared 1064 nm laser modulates migratory dendritic cells to augment the immune response to intradermal influenza vaccine'. In: The Journal of Immunology 199.4 (2017), pp. 1319–1332 (cited on page 16).

[109] Ji Wang et al. 'A micro-sterile inflammation array as an adjuvant for influenza vaccines'. In: Nature communications 5.1 (2014), pp. 1–11 (cited on page 17).

[110] Satoshi Kashiwagi. 'Laser adjuvant for vaccination'. In: The FASEB Journal 34.3 (2020), pp. 3485–3500 (cited on page 17).

[111] Xinyuan Chen et al. 'Facilitation of transcutaneous drug delivery and vaccine immunization by a safe laser technology'. In: Journal of controlled release 159.1 (2012), pp. 43–51 (cited on page 17).

[112] Barbara Zorec et al. 'The effect of pulse duration, power and energy of fractional Er: YAG laser for transdermal delivery of differently sized FITC dextrans'. In: International Journal of Pharmaceutics 516.1-2 (2017), pp. 204–213 (cited on page 17).

[113] Richard Weiss et al. 'Transcutaneous vaccination via laser microporation'. In: Journal of controlled release 162.2 (2012), pp. 391–399 (cited on pages 17, 64).

[114] O Chatzis et al. 'Safety and immunogenicity of the epicutaneous reactivation of pertussis toxin immunity in healthy adults: a phase I, randomized, double-blind, placebo-controlled trial'. In: Clinical Microbiology and Infection (2020) (cited on page 18).

[115] RStudio Team. RStudio: Integrated Development Environment for R. RStudio, PBC. Boston, MA, 2020 (cited on page 19).

[116] Hadley Wickham et al. 'Welcome to the tidyverse'. In: Journal of Open Source Software 4.43 (2019), p. 1686. DOI: 10.21105/joss.01686 (cited on page 19).

[117] Greg T Hermanson. '18. PEGylation and synthetic polymer modification'. In: Bioconjugate techniques. Academic press, 2013, pp. 787–838 (cited on page 20).

[118] Jiri Moravec and Jan Mares. 'A simple, time-saving, microwave-assisted periodic acid–Schiff´ s staining of glycoproteins on 1D electrophoretic gels'. In: Electrophoresis 38.24 (2017), pp. 3100–3103 (cited on page 23).

[119] Sabrina Wildner et al. 'Endolysosomal degradation of allergenic ole e 1-like proteins: analysis of proteolytic cleavage sites revealing T cell epitope-containing peptides'. In: International journal of molecular sciences 18.8 (2017), p. 1780 (cited on page 24).

[120] Francesca Granucci et al. 'Early events in dendritic cell maturation induced by LPS'. In: Microbes and infection 1.13 (1999), pp. 1079–1084 (cited on page 38).

[121] Beom Seok Park and Jie-Oh Lee. 'Recognition of lipopolysaccharide pattern by TLR4 complexes'. In: Experimental & molecular medicine 45.12 (2013), e66–e66 (cited on page 38).

[122] Albumin from hen egg white. URL: https://www.sigmaaldrich.com/catalog/product/sigma/a5503?lang=de&region=AT (cited on page 38).

[123] Seid Mahdi Jafari ... Milena Martelli Tosi Ana Paula Ramos. 'Chapter Six - Dynamic light scattering (DLS) of nanoencapsulated food ingredients'. In: Characterization of Nanoencapsulated Food Ingredi 1, volume 4. Elsevier, 2020, pp. 191–211 (cited on page 41).

[124] Jonathan K Armstrong et al. 'The hydrodynamic radii of macromolecules and their effect on red blood cell aggregation'. In: Biophysical journal 87.6 (2004), pp. 4259–4270 (cited on page 41).

[125] Harold P Erickson. 'Size and shape of protein molecules at the nanometer level determined by sedimentation, gel filtration, and electron microscopy'. In: Biological procedures online 11.1 (2009), p. 32 (cited on page 41).

[126] Maria Hrmova and Geoffrey B Fincher. 'Plant and microbial enzymes involved in the depolymerization of (1, 3)-$\beta$-d-glucans and related polysaccharides'. In: Chemistry, Biochemistry, and Biology of 1-3 Elsevier, 2009, pp. 119–170 (cited on page 42).

[127] Bruce A Burton and David A Brant. 'Comparative flexibility, extension, and conformation of some simple polysaccharide chains'. In: Biopolymers: Original Research on Biomolecules 22.7 (1983), pp. 1769–1792 (cited on pages 42, 66).

[128] GT Hermanson. 'Vaccines and immunogen conjugates'. In: Bioconjugate techniques, 3rd edn. Academic Pres (2013), pp. 839–865 (cited on page 42).

[129] Eric F Pettersen et al. 'UCSF Chimera—a visualization system for exploratory research and analysis'. In: Journal of computational chemistry 25.13 (2004), pp. 1605–1612 (cited on page 45).

[130] Mette M Nielsen et al. 'Unfolding of $\beta$-sheet proteins in SDS'. In: Biophysical journal 92.10 (2007), pp. 3674–3685 (cited on page 44).

[131] Kazuharu Sugawara et al. 'Electrochemically monitoring the binding of concanavalin A and ovalbumin'. In: Talanta 85.1 (2011), pp. 425–429 (cited on page 46).

[132] BB Agrawal and IJ Goldstein. 'Specific binding of concanavalin A to cross-linked dextran gels.' In: Biochemical Journal 96.3 (1965), 23contd (cited on page 46).

[133] Fohona S Coulibaly and Bi-Botti C Youan. 'Concanavalin A–Polysaccharides binding affinity analysis using a quartz crystal microbalance'. In: Biosensors and Bioelectronics 59 (2014), pp. 404–411 (cited on pages 46, 66).

[134] Fardous Musa et al. 'Compliance with allergen immunotherapy and factors affecting compliance among patients with respiratory allergies'. In: Human vaccines & immunotherapeutics 13.3 (2017), pp. 514–517 (cited on page 47).

[135] Pierre Brawand et al. 'Murine plasmacytoid pre-dendritic cells generated from Flt3 ligand-supplemented bone marrow cultures are immature APCs'. In: The Journal of Immunology 169.12 (2002), pp. 6711–6719 (cited on pages 48, 52, 67, 68).

[136] Yung-Yi C Mosley, Josiah E Radder, and Harm HogenEsch. 'Genetic Variation in the Magnitude and Longevity of the IgG Subclass Response to a Diphtheria-Tetanus-Acellular Pertussis (DTaP) Vaccine in Mice'. In: Vaccines 7.4 (2019), p. 124 (cited on page 53).

[137] Chunhui Lai et al. 'The enhanced antitumor-specific immune response with mannose-and CpG-ODN-coated liposomes delivering TRP2 peptide'. In: Theranostics 8.6 (2018), p. 1723 (cited on page 54).

[138] Christina Ekerfelt, Jan Ernerudh, and Maria C Jenmalm. 'Detection of spontaneous and antigen-induced human interleukin-4 responses in vitro: comparison of ELISPOT, a novel ELISA and real-time RT-PCR'. In: Journal of immunological methods 260.1-2 (2002), pp. 55–67 (cited on page 54).

[139] S. Ilyas and J. Yang. 'Landscape of Tumor Antigens in T Cell Immunotherapy'. In: The Journal of Immunology 195 (2015), pp. 5117–5122 (cited on page 60).

[140] Patricia M Santos and Lisa H Butterfield. 'Dendritic cell–based cancer vaccines'. In: The Journal of Immunology 200.2 (2018), pp. 443–449 (cited on page 60).

[141] A. Sandrini, J. Rolland, and R. O'hehir. 'Current developments for improving efficacy of allergy vaccines'. In: Expert Review of Vaccines 14 (2015), pp. 1073–1087 (cited on page 63).

[142] R. Hollingsworth and K. Jansen. 'Turning the corner on therapeutic cancer vaccines'. In: NPJ Vaccines 4 (2019) (cited on page 63).

[143] Boudewijn JH Dierick et al. 'Burden and socioeconomics of asthma, allergic rhinitis, atopic dermatitis and food allergy'. In: Expert review of pharmacoeconomics & outcomes research 20.5 (2020), pp. 437–453 (cited on page 63).

[144] C. Fitzmaurice et al. 'Global, Regional, and National Cancer Incidence, Mortality, Years of Life Lost, Years Lived With Disability, and Disability-Adjusted Life-years for 32 Cancer Groups, 1990 to 2015: A Systematic Analysis for the Global Burden of Disease Study'. In: JAMA Oncology 3 (2017), pp. 524–548 (cited on page 63).

[145] Cynthia Kanagaratham et al. 'IgE and IgG Antibodies as Regulators of Mast Cell and Basophil Functions in Food Allergy'. In: Frontiers in Immunology 11 (2020) (cited on page 63).

[146] C. Vizzardelli et al. 'Blocking antibodies induced by allergen-specific immunotherapy ameliorate allergic airway disease in a human/mouse chimeric model'. In: Allergy 73 (2018), pp. 851–861 (cited on page 63).

[147] Tatiana A Korolenko, N. Bgatova, and V. Vetvicka. 'Glucan and Mannan—Two Peas in a Pod'. In: International Journal of Molecular Sciences 20 (2019) (cited on pages 63, 66).

[148] Yuka Igarashi and T. Sasada. 'Cancer Vaccines: Toward the Next Breakthrough in Cancer Immunotherapy'. In: Journal of Immunology Research 2020 (2020) (cited on page 64).

[149] Andrew Almond and John K Sheehan. 'Predicting the molecular shape of polysaccharides from dynamic interactions with water'. In: Glycobiology 13.4 (2003), pp. 255–264 (cited on page 66).

[150] E. Amri and F. Mamboya. 'Papain, a Plant Enzyme of Biological Importance: A Review'. In: American Journal of Biochemistry and Biotechnology 8 (2012), pp. 99–104 (cited on page 66).

[151] Sakeen W Kashem, Muzlifah Haniffa, and Daniel H Kaplan. 'Antigen-presenting cells in the skin'. In: Annual review of immunology 35 (2017), pp. 469–499 (cited on page 67).

[152] Josh Gregorio et al. 'Plasmacytoid dendritic cells sense skin injury and promote wound healing through type I interferons'. In: Journal of Experimental Medicine 207.13 (2010), pp. 2921–2930 (cited on page 67).

[153] Yoshinori Mine and Prithy Rupa. 'Fine mapping and structural analysis of immunodominant IgE allergenic epitopes in chicken egg ovalbumin'. In: Protein engineering 16.10 (2003), pp. 747–752 (cited on page 70).

[154] Mudnakudu Nagaraju Kiran Kumar, Chang Zhou, and Mei X Wu. 'Laser-facilitated epicutaneous immunotherapy to IgE-mediated allergy'. In: Journal of Controlled Release 235 (2016), pp. 82–90 (cited on page 71).

[155] Juliane Fornefett et al. 'Comparative analysis of humoral immune responses and pathologies of BALB/c and C57BL/6 wildtype mice experimentally infected with a highly virulent Rodentibacter pneumotropicus (Pasteurella pneumotropica) strain'. In: BMC microbiology 18.1 (2018), pp. 1–11 (cited on page 71).

[156] Ewoud Bernardus Compeer et al. 'Antigen processing and remodeling of the endosomal pathway: requirements for antigen cross-presentation'. In: Frontiers in immunology 3 (2012), p. 37 (cited on page 71).

[157] Sukrut Hemant Karandikar et al. 'Identification of epitopes in ovalbumin that provide insights for cancer neoepitopes'. In: JCI insight 4.8 (2019) (cited on page 71).

[158] Kyle E Broaders et al. 'Acetalated dextran is a chemically and biologically tunable material for particulate immunotherapy'. In: Proceedings of the National Academy of Sciences 106.14 (2009), pp. 5497–5502 (cited on pages 71, 73).

[159] Amy S Rosenberg. 'Effects of protein aggregates: an immunologic perspective'. In: The AAPS journal 8.3 (2006), E501–E507 (cited on page 72).

[160] Eric M Bachelder et al. 'Acetal-derivatized dextran: an acid-responsive biodegradable material for therapeutic applications'. In: Journal of the American Chemical Society 130.32 (2008), pp. 10494–10495 (cited on page 73).

[161] C. Galustian et al. 'High and low affinity carbohydrate ligands revealed for murine SIGN-R1 by carbohydrate array and cell binding approaches, and differing specificities for SIGN-R3 and langerin.' In: International immunology 16 6 (2004), pp. 853–66 (cited on page 73).

[162] Pallavi Kiran et al. 'Synthesis and comparison of linear and hyperbranched multivalent glycosides for C-type lectin binding'. In: New Journal of Chemistry 43.40 (2019), pp. 16012–16016 (cited on page 74).

[163] Lina Cui et al. 'Mannosylated dextran nanoparticles: a pH-sensitive system engineered for immunomodulation through mannose targeting'. In: Bioconjugate chemistry 22.5 (2011), pp. 949–957 (cited on page 74).

[164] Miao Yu et al. 'Dextran and polymer polyethylene glycol (PEG) coating reduce both 5 and 30 nm iron oxide nanoparticle cytotoxicity in 2D and 3D cell culture'. In: International journal of molecular scien 13.5 (2012), pp. 5554–5570 (cited on page 74).

# List of Figures

# List of Tables